Exploring Novel Enzymology in Bacterial Metabolism: Cysteine Synthase, Urate Oxidase, and Bacimethrin Biosynthesis.

by Sean O'Leary

EXPLORING NOVEL ENZYMOLOGY IN BACTERIAL METABOLISM: CYSTEINE SYNTHASE, URATE OXIDASE, AND BACIMETHRIN BIOSYNTHESIS.

A Dissertation

Presented to the Faculty of the Graduate School

of Cornell University

In Partial Fulfillment of the Requirements for the Degree of

Doctor of Philosophy

by

Seán O'Leary

August 2010

EXPLORING NOVEL ENZYMOLOGY IN BACTERIAL METABOLISM: CYSTEINE SYNTHASE, URATE OXIDASE, AND BACIMETHRIN BIOSYNTHESIS.

Seán O'Leary, Ph. D.

Cornell University 2010

The practice of biological chemistry in the post-genomic era has included increasingly broad and detailed interrogation of cellular processes at the molecular level. In particular, enzymology has been equipped with a wide range of physical and analytical tools to study in detail chemical reactions catalyzed by enzymes.

The present work describes studies aimed at characterizing enzymes involved in bacterial metabolism. First, a pre-steady-state kinetic analysis is described of CysM, a cysteine synthase from *Mycobacterium tuberculosis*. This analysis led to two principal results. *O*-phospho-L-serine was identified as the immediate biosynthetic precursor for cysteine in its CysM-mediated biosynthesis in *M. tuberculosis*. The substrate for CysM and related enzymes in bacteria was previously assumed to be *O*-acetyl-L-serine. The study also resulted in the first detailed pre-steady-state kinetic characterization of sulfur transfer from a small sulfur carrier protein (CysO) to an enzyme-bound intermediate in a biosynthetic pathway.

The second study involved biochemical characterization of the HpxO enzyme from *Klebsiella pneumoniae*. This enzyme catalyzes the oxidation of uric acid to 5-hydroxyisourate as part of the purine catabolic pathway. The activity of HpxO was shown to depend on flavin adenine dinucleotide (FAD), in contrast to all previously-studied urate oxidase enzymes, which employ a cofactor-independent chemical

mechanism. The results confirmed the existence of a novel mechanistic paradigm in purine catabolism. A series of HpxO active-site mutants were generated and characterized kinetically in order to gain further insight into the HpxO-catalyzed mechanism of urate hydroxylation, in the context of its X-ray crystal structure.

The third study reported here involved characterization of a biosynthetic pathway for bacimethrin, a thiamin antimetabolite. We identified a previously unknown biosynthetic pathway for bacimethrin in *Clostridium botulinum* and reconstituted *in vitro* the three enzymatic activities which are responsible for conversion of cytidine monophosphate to bacimethrin. We also investigated the activity of a thiaminase I enzyme found in the *C. botulinum* bacimethrin biosynthetic cluster. Our results implicate thiaminase I as a potentiator of bacimethrin toxicity and indicate a possible role for this enzyme in extracellular salvage of thiazole for thiamin biosynthesis.

BIOGRAPHICAL SKETCH

Seán O'Leary was born in Co. Wexford, Ireland. He received a B.Sc.(Hons.) in Chemistry, from the National University of Ireland, University College Dublin, in 2005. He then moved to Ithaca, N.Y. and later College Station, Tex., to work in the laboratory of Tadhg P. Begley. He received an M. S. in Chemistry and Chemical Biology in 2008, and later a Ph.D. in the same field, both from Cornell University.

ACKNOWLEDGMENTS

Colleagues, friends, and family are gratefully acknowledged for their enabling contributions and support, both throughout and beyond the period when the work described here was carried out. In particular, Tadhg Begley is acknowledged for insight, help, good humor, and the habitual indulgence of considerable idiosyncrasy. Brian Crane and Hening Lin are thanked for their input and participation in the doctoral committee. Thanks are also due to Steve Ealick for collaborative input into several studies including the CysM and HpxO work described here.

The research described in this work was funded by NIH (grants AI066244-02 and DK44083 to T. P. B.).

TABLE OF CONTENTS

Chapter 4. Identification and initial characterization of a biosynthetic pathway for bacimethrin in *Clostridium botulinum A ATCC 19397*.

Chapter 5. Summary and outlook.

LIST OF FIGURES

LIST OF TABLES

LIST OF ABBREVIATIONS

ATP	Adenosine 5′-triphosphate
CMP	Cytidine 5′-monophosphate
dUMP	2′-deoxyuridine 5′-monophosphate
BLAST	Basic Local Alignment Search Tool
FAD	Flavin adenine dinucleotide
HMP-OH	2-Methyl-4-amino-5-(hydroxymethyl)pyrimidine
HMP-PP	2-Methyl-4-amino-5-(diphosphomethyl)pyrimidine
MeOThOH	2′-Methoxythiamin
MeOThDP	2′-Methoxythiamin pyrophosphate
MWCO	Molecular weight cut-off
NADH	β-Nicotinamide adenine dinucleotide, reduced form
NADPH	β-Nicotinamide adenine dinucleotide phosphate, reduced form
OAS	*O*-acetyl-L-serine
OASS	*O*-acetylserine sulfhydrylase
OPS	*O*-phospho-L-serine
PLP	Pyridoxal 5′-phosphate
SAM	*S*-Adenosyl-L-methionine
TCEP	*tris*(2-carboxyethyl)phosphane
ThOH	Thiamin
ThDP	Thiamin pyrophosphate
Tris	*tris*-(hydroxymethyl)aminomethane

LIST OF SYMBOLS

ε_λ	Molar absorptivity coefficient at wavelength λ
E_o	Total enzyme concentration.
K_d	Dissociation constant.
K_m	Michaelis constant.
k_{cat}	Michaelis-Menten turnover number.
V	Observed rate of enzymatic turnover (concentration time^{-1}).

CHAPTER 1

Pre-steady-state kinetic studies on CysM, a cysteine synthase from *Mycobacterium tuberculosis* with novel substrate specificity.[1]

1.1. Introduction.

Mycobacterium tuberculosis is a widespread and dangerous pathogen which exerts significant deleterious effects on humans both from health and economic standpoints (*1*). An understanding of the metabolism of this bacterium is clearly advantageous in order to establish means for its control and treatment of the symptoms which infection produces in humans. This is particularly the case where the possibility of discovering new metabolic pathways specific to *M. tuberculosis* exists, as these may be exploited by the development of therapeutic agents.

The biosynthesis of L-cysteine is thought to occur *via* at least four pathways (Figure 1.1). The first of these was reported by Kredich and Tompkins and involves two enzymatic steps (*2*) beginning with L-serine. The first step is activation as a leaving group of the serine hydroxyl by acetylation, catalyzed by the acetyl-CoA-dependent enzyme serine acetyltransferase (*3*). *O*-acetyl-L-serine then undergoes a β-replacement reaction catalyzed by a PLP-dependent cysteine synthase. In *Salmonella typhimurium* bisulfide (HS^-) has been shown to be a nucleophilic substrate for the β-replacement

---

[1]Reproduced with permission from O'Leary, S. E., Jurgenson, C. T., Ealick, S. E., Begley, T. P. (2008) *O*-Phospho-L-serine and the thiocarboxylated sulfur carrier protein CysO-COSH are substrates for CysM, a cysteine synthase from *Mycobacterium tuberculosis*, *Biochemistry 47*, 11606–11615. Copyright 2008, American Chemical Society.

reaction, and the kinetics of the *S. typhimurium* enzyme have been studied extensively. These studies have been reviewed by Tai and Cook (*4*).

A variation on this pathway has been identified in the hyperthermophilic archaeon *Aeropyrum pernix*, where *O*-phospho-L-serine is the immediate biosynthetic precursor for L-cysteine (*5, 6*). The catabolism of L-cystathionine by L-cystathionine *γ*-lyase to produce L-cysteine, 2-oxobutyrate and ammonia is thought to be the predominant biosynthetic route for cysteine in eukaryotic and mammalian systems but also has been shown to take place in some bacteria (*7*). A fourth pathway in the methanogenic archaea was recently described which is tRNA-dependent and proceeds *via* an *O*-phosphoseryl-tRNA^{Cys} intermediate which can be converted to cysteinyl-tRNA^{Cys} and thence to cysteine (*8*).

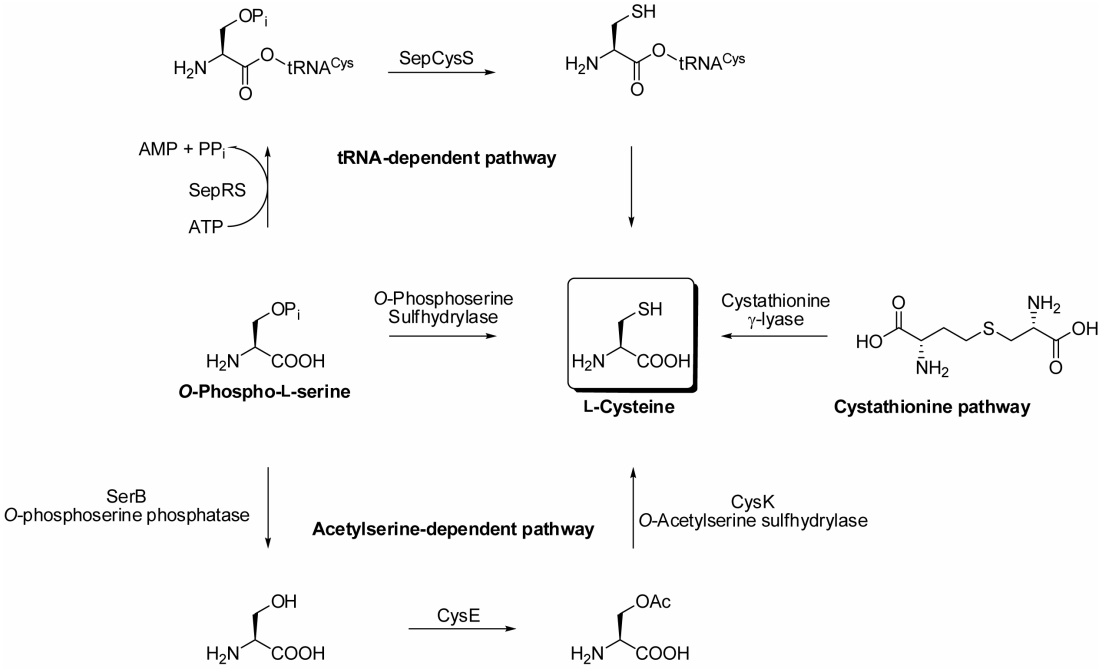

Figure 1.1. Biosynthetic pathways for L-cysteine.

Inspection of the sequenced *M. tuberculosis* H37Rv genome reveals the presence of four loci assigned as coding for cysteine synthase enzymes. Locus Rv2334, coding for the *cysK* gene is contiguous with locus Rv2335 (*cysE*), proposed to code for serine acetyltransferase. A second open reading frame (Rv0848) contains the *cysK1* gene but no serine acetyltransferase is present. Locus Rv3684 is also proposed to code for a cysteine synthase gene, but is also not clustered with the serine acetyltransferase, instead being neighbored by regions coding for a proposed phosphohydrolase enzyme (Rv3683) and prolyl tRNA (Rvnt40). The fourth and final open reading frame, Rv1336, codes for a cysteine synthase (CysM) which is found clustered with, amongst others, a gene coding for a small sulfur carrier protein (CysO).

Previous work from our laboratory reported the reconstitution of a new cysteine biosynthetic pathway in *M. tuberculosis* (*9*) which involves CysM. This enzyme has extensive sequence homology to the *O*-acetylserine sulfhydrylases and is predicted on this basis to belong to the *O*-acetylserine sulfhydrylase B family of enzymes. The new pathway utilizes the 93-amino acid sulfur carrier protein (CysO), which clusters with CysM in the *M. tuberculosis* H37Rv genome. Similar sulfur carrier proteins have been identified in the biosynthetic pathways for thiamin (*10*) and molybdopterin (*11*) and quinolobactin (*12, 13*). These proteins also show homology to components of the system which targets doomed proteins by ubiquitination for degradation by the proteasome (*14*). A key feature of these proteins is a flexible *C*-terminal Gly-Gly tail which can insert into the active site of their partner enzymes to facilitate sulfur transfer. It has been shown that to form the *C*-terminal thiocarboxylate, the proteins are first activated by adenylation of their *C*-termini and then undergo nucleophilic addition-elimination chemistry with a sulfide equivalent, the production of which involves enzymes such as cysteine desulfurases or rhodanese homology domain proteins. The *M. tuberculosis moeZ* (Rv3206) gene product (*15*) contains such a

rhodanese homology domain as well as a ThiF-like domain and was shown to catalyze the formation of the CysO thiocarboxylate using an unidentified sulfur source in cell-free extract. ThiF is the enzyme responsible for the adenylation of ThiS-COOH in the thiamin biosynthetic pathway in prokaryotes (*16*). The expression of MoeZ is upregulated under the same conditions that produce upregulation of CysO and CysM expression. A zinc-dependent hydrolase Mec^{+} (*17*) was shown to catalyze the selective hydrolysis of the CysO-cysteine adduct formed after attack of thiocarboxylated CysO (CysO-COSH) at the α-aminoacrylate intermediate formed at the CysM active site. The mec^{+} gene (Rv1334) clusters with the *cysO* and *cysM* genes.

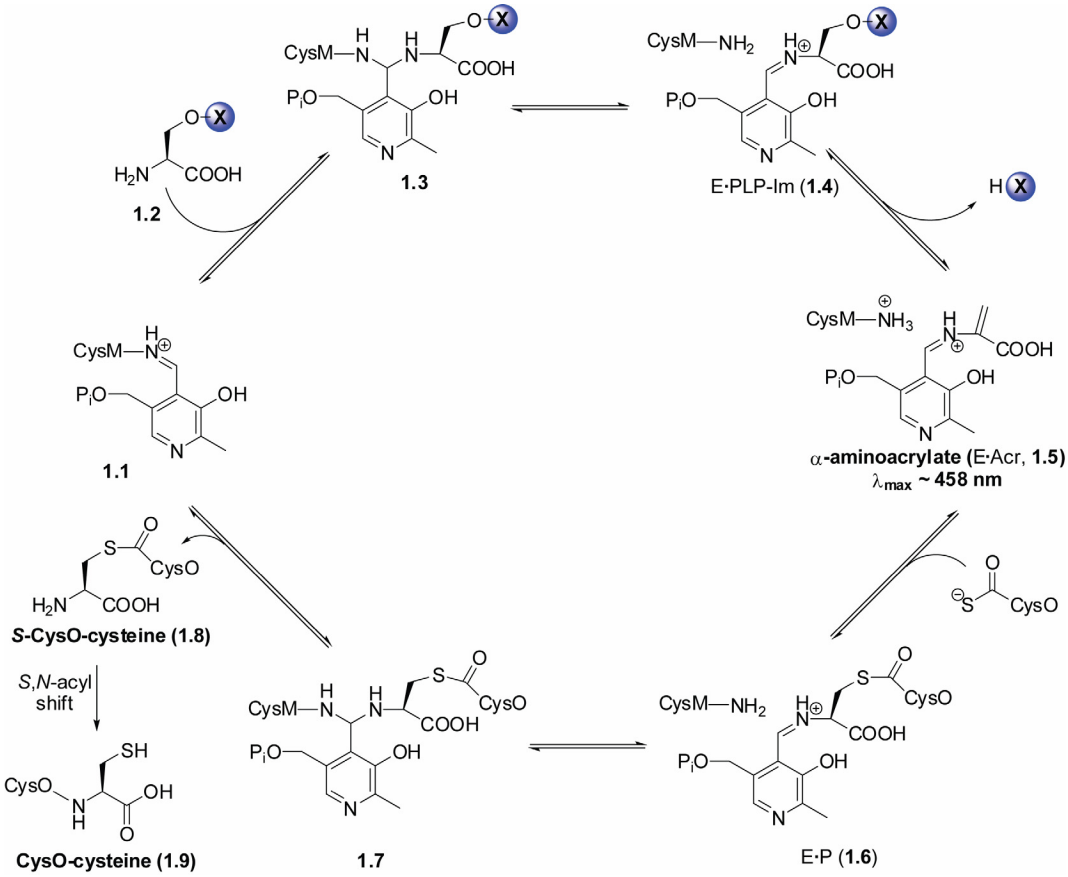

Figure 1.2. Proposed catalytic mechanism for CysM, based on studies on the related *O*-acetylserine sulfhydrylase family of PLP-dependent β-replacement enzymes.

Given that no acetyltransferase gene is found clustered with the *cysM* and *cysO* genes, there is no reason to assume *a priori* that *O*-acetyl-L-serine is the physiological amino acid substrate for CysM. In order to test this hypothesis, and to investigate the reaction of CysO-COSH as the nucleophilic substrate for CysM, we have characterized the CysM kinetic pathway under transient-state and single-turnover conditions using both *O*-acetyl- and *O*-phospho-L-serine as the amino acid substrates and CysO-COSH and bisulfide as the nucleophilic substrates. The proposed chemical mechanism for CysM is shown in Figure 1.2. In brief, this mechanism involves formation of an imine (**1.4**) between CysM-bound pyridoxal 5′-phosphate and the amino acid substrate *via* a transient geminal diamine intermediate (**1.3**), followed by elimination across the α,β bond of the substrate to form a relatively stable α-aminoacrylate intermediate (**1.5**). 1,4-Addition of a suitable nucleophile such as CysO-COSH to this intermediate affords the β-substituted amino acid imine (**1.6**), which undergoes transimination with an active site lysine residue to release the product (**1.8**) and regenerate the active site for catalysis.

1.2. Results.

1.2.1. Formation of the a-aminoacrylate from O-acetyl-L-serine.

The aminoacrylate intermediate could be formed from *O*-acetyl-L-serine (Figure 1.3A) and the increase in absorbance at 465 nm due to its formation on treatment of CysM with OAS could be best fit using a single exponential function at each of the various concentrations of OAS employed, to give the first order rate constants for formation. The dependence of these rate constants on the OAS concentration was best described by a hyperbolic function. A dissociation constant ($K_d = 1/K_1$) for OAS of 5 ± 2 mM and a first order rate constant of 0.025 ± 0.004 s^{-1} were determined for formation of the aminoacrylate intermediate. This intermediate was stable for more than 30 minutes

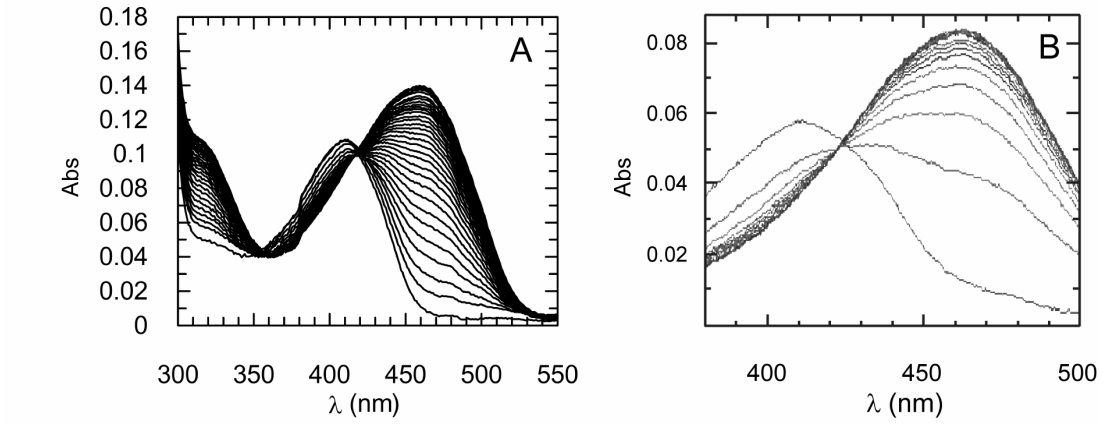

Figure 1.3. Ultraviolet-visible spectroscopy of formation of the CysM-bound α-aminoacrylate intermediate. (A) Mixing of CysM (14 μM) with *O*-acetyl-L-serine (5 mM) produces a decrease in the absorbance due to enzyme-bound pyridoxal-5′-phosphate (**1.1**) at 412 nm and an increase in the absorbance at 458 nm due to the formation of an α-aminoacrylate intermediate (**1.5**). The traces were recorded at intervals of approximately 34 s after mixing, in 50 mM Tris-HCl, pH 8.0 and at room temperature. (B) Absorbance changes due to mixing of *O*-phospho-L-serine (10 μM) with CysM (14 μM) in 50 mM Tris-HCl at pH 8.0 and at room temperature. Individual traces were recorded at intervals of approximately 30 s. The changes reflect conversion of the enzyme-bound PLP imine (**1.1**, λ_{max} = ~412 nm) to a stable α-aminoacrylate intermediate (**1.5**, λ_{max} = ~462 nm).

(data not shown). Additionally, the hyperbolic function was found to pass through the origin. The limiting initial slope of the hyperbola, determined as k_{max}/K_d provides an estimate of the second order rate constant for formation of the aminoacrylate intermediate, and was found to be 0.005 ± 0.002 mM^{-1} s^{-1}. This estimate is model-dependent and applies only in the case of rapid-equilibrium binding followed by a single rate-limiting step, consistent with the proposed chemical mechanism. No

evidence for reversibility of the formation of the aminoacrylate was found under the conditions of its formation.

1.2.2. Formation of the a-aminoacrylate from O-phospho-L-serine

The α-aminoacrylate intermediate could also be formed from *O*-phospho-L-serine (Figure 1.3B) and the increase in absorbance at 465 nm due to its formation on treatment of CysM with OPS could also be fit using a single exponential function at the various concentrations of OPS examined (Figure 1.4). The data for this substrate was treated as described for *O*-acetyl-L-serine to give a first order rate constant of 17 ± 2 s^{-1} for formation of the aminoacrylate and a K_d of 6 ± 1 mM. The second order rate constant for formation of the aminoacrylate intermediate was thus estimated at 2.8 ± 0.7 mM^{-1} s^{-1}. The intermediate could be partially quenched by addition of high concentrations of potassium phosphate (> 10 mM, data not shown).

1.2.3. Formation and decay of the a-aminoacrylate with L-cysteine.

When CysM was treated with L-cysteine, an increase in the absorbance at 465 nm was detected consistent with formation of the α-aminoacrylate intermediate. However, this was found to subsequently decay on a longer timescale. The resulting traces at the various concentrations of L-cysteine examined were best fit by double exponential functions to give two sets of first order rate constants at the various cysteine concentrations, one for formation and one for decay of the aminoacrylate intermediate (Figure 1.5). The first order rate constants for formation of the aminoacrylate were plotted as a function of the concentration of L-cysteine and the resulting data were best fit by a line with a slope of 0.0044 ± 0.0004 mM^{-1} s^{-1}. The rate of decay of the aminoacrylate intermediate was independent of the concentration of L-cysteine within experimental error, being of the order of 0.001 s^{-1} (data not shown).

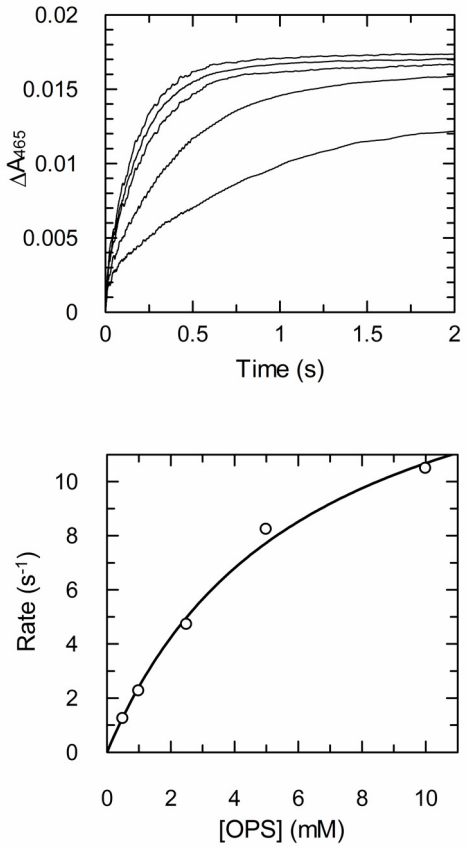

Figure 1.4. Kinetics of formation of α-aminoacrylate intermediate from *O*-phospho-L-serine. (A) Changes in absorbance at 465 nm following rapid mixing of *O*-phospho-L-serine (OPS; 0.5, 1, 2, 5 and 10 mM in order of increasing rate) with CysM (4.5 μM) in 50 mM Tris-HCl at pH 8 and at ~22 °C. The resulting data were fit to single exponential functions to give the first order rates at the various concentrations of *O*-phospho-L-serine. (B) Plot of the rates of acrylate formation as a function of *O*-phospho-L-serine concentration, fit to a hyperbolic function describing a rapid equilibrium binding model. From this fit, the K_d for OPS was found to be 6 ± 1 mM and the second order rate constant for formation of the aminoacrylate intermediate was 2.8 ± 0.7 mM^{-1} s^{-1}.

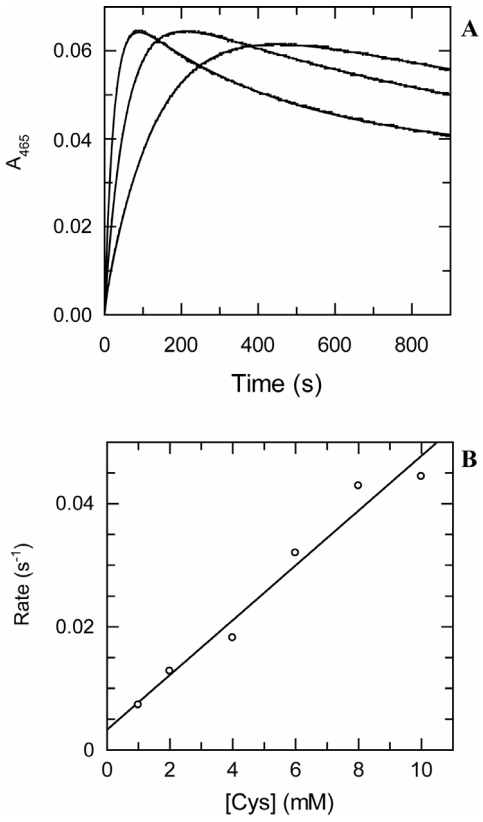

Figure 1.5. Kinetics of formation and decay of the α-aminoacrylate intermediate in the presence of cysteine. (A) CysM (31 μM) was mixed with cysteine (1, 4 and 8 mM in order of increasing rate) in 50 mM Tris-HCl, pH 8.0 and at ~22 °C and the change in absorbance at 465 nm was monitored. The data are shown fit to functions of the form $y = Ae^{-kt} + Be^{-kt} + C$. (B) Dependence of the rate of formation of the aminoacrylate intermediate on the concentration of cysteine. The slope of the line fitting the data is a measure of the specificity of the enzyme for this amino acid substrate and was found to be 0.0044 ± 0.0004 mM^{-1} s^{-1}. The rate of decay of the aminoacrylate intermediate was independent of the concentration of L-cysteine within experimental error, being of the order of 0.001 s^{-1}.

1.2.4. Quenching of the α-aminoacrylate intermediate by bisulfide.

The α-aminoacrylate intermediate was pre-formed under single turnover conditions by treatment of CysM (25 μM) with *O*-phospho-L-serine (20 μM) in 50 mM Tris-HCl at pH 8. Addition of sodium sulfide (0.1 – 15 mM final bisulfide concentration) caused a decrease in the absorbance at 465 nm (Figure 1.6). This decrease was fit to a single exponential function to give the observed rates for decay at the various bisulfide concentrations employed. The rate constants exhibited the hyperbolic dependence on the concentration of bisulfide consistent with a rapid-equilibrium binding model, with a predicted rate constant for quenching of 0.48 ± 0.07 s^{-1} and a K_d for bisulfide of 7 ± 2 mM, yielding an apparent second order rate constant for quenching of 0.07 ± 0.02 mM^{-1} s^{-1}.

1.2.5. Quenching of the α-aminoacrylate intermediate by CysO-COSH.

Addition by rapid mixing of a solution of CysO-COSH to a pre-formed solution of the α-aminoacrylate under single turnover conditions also caused a decay in the absorbance at 465 nm (Figure 1.7). This decay could be fit to a single exponential function to give the observed rate for decay at the various concentrations of CysO-COSH examined. The rate of reaction of CysO-COSH with the CysM-bound aminoacrylate intermediate could not be saturated at the highest available CysO-COSH concentration (250 μM), which approached the solubility limit for the protein. We therefore restricted our analysis to the reaction of CysO-COSH in the 0–125 μM concentration range. A comparison of the specificity of CysM for the nucleophilic substrates, which was the aim of the present study, is readily obtained from such an analysis. The data describing the dependence of the rate of reaction of CysO-COSH in this concentration range with the CysM-bound aminoacrylate intermediate fit well to a line with a slope of 88 ± 6 mM^{-1} s^{-1}. This value can be interpreted as an estimate of the

second order rate constant for the reaction (Figure 5). The *y*-intercept of this line had a value of 0.61 ± 0.43 s^{-1}.

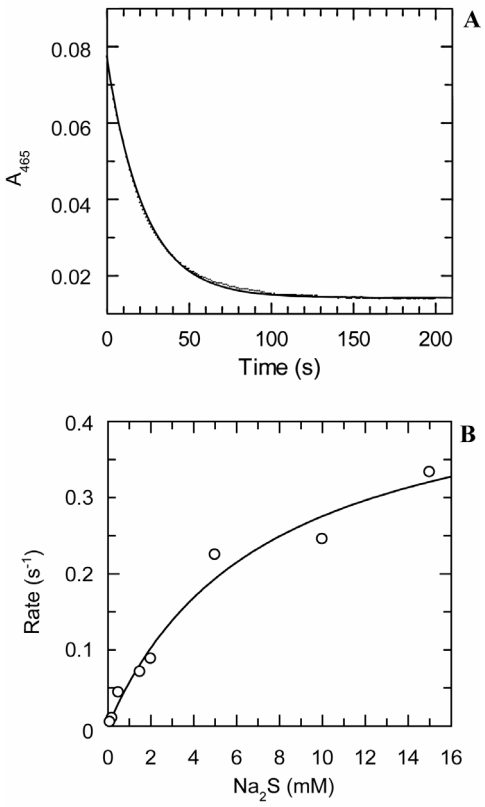

Figure 1.6. Kinetics of quenching of the α-aminoacrylate intermediate by bisulfide. The CysM/*O*-phospho-L-serine α-aminoacrylate intermediate was pre-formed by mixing CysM with a stoichiometric quantity of *O*-phospho-L-serine in 50 mM Tris-HCl, pH 8.0 at room temperature (~22 °C), then mixed with a solution of sodium sulfide in the same buffer. (A) Representative trace with exponential fit showing decay of absorbance at 465 nm after rapid mixing of the pre-formed CysM/*O*-phospho-L-serine α-aminoacrylate intermediate (11 μM) with sodium sulfide (0.5 mM). (B) Dependence of the rate of reaction on the bisulfide concentration (0.1 – 15 mM), fit to a hyperbolic function, The K_d for bisulfide was found to be 7 ± 2 mM and the first order rate constant for the carbon-sulfur bond-forming addition reaction was 0.48 ± 0.07 s^{-1}.

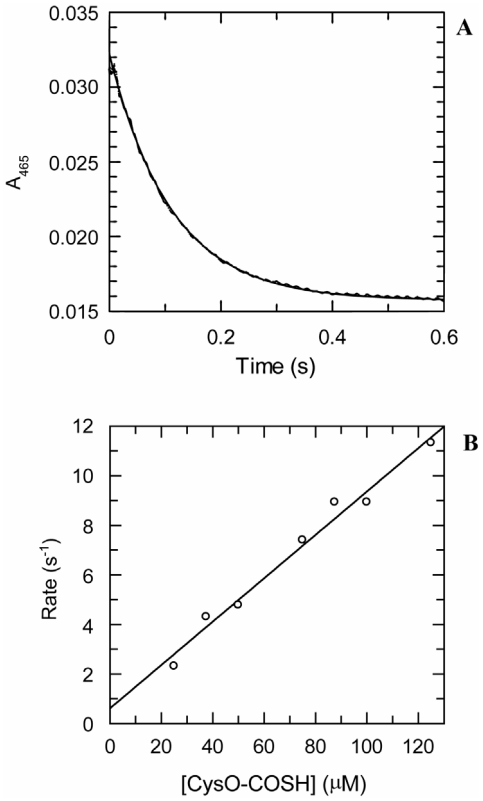

Figure 1.7. Kinetics of quenching of the α-aminoacrylate intermediate by CysO-COSH. The CysM/*O*-phospho-L-serine α-aminoacrylate intermediate was pre-formed by mixing CysM (14 μM) with *O*-phospho-L-serine (11 μM) in 50 mM Tris-HCl, pH 8.0 at room temperature (~22 °C). This solution was then rapidly mixed with a solution containing CysO-COSH in the same buffer. (A) Representative trace with exponential fit showing decay of absorbance at 465 nm after rapid mixing of the CysM/*O*-phospho-L-serine α-aminoacrylate intermediate with CysO-COSH (0.05 mM) in 50 mM Tris-HCl at pH 8 and at room temperature. (B) Plot of the first-order rates of decay at the various CysO-COSH concentrations with a linear fit. The slope of this line is a measure of the specificity of the enzyme for this nucleophilic substrate and was found to be 88 ± 6 mM^{-1} s^{-1}.

1.3. Discussion.

1.3.1. Kinetic scheme for CysM.

The minimal kinetic scheme for CysM (Figure 1.8) can be derived from the full pathway (Figure 1.2) by its collapse due to the kinetic silence of the geminal diamine intermediates (**3** and **7**) and the aldimine intermediate **1.4.**. There was neither a lag in formation of the observable α-aminoacrylate intermediate, nor a dependence of the amplitude for aminoacrylate formation on the substrate concentration, suggesting that the forward partitioning of all intermediates up to and including the imine **1.4** must be, respectively, rapid and favorable. Indeed in the case of the cysteine synthase OASS-A from *Salmonella typhimurium* LT-2, the CysM-bound PLP-OAS aldimine intermediate (equivalent to structure **1.4**) could only be observed on a low millisecond timescale and a precise rate for its formation was not reported (*22*). The kinetic pathway of CysM thus resembles that reported for the *O*-acetylserine sulfhydrylase enzymes with respect to the "elimination" half-reaction which generates the aminoacrylate intermediate. However, in the second CysM half-reaction a hitherto unexplored mechanistic variation presents itself in the form of CysO-COSH, which acts as a sulfide equivalent. Additionally, this half-reaction of CysM offered a more detailed insight than had been previously available in any system into the kinetics of sulfur transfer mediated by CysO-like proteins. The biosynthetic enzymes for thiamin (*23*) and quinolobactin (*12*) are experimentally much less tractable with regard to making detailed kinetic measurements on the sulfur transfer reaction.

1.3.2. Formation of the α-aminoacrylate intermediate.

Mixing of CysM with an excess of *O*-acetyl-L-serine or *O*-phospho-L-serine (Figure 1A and 1B, respectively) produces initially a red shift of the absorbance at 412 nm due

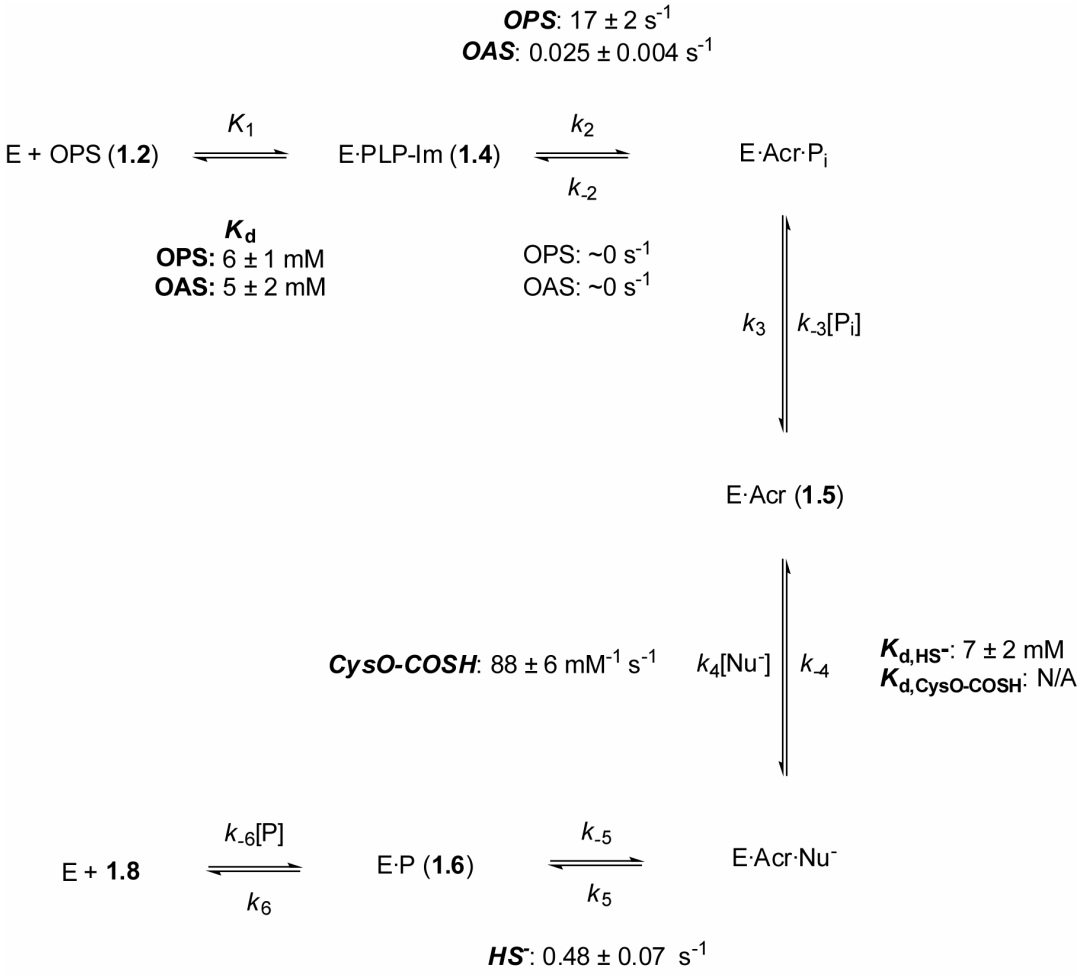

Figure 1.8. Minimal kinetic model for CysM.

to the enzyme-PLP internal aldimine (**1.1**). This is consistent with the data observed for reaction of the previously-studied *O*-acetylserine sulfhydrylase A enzyme from *Salmonella typhimurium* with OAS, and is attributed to the transient formation of the enzyme-PLP external aldimine (**1.4**), which then rapidly converts to the aminoacrylate intermediate. The lack of an isosbestic point in the data obtained with CysM contrasts with the situation for the reaction of OAS with the B-isozyme from *S. typhimurium* (*24*).

The kinetics of formation of the aminoacrylate may be described in terms of a rapid equilibrium binding model (Figure 1.8) where the rate of dissociation of the ES complex, k_{-1}, is much greater than the rate of the subsequent, kinetically significant, chemical step, i.e. the β-elimination reaction (k_2). This model has been used previously to describe the formation of the aminoacrylate intermediate from OAS, catalyzed by *O*-acetylserine sulfhydrylase enzymes from *Salmonella typhimurium* and *Escherichia coli*, and predicts a hyperbolic dependence of the observed rate constant for chemistry on the substrate concentration, with saturation of the rate of the chemical step at concentrations of substrate which saturate the ES complex. In this model, an aminoacrylate intermediate at a CysM active site under conditions of zero substrate concentration may only undergo reverse reaction. Hence, the *y*-intercept of such a hyperbola corresponds to the back-rate for the chemical reaction (k_{-2}). Equation (2) also defines the equilibrium constant K_1 for substrate association, which is the reciprocal of the dissociation constant (K_d) The quotient $K_1[S]/(K_1[S] + 1)$ is a fraction that ranges from 0 to 1, reflecting the formation of the ES complex. The rates of formation of the aminoacrylate intermediate in a single turnover from both *O*-acetyl- and *O*-phospho-L-serine were found to exhibit hyperbolic dependence on the substrate concentrations, consistent with this model. Both substrates have comparable dissociation constants (K_d) of 6 mM (OPS) and 5 mM (OAS). The Michaelis constants (K_m) for these amino acids with respect to enzymes which utilize them as substrates appear to be, broadly speaking, in the mid-micromolar to low millimolar range (*25, 26*). The relatively high dissociation constants for the amino acid substrates are similar to that determined for OAS in studies on the *O*-acetylserine sulfhydrylase A enzyme from *Salmonella typhimurium*. However, the rates of the elimination reaction to form the aminoacrylate intermediate were found to vary substantially between *O*-acetyl- and *O*-phospho-L-serine. The rate of the β-elimination reaction of acetic acid to give

the aminoacrylate intermediate (0.025 s^{-1}) is 850-fold slower than that of the elimination of, formally, $[HPO_4]^{2-}$ (17 s^{-1}), suggesting the presence of stabilizing interactions at the CysM active site which facilitate such a rate enhancement.

In the case of OAS, the apparent second order rate constant for formation of the aminoacrylate was found to be 0.005 mM^{-1} s^{-1}, compared with 2.8 mM^{-1} s^{-1} for *O*-phospho-L-serine. This 560-fold specificity suggests that *O*-phospho-L-serine and not *O*-acetyl-L-serine is the physiologically relevant substrate for CysM. Given the similarity of the dissociation constants for both substrates, the ultimate origin of this specificity appears to be the chemical reactivity of OPS at the CysM active site.

In order to further evaluate the plausibility of OPS as a substrate for CysM, we investigated the CysM-catalyzed reaction of cysteine. It would seem logical that physiologically-relevant substrates for cysteine synthases must greatly out-compete the intrinsic cysteine synthase-catalyzed reactivity of cysteine itself. Cysteine reacts with biphasic kinetics in the presence of CysM as it both forms and quenches the aminoacrylate intermediate. In the case of OASS-A from *Salmonella typhimurium*, the quenching reaction has been reported to form a thioether product (*27*). The time course of reaction of cysteine with CysM is thus described by a double exponential function with the first and second phases resulting from the formation and quenching of the aminoacrylate, respectively (Figure 1.5). The formation of the aminoacrylate from cysteine also exhibits rapid-equilibrium binding kinetics, with the apparent second order rate constant (0.0044 mM^{-1} s^{-1}) suggesting that L-cysteine itself is an equally-good substrate for CysM as OAS. Such an observation points strongly to OPS as a more likely substrate for CysM than OAS. This contrasts with the situation for the previously-studied OASS-B from *Salmonella typhimurium*, which does not utilize OPS as a substrate (*28*).

1.3.3. Quenching of the α-aminoacrylate intermediate.

The reaction of the CysM-bound α-aminoacrylate intermediate in the carbon-sulfur bond-forming conjugate addition constitutes the second half-reaction characteristic of cysteine synthases. In all previously-studied systems bisulfide is the sulfur donor. CysM offers a hitherto unexplored mechanistic variation on the existing paradigm in the form of CysO-COSH, the thiocarboxylated sulfide carrier protein which acts as a sulfide source for this second half reaction. Additionally, the CysM system allowed kinetic characterization of the sulfide transfer event mediated by CysO-COSH. This characterization has not been possible for any of the other sulfide carrier proteins. To characterize this second half-reaction of CysM we examined the reaction of the pre-formed aminoacrylate intermediate with both CysO-COSH and bisulfide.

The aminoacrylate intermediate could be quenched by bisulfide to give L-cysteine. The dependence of the observed rate for quenching on the concentration of bisulfide was hyperbolic, also consistent with a rapid-equilibrium binding model. From the hyperbolic fit to the data, the rate constant k_5 for quenching of the aminoacrylate by bisulfide was found to be 0.48 s^{-1}, with a K_d for bisulfide of 7 mM. This value suggests that appreciable binding of bisulfide to CysM should occur only at a bisulfide concentration generally regarded as toxic to *M. tuberculosis* (*29*). In contrast, the rate of quenching of the aminoacrylate in the presence of CysO-COSH depended linearly on the CysO-COSH concentration in the 0–125 μM range. The rate of quenching of the aminoacrylate by CysO-COSH could not be fully saturated at a CysO-COSH concentration of 250 μM, which approaches the solubility limit of the protein. The kinetic difference between CysO-COSH and bisulfide as nucleophiles provides an insight into the physical processes involved with the two sulfur sources. The quenching of the aminoacrylate by CysO-COSH requires association of the two proteins, likely followed by conformational changes in one or both proteins to place

the Gly-Gly-SH *C*-terminal sulfur atom of CysO-COSH in a position optimal for *β*-addition to the aminoacrylate intermediate (**1.5**). It is not surprising that these steps should be slower than the subsequent chemical reaction. The slope of the line describing the concentration dependence of the quenching rate (88 mM^{-1} s^{-1}) may thus be regarded as an estimate of the second order rate constant k_4 for binding of CysO-COSH to CysM. This is three orders of magnitude greater than the value of k_5/K_d for bisulfide, computed for that substrate to be 0.07 mM^{-1} s^{-1}, and which is an estimate of the specificity of the enzyme for this substrate. Comparison of these values strongly suggests that CysO-COSH is the nucleophilic substrate *in vivo*. The CysM active site with the aminoacrylate intermediate present cannot be readily accessible to the bulk solvent in the absence of CysO, as demonstrated by the longevity of the aminoacrylate even under conditions of exposure to nucleophiles such as cysteine, and its slow rate of reaction with bisulfide. In the case of OASS-A from *Salmonella typhimurium*, the rate of the *β*-addition reaction is thought to be diffusion-limited when bisulfide is the nucleophilic substrate (*30*). Therefore it is likely that binding of CysO causes a conformational change in CysM which facilitates the nucleophilic addition.

The *y*-intercept of the linear fit describing the concentration-dependence of the rate of quenching of the OPS-derived CysM-aminoacrylate intermediate by CysO-COSH is nonzero and has a value of 0.61 ± 0.43 s^{-1}, which is likely to estimate the rate of the rate-limiting step for back-reaction of the *S*-CysO-Cys external aldimine (**1.6**), i.e. re-formation of the aminoacrylate and CysO-COSH.

1.3.4. Role of CysM and CysO-COSH.

Formation of the CysO-COSH thiocarboxylate represents a considerable energy investment for *M. tuberculosis*, with the direct involvement of at least two nucleoside

triphosphate molecules required to produce *O*-phospho-L-serine and activate CysO for formation of the *C*-terminal thiocarboxylate. The underlying reasons justifying this investment are not clear, but it is possible that the thiocarboxylate moiety represents a stable, oxidation-resistant and relatively non-toxic source of sulfide from which cysteine can be produced in the highly oxidizing environment of the macrophage. Inhibitors of CysM may thus have potential as antimycobacterial chemotherapeutic agents.

1.4. Conclusions.

A new cysteine biosynthetic pathway, in *Mycobacterium tuberculosis*, involving a sulfide carrier protein (CysO) and a cysteine synthase (CysM) has previously been described. Here we report the kinetic characterization of this system and determine that *O*-phospho-L-serine rather than *O*-acetyl-L-serine is the cosubstrate. The chemical mechanism of CysM involves formation of an α-aminoacrylate intermediate consistent with its assignment as a member of the PLP-dependent β-replacement family of enzymes. *O*-acetyl-L-serine has a comparable K_d to that of *O*-phospho-L-serine, but the elimination of acetic acid is substantially slower than that of $[HPO_4]^{2-}$, resulting in a much smaller apparent second order rate constant for formation of the aminoacrylate intermediate. This appears to be analogous to the situation described for the hyperthermophilic archaeon *Aeropyrum pernix* K1, which has been shown to possess a cysteine synthase enzyme which selectively catalyzes the *O*-phosphoserine sulfhydrylation reaction (*6*). Our data show that the thiocarboxylated sulfur carrier protein (CysO-COSH) is likely to serve as the endogenous nucleophilic substrate in *M. tuberculosis*, having an apparent second order rate constant for quenching of the aminoacrylate intermediate that is more than 1200 times faster than bisulfide, the nucleophilic substrate assigned for homologous bacterial cysteine synthases. The

underlying reasons for involvement of a sulfur carrier protein in this pathway remain unclear. One possibility is that the oxidation-resistance of the thiocarboxylate moiety may be a important key factor in protecting sulfide from oxidation in the macrophage.

1.5. Experimental.

All reagents and chemicals were of the highest purity commercially available. Sodium sulfide (90 % dry, balance water) was obtained from Acros Organics. Stopped-flow experiments were performed using a KinTek stopped-flow spectrophotometer (KinTek Corporation). All reactions were carried out in 50 mM Tris-HCl at pH 8. Protein concentrations were determined by the method of Bradford (*18*) and the concentrations thus-determined for CysM were in agreement with those calculated from the absorbance (*19*) of the enzyme-PLP internal imine (**1.1**, ε_{412} = 7600 M^{-1} cm^{-1}) and the α-aminoacrylate intermediate (**1.5**, ε_{465} ~ 9800 M^{-1} cm^{-1}).

1.5.1. Overexpression and purification of proteins.

CysM was overexpressed in *Escherichia coli* BL21(DE3) using a pET16b vector and purified by nickel affinity chromatography. The thiocarboxylated sulfur carrier protein CysO-COSH was overexpressed as a fusion with an intein protein possessing a chitin binding domain using a modification of the method of Kinsland *et al.* (*20*). The *cysO* gene was expressed in pTYB1 in *E. coli* grown at 24 °C. The protein was purified using chitin affinity chromatography. The *C*-terminal thiocarboxylate was generated by soaking the chitin resin-bound protein obtained from clarified cell lysate in a cleavage buffer containing 25 mM $(NH_4)_2S$, 50 mM NaCl and 1 mM EDTA at pH 8 and at 4 °C for 40 h before elution. All proteins were buffer-exchanged into 50 mM Tris-HCl, pH 8 and concentrated prior to use.

1.5.2. Data analysis.

Single-wavelength stopped-flow data for formation and decay of the α-aminoacrylate were fit to exponential functions with the general form of equation (1.1):

$$A_t = A_\infty \pm \sum_i A_i e^{-k_i t} \tag{1.1}$$

where A_t is the absorbance at time t, A_∞ is the absorbance at time ∞, A_i is the amplitude of the ith transient and k_i is the phenomenological observed first order rate constant (k_{obs}) for the ith transient. The data for formation and quenching of the α-aminoacrylate intermediate which showed a hyperbolic dependence of the phenomenological first order rate constants for formation on the concentration of substrates were fit to equation (2) which describes a rapid equilibrium binding model. Details of this model are treated in the discussion. The kinetic and thermodynamic constants $K_1 = 1/K_d$, k_2 and k_{-2} are defined in Scheme 2. [S] is the substrate concentration.

$$k_{obs} = \frac{k_2 K_1 [S]}{K_1 [S] + 1} + k_{-2} \tag{1.2}$$

Linear data for dependence of the first order rate constants for decay of the aminoacrylate were fit to equation (3):

$$k_{obs} = k_q^{app}[S] + k_b \tag{1.3}$$

where k_q^{app} is the apparent second order rate constant for quenching and k_b is a complex function of mechanistic rate constants contributing to re-formation of the aminoacrylate. Linear data for formation of the aminoacrylate were fit to equation (4):

$$k_{obs} = k_f^{app}[S] + k_c \quad (1.4)$$

where k_f^{app} is the apparent second order rate constant for quenching and k_c is a complex function of mechanistic rate constants contributing to the reverse reaction.

1.5.3. Ultraviolet-visible spectroscopy of formation of the α-aminoacrylate intermediate.

CysM (0.76 mg/mL) was treated with excess *O*-acetyl-L-serine (5 mM) in 50 mM Tris at pH 8 and at room temperature. Absorbance spectra in the region 300 – 550 nm were taken manually at intervals of approximately 34 s until no further change in the spectra was observed. In the case of *O*-phospho-L-serine, the enzyme (14 μM) was mixed with OPS (10 μM) and the absorbance spectra were recorded in the 380-500 nm region, with individual traces recorded at intervals of approximately 30 s.

1.5.4. Single-wavelength kinetics of formation of the α-aminoacrylate intermediate.

The instrumentation used varied with the timescale for aminoacrylate formation. Solutions of *O*-acetyl-L-serine were prepared freshly immediately before each experiment. All concentrations are final after mixing. In the case of *O*-acetyl-L-serine, CysM (20 μM) was treated with solutions of *O*-acetyl-L-serine (500 μM – 10 mM). The absorbance at 465 nm was recorded for 900 s after mixing. The concentration of OAS was not corrected for its first order conversion to *N*-acetyl-L-serine, which occurs at ~1% min^{-1} (*21*). The reaction conditions to form the aminoacrylate intermediate were still *pseudo*-first-order in OAS even taking a conversion of ~15% to *N*-acetyl-l-serine into account. No evidence suggesting inhibition of formation of the aminoacrylate intermediate by *N*-acetyl-L-serine was observed. The absorbance as a

function of time after mixing was fit in each case to a single exponential function to give the rates of formation of the aminoacrylate intermediate at the various concentrations of OAS. These rates were plotted as a function of the concentration of OAS and the resulting data were fit to a hyperbolic function. In the case of *O*-phospho-L-serine, where formation of the aminoacrylate intermediate was found to occur on a much faster timescale, the mixing was carried out using a stopped-flow device. CysM (4.5 μM) was rapidly mixed with OPS (1 mM – 10 mM) and the absorbance at 465 nm was recorded after mixing. The data from this experiment were analyzed as described above for OAS.

1.5.5. Single-wavelength kinetics of formation and decay of the α-aminoacrylate intermediate with L-cysteine.

CysM (31 μM) was treated with L-cysteine (1 mM – 10 mM). The absorbance at 465 nm was monitored as a function of time (900 s) after mixing. The resulting trace showed an increase and subsequent decrease in absorbance over the course of the experiment and this was best fit to a double exponential to obtain the two first order rate constants for formation and decay of the absorbance at 465 nm. These were plotted as a function of L-cysteine concentration and in the case of both sets of rate constants fitted to linear functions.

1.5.6. Effect of phosphate on the α-aminoacrylate intermediate.

CysM (19 μM), in 50 mM Tris-HCl at pH 8 was treated with potassium phosphate (10 mM – 100 mM) prepared from a 1.0 M stock solution, the pH of which was adjusted to 8 before dilution.

1.5.7. Single-wavelength kinetics of quenching of the α-aminoacrylate intermediate.

The instrumentation in this case also varied with the nucleophilic substrate. In both the case of CysO-COSH and sodium sulfide, the aminoacrylate intermediate was pre-formed by treatment of CysM (14 μM) with a solution of *O*-phospho-L-serine (11 μM) under single turnover conditions. This was then mixed with solutions of CysO-COSH (25 – 250 μM) or sodium sulfide (100 μM – 15 mM). In the case of CysO-COSH, the lowest concentration used (25 μM) was not under *pseudo*-first order conditions. For CysO-COSH, the aminoacrylate and CysO-COSH solutions were mixed rapidly in a stopped-flow device and the decay of absorbance at 465 nm due to reaction of the aminoacrylate intermediate was observed. In the case of sodium sulfide, the aminoacrylate and bisulfide-containing solutions were mixed manually and the decay of absorbance was recorded in the presence of the reductant TCEP (2 mM). In both cases these decays were fit by non-linear regression to single exponential functions to yield the first order rate constants for quenching of the aminoacrylate under the varying conditions of nucleophile concentration. These rate constants were then plotted as a function of nucleophile concentration. In the case of CysO-COSH the data thus obtained were fit to a line, whereas in the case of bisulfide the dependence of the first order rate constants on the nucleophile concentration was fit to a hyperbola.

REFERENCES

1. *Scientific Working Group Report on Tuberculosis*, 2006, World Health Organization, Geneva
2. Kredich, N. M. & Tomkins, G. M. (1966) The enzymic synthesis of L-cysteine in *Escherichia coli* and *Salmonella typhimurium*, *J. Biol. Chem. 241*, 4955–4965.
3. Johnson, C. M., Roderick, S. L., Cook, P. F. (2007) The serine acetyltransferase reaction: acetyl transfer from an acylpantothenyl donor to an alcohol, *Arch. Biochem. Biophys. 433*, 85–95.
4. Tai, C.-H., and Cook, P. F. (2001) Pyridoxal-5′-phosphate-dependent α,β-elimination reactions: Mechanism of *O*-acetylserine sulfhydrylase, *Acc. Chem. Res. 34*, 49–59.
5. Mino, K., and Ishikawa, K. (2003) Characterization of a novel thermostable *O*-acetylserine sulfhydrylase from *Aeropyrum pernix* K1, *J. Bacteriol.185*, 2277–2284.
6. Mino, K., and Ishikawa, K. (2003) A novel *O*-phospho-L-serine sulfhydrylation reaction catalyzed by *O*-acetylserine sulfhydrylase from *Aeropyrum pernix* K1, *FEBS Lett. 551*, 133–138.
7. Wheeler, P. R., Coldham, N. G., Keating, L., Gordon, S. V., Wooff, E. E., Parish, T., and Hewinson, R. G. (2005) Functional demonstration of reverse transsulfuration in the *Mycobacterium tuberculosis* complex reveals that methionine is the preferred sulfur source for pathogenic mycobacteria, *J. Biol. Chem. 280*, 8069–8078.

8. Sauerwald, A., Zhu, W., Major, T., Roy, H., Palioura, S., Jahn, D., Whitman, W. B., Yates 3rd, J. R., Ibba, M., and Söll, D. (2005) RNA-dependent cysteine biosynthesis in Archaea, *Science 307*, 1969–1972.

9. Burns, K. E., Baumgart, S., Dorrestein, P. C., Zhai, H., McLafferty, F. W., and Begley, T. P. (2005) Reconstitution of a new cysteine biosynthetic pathway in *Mycobacterium tuberculosis*, *J. Am. Chem. Soc. 127*, 11602–11603.

10. Park, J.-H., Dorrestein, P. C., Zhai, H., Kinsland, C., McLafferty, F. W., Begley, T. P. (2003) Biosynthesis of the thiazole moeity of thiamin pyrophosphate (vitamin B1), *Biochemistry 42*, 12430–12438.

11. Rudolph, M. J., Wuebbens, M. M., Rajagopalan, K. V., Schindelin, H. (2001) Crystal structure of molybdopterin synthase and its evolutionary relationship to ubiquitin activation, *Nat. Struct. Biol., 8*, 42–46.

12. Godert, A. M. *Investigating the Biosynthesis of Thio-Quinolobactin and the Development of a Proteomics Probe for Thiamin Utilizing Enzymes* (2006); Dissertation, Cornell University.

13. Matthijs, S., Baysse, C., Koedam, N., Tehrani, K. A., Verheyden, L., Budzikiewicz, H., Schäfer, M., Hoorelbeke, B., Meyer, J.-M., De Greve, H., Cornelis, P., (2004) The Pseudomonas siderophore quinolobactin is synthesized from xanthurenic acid, an intermediate of the kynurenine pathway, *Mol. Microbiol. 52*, 371–374.

14. Hershko, A. Ciechanover, A. (1998) The ubiquitin system, *Ann. Rev. Biochem. 67*, 425–479.

15. Mueller, E. G. (2006) Trafficking in persulfides: delivering sulfur in biosynthetic pathways, *Nat. Chem. Biol. 2*, 185–194.

16. Lehmann, C., Begley, T. P., Ealick, S. E. (2006) Structure of the *Escherichia coli* ThiS–ThiF complex, a key component of the sulfur transfer system in thiamin biosynthesis, *Biochemistry 45*, 11–19.

17. Yao, T., Cohen, R. E. (2002) A cryptic protease couples deubiquitination and degradation by the proteasome, *Nature 419*, 403–407.

18. Bradford, M. M. (1976) A rapid and sensitive method for quantitation of microgram quantities of protein utilizing the principle of protein dye binding, *Anal. Biochem. 131*, 248–254.

19. Cook, P. F., Hara, S., Nalabolu, S. R., and Schnackerz, K. D. (1992) pH Dependence of the absorbance and phosphorus-31 NMR spectra of *O*-acetylserine sulfhydrylase in the absence and presence of *O*-acetyl-L-serine, *Biochemistry 31*, 2298–2303.

20. Kinsland, C. L., Taylor, S. V., Kelleher, N. L., McLafferty, F. W., and Begley, T. P. (1998) Overexpression of recombinant proteins with a *C*-terminal thiocarboxylate: Implications for protein semisynthesis and thiamin biosynthesis, *Protein Science 7*, 1839–1842.

21. Ostrowski, J., Kredich, N. M. (1989) Molecular characterization of the *cysJIH* promoters of *Salmonella typhimurium* and *Escherichia coli*: Regulation by *cysB* protein and *N*-acetyl-L-serine, *J. Bacteriol. 171*(1), 130–140.

22. Woehl, E. U., Tai, C.–H., Dunn, M. F., Cook, P. F. (1996) Formation of the α-aminoacrylate intermediate limits the overall reaction catalyzed by *O*-acetylserine sulfhydrylase, *Biochemistry 35*, 4776–4783.

23. Dorrestein, P. C., Zhai, H., McLafferty, F. W., Begley, T. P. (2004) The biosynthesis of the thiazole phosphate moiety of thiamin: the sulfur transfer mediated by the sulfur carrier protein ThiS, *Chem. Biol. 11*, 1373–1381.

24. Chattopadhyay, A., Meier, M., Ivaninskii, S., Burkhard, P., Speroni, F., Campanini, B., Bettati, S., Mozzarelli, A., Rabeh, W., Li, L., Cook, P. F. (2007) Structure, mechanism, and conformational dynamics of *O*-acetylserine sulfhydrylase from *Salmonella typhimurium*: comparison of A and B isozymes, *Biochemistry*, *46*, 8315–8330.

25. (a) Ho, C.-L.; Noji, M.; Saito, K. (1999) Plastidic pathway of serine biosynthesis. Molecular cloning and expression of 3-phosphoserine phosphatase from *Arabidopsis thaliana*, *J. Biol. Chem. 274*(16), 11007–11012; (b) Singh, S. K.; Yang, K.; Karthikeyan, S.; Huynh, T.; Zhang, X.; Phillips, M. A.; Zhang, H. (2004) The *thrH* gene product of *Pseudomonas aeruginosa* is a dual activity enzyme with a novel phosphoserine:homoserine phosphotransferase avtivity, *J. Biol. Chem. 279*(13), 13166–13173.

26. Kredich, N. M.; Becker, M. A. (1971) Cysteine biosynthesis: serine transacetylase and *O*-acetylserine sulfhydrylase (*Salmonella typhimurium*), *Methods Enzym. 17*(B), 459–470.

27. Flint, D. H., Tuminello, J. F., Miller, T. J. (1996) Studies on the synthesis of the Fe-S cluster of dihydroxyacid dehydratase in *Escherichia coli* crude extract, *J. Biol. Chem.*, *271*, 16053–16067.

28. Nakamura, T., Iwahashi, H., Eguchi, Y. (1984) Enzymatic proof for the identity of the *S*-sulfocysteine synthase and cysteine synthase B of *Salmonella typhimurium*, *J. Bacteriol. 158*, 1122–1127.

29. Kaksonen, A. H.; Franzmann, P. D.; Puhakka, J. A. (2004) Effects of hydraulic retention time and sulfide toxicity on ethanol and acetate oxidation in sulfate-reducing metal-precipitating fluidized-bed reactor, *Biotechnol. Bioeng. 86*(3), 332–343.

30. Rabeh, W. M., Alguindigue, S. S., Cook, P. F. (2005) Mechanism of the addition half of the *O*-acetylserine sulfhydrylase A reaction, *Biochemistry 44*, 5541–5550.

CHAPTER 2

Biochemical characterization of the HpxO enzyme from *Klebsiella pneumoniae*, a novel FAD–dependent urate oxidase.[1]

2.1. Introduction

Catabolism of purine nucleobases is an important mechanism for nitrogen assimilation by many organisms when their growth is limited by the availability of ammonia or alternative nitrogen sources (*1*, *2*). The bases are converted to hypoxanthine **2.1** or xanthine **2.2**, then oxidized to uric acid **2.3** (Figure 2.1). The steps to this point are ubiquitous in Nature but humans, amongst other organisms, lack the ability to metabolize urate to allantoin **2.6** (*3*). In contrast, the pathway from urate, in a variety of microbes and plants, has been intensively studied and proceeds under aerobic conditions in three steps from urate to allantoin **2.6**. The first step is the hydroxylation of urate, catalyzed by urate oxidase (*1*, *4*, *5*). In all previously-studied cases, the catalytic mechanism of urate oxidase is remarkable in that it does not require a cofactor (*6*). Detailed studies have implicated the electron-rich urate dianion as an enzyme-bound intermediate which can react spontaneously with molecular oxygen in its triplet ground state, forming a peroxide intermediate. Analogy has thus been made between urate and the isoalloxazine moiety of flavins which in its reduced form undergoes a similar oxidation.

---

[1]Reproduced with permission from O'Leary, S. E., Hicks, K. A., Ealick, S. E., Begley, T. P. (2009) Biochemical characterization of the HpxO enzyme from *Klebsiella pneumoniae*, a novel FAD-dependent urate oxidase, *Biochemistry 48*, 3033–3035. Copyright 2009, American Chemical Society.

In extension of the analogy, EPR spin trapping experiments have suggested the presence of transient radical intermediates in the steps leading to the urate hydroperoxide intermediate (*7*).

The urate oxidase product, 5-HIU **2.4**, is unstable in aqueous buffer, hydrolyzing spontaneously to 2-oxo-4-hydroxy-4-carboxy-5-ureidoimidazoline (OHCU) **2.5** (*8*). Notwithstanding the operation of this spontaneous reaction under physiological conditions, all known organisms which express the cofactorless urate oxidase also

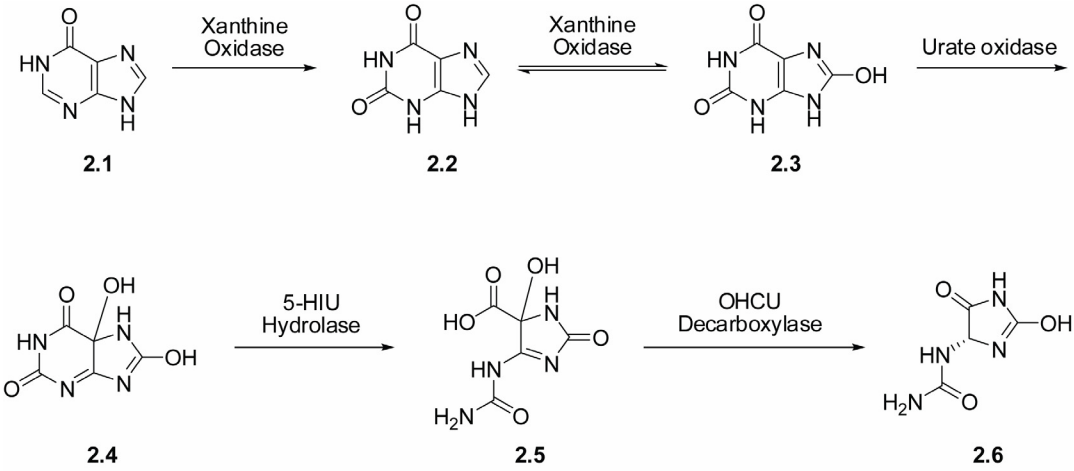

Figure 2.1. Purine catabolic pathway from hypxanthine to allantoin.

possess a hydrolase enzyme which accelerates the conversion of **2.4** to **2.5**. The decarboxylation of OHCU **2.5** to allantoin **2.6** is also spontaneous under physiological conditions, but nonenzymatically produces racemic allantoin (*3*). A stereospecific decarboxylating enzyme, which produces only (*S*)-allantoin, is found in organisms with urate oxidase and 5-HIU hydrolase (*9*, *10*); some organisms also possess a racemase enzyme (*1*, *11*). Allantoin can be futher catabolized to ammonia and carbon dioxide, thus utilizing the remaining nitrogen atoms in the imidazoline ring (*1*,*12*).

While the enzymology of the pathway outlined above has been thoroughly investigated, two very recent reports (*13*, *14*) have suggested that the pathway from

hypoxanthine to allantoin, involving the same intermediates but different catalytic strategies for their interconversion, exists in the facultative anaerobe *Klebsiella pneumoniae*, a ubiquitous human pathogen (*15*, *16*). In particular, the enzyme proposed to catalyze the conversion of urate to 5-hydroxyisourate **2.4** shows sequence similarity to FAD-dependent monooxygenases catalyzing the hydroxylation of aromatic compounds. It was noted that the enzyme sequence includes residues which are conserved across this group of enzymes that contain an FAD-binding domain and a small NADH-binding domain (Figure 2.2) (*17*). Both groups proposed that HpxO catalyzes the hydroxylation of urate by a mechanism similar to the well-studied *p*-hydroxybenzoate hydroxylase (*18*, *19*), and that HpxO is the first example of an FAD-dependent urate oxidase. However, de la Riva *et al*. also reported that in their study, cells with *hpxO,* expressed from a high-copy plasmid, lacked discernible urate oxidase activity (*14*).

2.2. Results and discussion.

2.2.1. HpxO is a flavoprotein.

To test the prediction that HpxO is an FAD-dependent urate oxidase, we cloned, heterologously overexpressed and purified the recombinant, *N*-terminally His_6-tagged protein, and then reconstituted its activity *in vitro*. The isolated protein was more than 95% pure, as determined by SDS-PAGE analysis (Figure 2.2A), with a molecular weight (including the *N*-terminal tag) of ~45 kDa. The HpxO protein solution, after gel filtration, was yellow, suggesting the presence of a tightly-bound cofactor. The UV-visible spectrum of the protein solution (Figure 2.2B) had maxima at 454, 381, 273 and <220 nm. Reverse-phase HPLC analysis of the small molecule released from the protein upon heat denaturation confirmed that the cofactor was FAD (Figure 2.2C, 2.2D). We determined the HpxO:FAD stoichiometry by measurement of the FAD-

derived absorbance in a solution of HpxO denatured by the addition of urea to a concentration of 6 M. The 450 nm absorbance (ε_{450} = 9.7 mM^{-1} cm^{-1}, Figure 2.3) was used to compute the FAD- derived 280 nm absorbance (A_{280}/A_{450} = 1.84), which in turn was subtracted from the total absorbance at 280 nm to give the protein absorbance at that wavelength. The protein absorbance was then used to determine its concentration based on the theoretical HpxO molar extinction coefficient (57.4 mM^{-1} cm^{-1}) at 280 nm (*20*). The FAD concentration and the protein concentration agreed to within 10%, and also agreed with the protein concentration determined by the Bradford method (*21*). Taken together, these results suggest that the FAD:HpxO stoichiometry is 1:1.

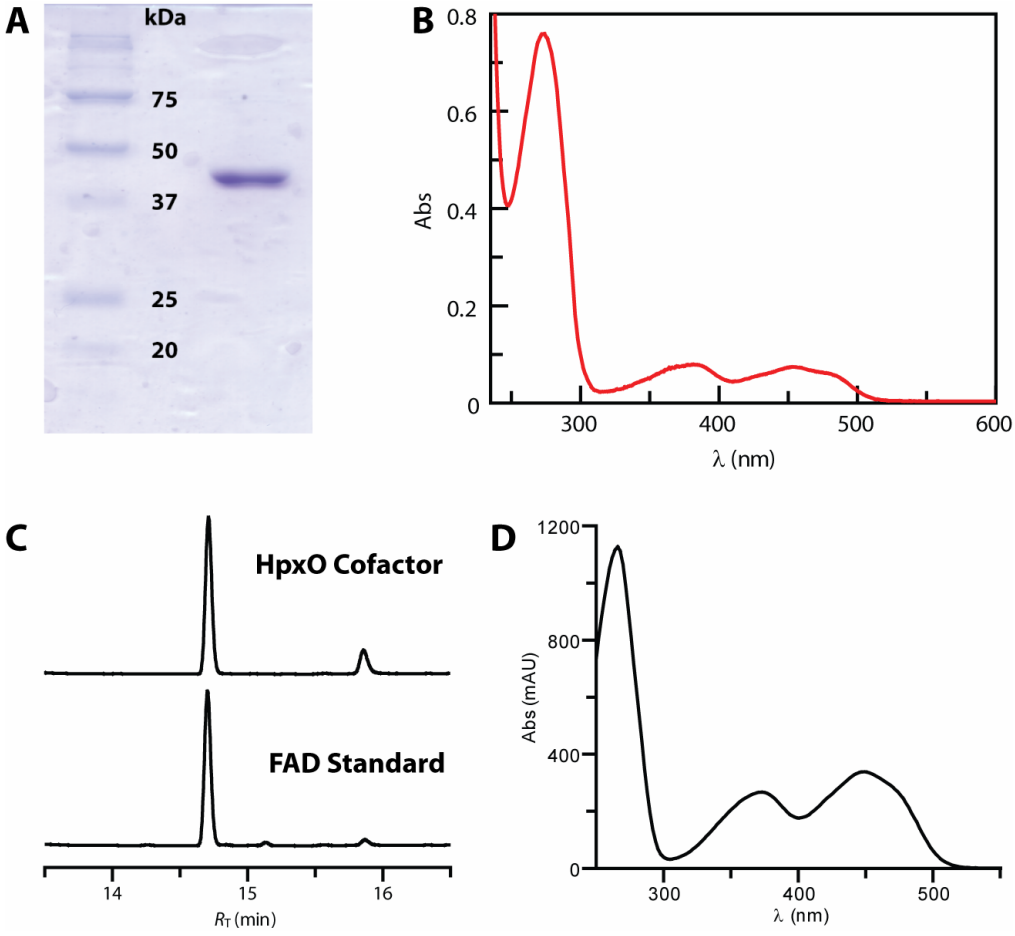

Figure 2.2. Isolation and cofactor content of recombinant *K. pneumoniae* HpxO.

2.2.2. Urate oxidase activity of HpxO.

Having demonstrated that HpxO is a flavoprotein, we investigated its catalytic activity towards uric acid. Treatment of uric acid with HpxO in the presence of NAD(P)H resulted in a decrease in the 340 nm absorbance, consistent with the oxidation of the NAD(P)H to $NAD(P)^+$. The rate of this decrease in A_{340} depended linearly on the enzyme concentration and could be saturated at high concentrations of urate or NADH. At saturating concentrations of NADH (1.5 mM, see below) the 385 nm

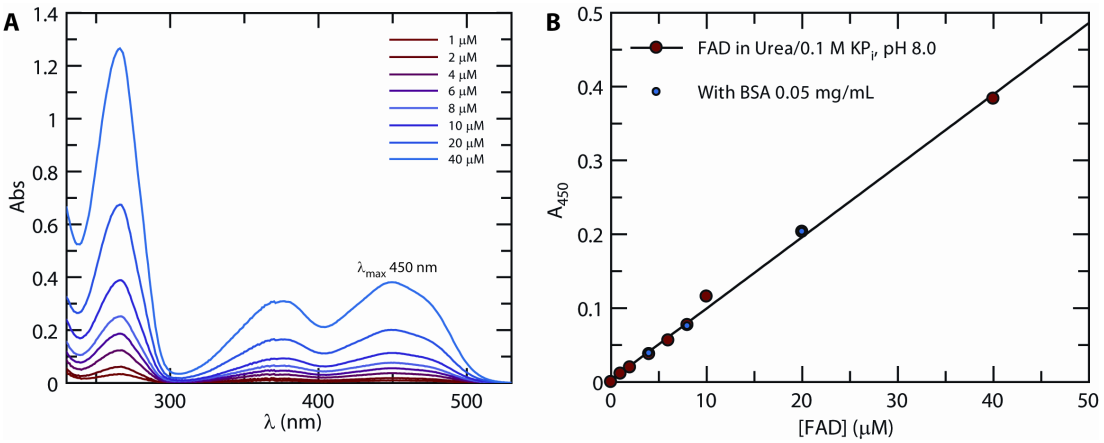

Figure 2.3. Determination of absorption characteristics of flavin adenine dinucleotide (FAD) under conditions used to produce denatured HpxO. A: UV-visbile spectra of standard solutions of FAD (1 − 40 μM) in 6 M urea buffered with 0.1 M potassium phosphate, pH 8.0; B: Beer-Lambert plot for the FAD absorbance at 450 nm. The blue circles indicate samples where BSA was added to a final concentration of 50 μg/mL to ensure that the presence of protein did not alter the observed absorbance. The linear fit gives ε_{450} = 9.7 mM^{-1} cm^{-1}. Additionally, the A_{280}/A_{450} ratio was 1.84.

absorbance was monitored (ε_{385} = 0.745 mM^{-1} cm^{-1}). When urate was omitted there was a detectable, enzyme-dependent rate of NAD(P)H oxidation, but this was not significant relative to the rates observed in the presence of urate. A fit of the kinetic

data when NADH was used as the nucleotide cosubstrate to the Michaelis–Menten equation gave values for K_m and k_{cat} of 42 ± 8 μM and 42 ± 2 s^{-1} (k_{cat}/K_m = 1.0 ± 0.2 μM^{-1} s^{-1}) for urate (Figure 2.4). Previous studies on the stability of the proposed HpxO product, 5-HIU **2.4**, have shown that it should react spontaneously under our assay conditions to form allantoin; full conversion should occur in ~1 h. HPLC analysis of samples of urate, incubated with HpxO for 1 h in the presence of NADPH followed by removal of the enzyme, confirmed the presence of allantoin and $NADP^+$ (Figure 2.5E). Assignment of the product as allantoin was confirmed by comparison with an authentic standard and also with the reaction products from a commercially available, FAD-independent urate oxidase (Figure 2.5D). Control experiments where urate was omitted confirmed that HpxO can catalyze the slow conversion of NADPH to $NADP^+$ in the absence of urate (Figure 2.5A-2.5C). These results suggest 5-HIU **2.4** to be the immediate product of the HpxO-catalyzed reaction. This proposal is further supported by the presence of genes in the *hpx* cluster which are proposed to encode 5-HIU hydrolase and OHCU decarboxylase.

Analysis of the time course of the HpxO catalyzed reaction from uric acid to allantoin by UV–visible spectrophotometry also indicated that 5-HIU and OHCU accumulated and decayed on the expected time scales (Figure 2.6).

2.2.3. Selectivity for NADH as the reduced nicotinamide substrate.

HpxO shows selectivity (*V*/*K* ratio of ~10) for NADH over NADPH. The HpxO steady-state rate showed no saturation at concentrations of NADPH up to 1 mM, suggesting this value as a lower limit for $K_{m,NADPH}$. A linear fit to the rate-concentration data gave an estimate of 9.7 ± 0.3 mM^{-1} s^{-1} for the k_{cat}/K_m value (Figure 2.7A). In contrast the steady-state rate showed saturation at NADH concentrations

above 0.5 mM, and a hyperbolic fit to this data gave 125 ± 30 mM^{-1} s^{-1} as an estimate of $k_{cat,NADH}/K_{m,NADH}$, (Figure 2.7B).

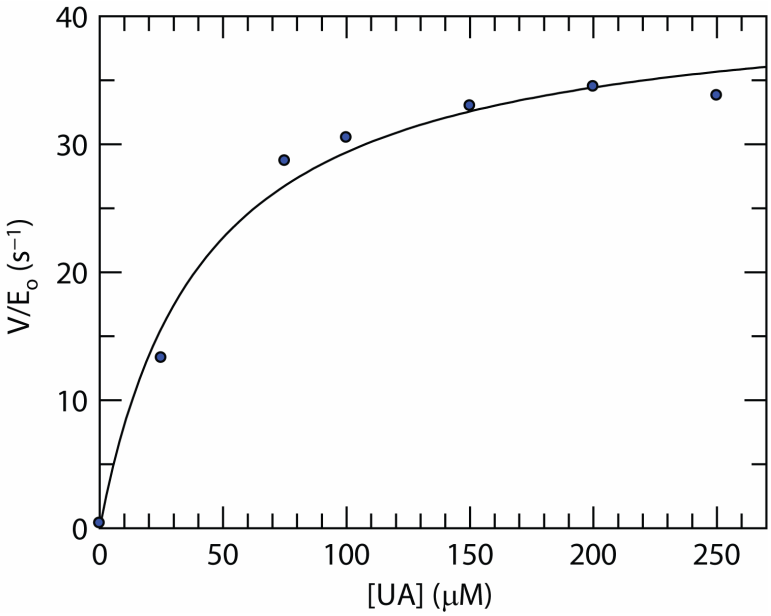

Figure 2.4. Steady-state kinetics of urate (UA) hydroxylation catalyzed by HpxO. All stocks were prepared in 0.1 M potassium phosphate, pH 8.0. Concentrations are final in a volume of 0.4 mL. Enzyme (40 μL, 40 nM) was pre-mixed with uric acid (0 – 50 μL, 0 – 250 μM) and buffer was added to a total volume of 340 μL. The reaction was initiated by addition of NADH (60μL, 1.5 mM), then the sample was manually mixed and the 385 nm absorbance was monitored as a function of time. The rates of NADH oxidation at the various concentrations of UA were determined by linear fits to the absorbance-time data, and these rates were fit to the Michaelis-Menten equation. The hyperbolic fit gives k_{cat} = 42 ± 2 s^{-1} and K_m = 42 ± 8 μM.

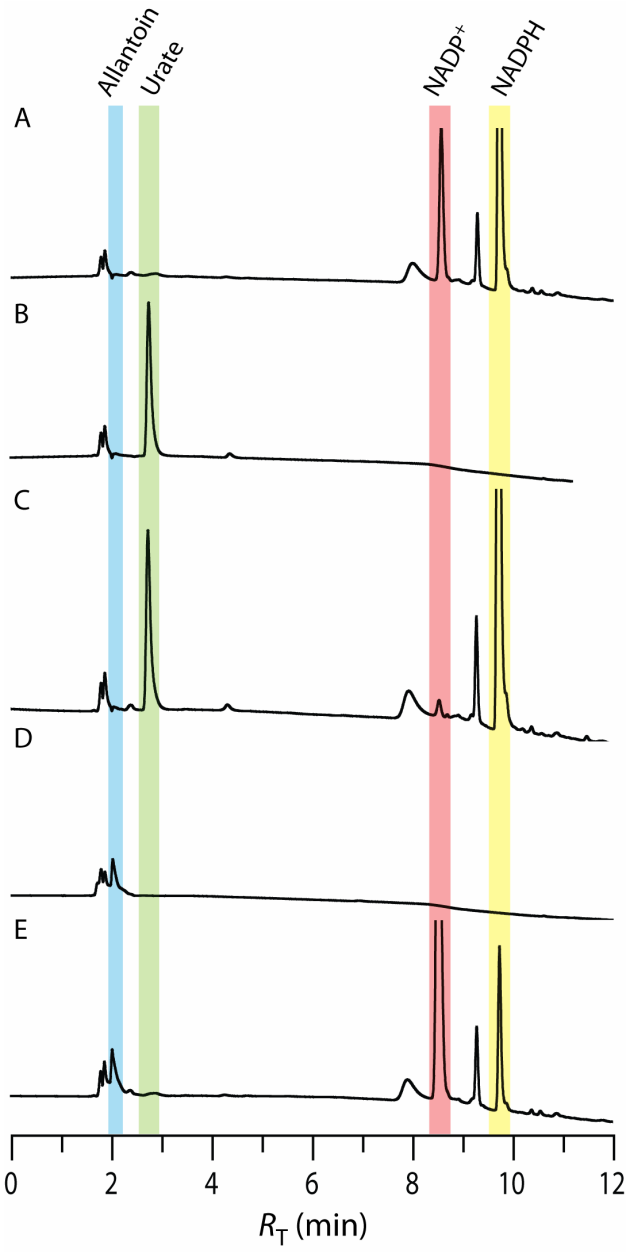

Figure 2.5. HPLC analysis of HpxO-catalyzed oxidation of uric acid in the presence of NADPH.

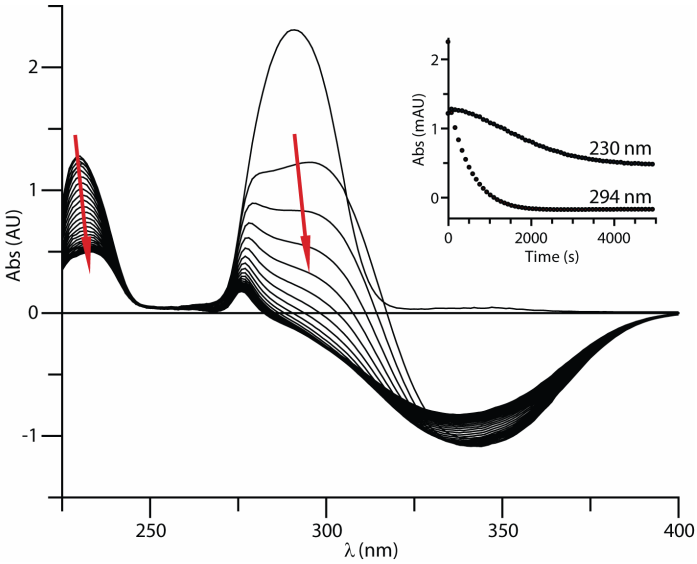

Figure 2.6. Time course of HpxO-catalyzed reaction of urate monitored by UV-visible spectrophotometry. Both the sample and reference cell contained NADH (0.2 mM) and HpxO (0.5 μM). The reaction mixture additionally contained 0.2 mM uric acid (λ_{max} = 290 nm, 230 nm). The traces shown were recorded before the addition of HpxO (uppermost trace) and then at 15 s, 100 s and (100 + 170n) s after addition of enzyme, where $1 \leq n \leq 29$. The spectra show initial rapid conversion of uric acid to a species with an absorbance maximum around 300 nm (reported for HIU, 302 nm, ref. 5), followed by the conversion of this species ($\tau_{½}$ ~ 500 s) to an intermediate with maximal absorbance at ~230 nm (reported for OHCU, < 240 nm). This intermediate then reacts further ($\tau_{½}$ ~ 500 s) with an associated decrease in the 230 nm absorbance. The absorption characteristics of the intermediates and the rates of their interconversion are consistent, based on previous studies, with the 5-HIU → OHCU → allantoin model proposed for decomposition of the 5-HIU HpxO reaction product. Inset: Single-wavelength time courses at 294 nm (with absorbance contributed by uric acid, 5-HIU and NADH) and 230 nm (uric acid, 5-HIU and OHCU). The small band centered around 276 nm is due to HpxO.

2.2.4. Formation of the **HpxO** *dihydroflavin intermediate under anoxic conditions.*

We also sought to demonstrate the formation of the dihydroflavin intermediate **2.8** by the reaction of NADPH with HpxO under anaerobic conditions. HpxO was incubated in the presence of glucose, glucose oxidase and catalase for 15 minutes in a sealed spectrophotometer cuvette prior to the introduction of an excess of NADPH. The absorbance spectrum in the 400-550 nm region was recorded after a further incubation of 10 minutes to allow for consumption of residual oxygen. The spectrum (Figure 2.8) showed complete removal of the 454 nm-centered absorbance, consistent with the formation of dihydro-FAD **2.8**. Considered along with the evidence that molecular oxygen is a substrate and the precedent available from previously well-studied systems, this result suggests that the mechanism presented in Figure 2.9 is in operation during the HpxO catalytic cycle.

***2.2.5. Estimation of k_{cat}/K_m* for molecular oxygen.** We estimated the K_m for molecular oxygen for the HpxO reaction to be no more than 0.05 mM, yielding a value of k_{cat}/K_m of at least ~0.7 μM^{-1} s^{-1} (Figure 2.10). This value is at least one order of magnitude greater than the equivalent value for the cofactor-independent urate oxidase (0.034 μM^{-1} s^{-1}). This suggests that the enzyme activity may have evolved to allow efficient flux through the purine catabolic pathway when the organisms are living in conditions where oxygen is not abundant.

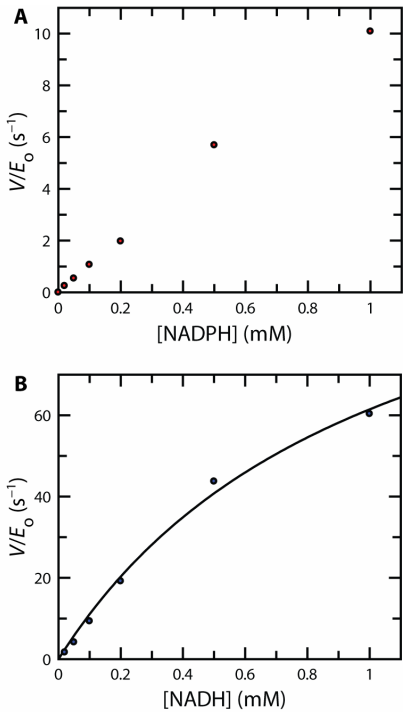

Figure 2.7. Dependence of HpxO steady-state rate on concentrations of NADPH and NADH. (A) Dependence on NADPH concentration. Enzyme (0.25 μM) was pre-mixed with urate (0.5 mM). The appropriate volume of NADPH solution was then added from a 10 mM stock to initiate the reaction after addition of buffer (0.1 M potassium phosphate, pH 8.0) to produce a total volume of 0.5 mL The rates of NADPH oxidation were measured by monitoring the absorbance at 340 nm (0 – 0.2 mM NADPH) or at 385 nm (>0.2 mM NADPH), using ε_{340} = 6.22 mM^{-1} cm^{-1} and ε_{385} = 0.745 mM^{-1} cm^{-1}. A linear fit to the low-concentration data ($\leq$ 200 μM) gives 9.7 ± 0.3 mM^{-1} s^{-1}; (B) Dependence on NADH concentration. Conditions were as for NADPH, with the exception that the enzyme concentration was 25 nM. The hyperbolic fit estimates k_{cat}/K_m = 125 ± 30 mM^{-1} s^{-1}.

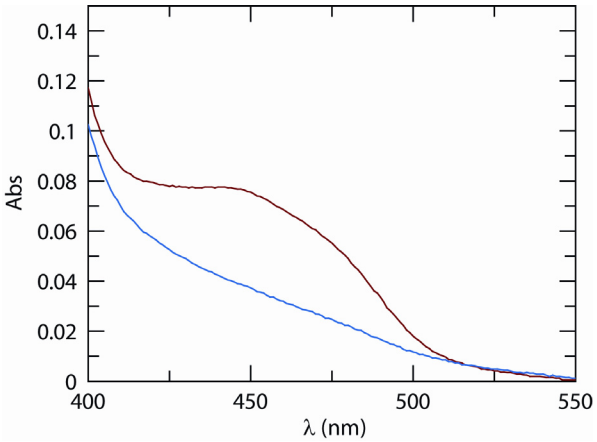

Figure 2.8. Reaction of HpxO-bound FAD with NADPH under anaerobic conditions. NADPH (final concentration 0.50 mM) was added to a solution, in a sealed quartz spectrophotometer cuvette, containing HpxO (6 μM), glucose (initial concentration 10 mM), glucose oxidase (10 units) and catalase (12.5 units), in 0.1 M potassium phosphate, pH 8.0. The red trace shows the 400 – 550 nm spectrum recorded immediately after the addition of the NADPH. The blue trace shows the spectrum of the same sample recorded after incubation for ~10 minutes.

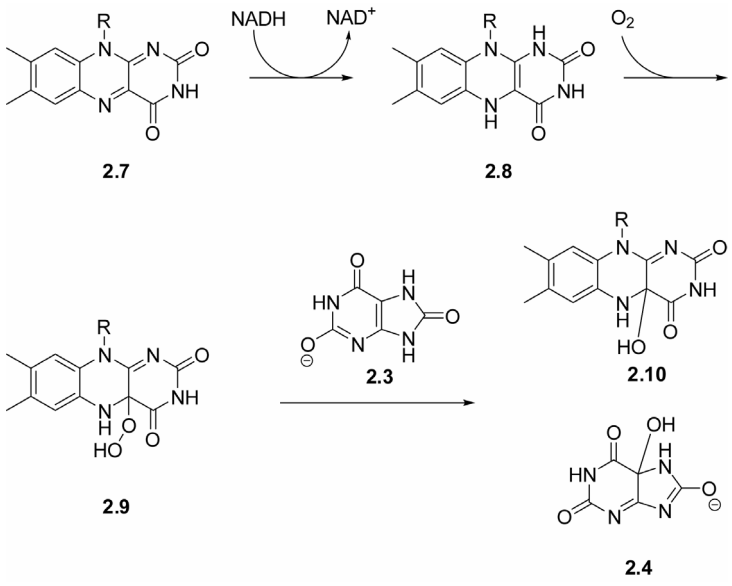

Figure 2.9. Proposed reaction mechanism for HpxO.

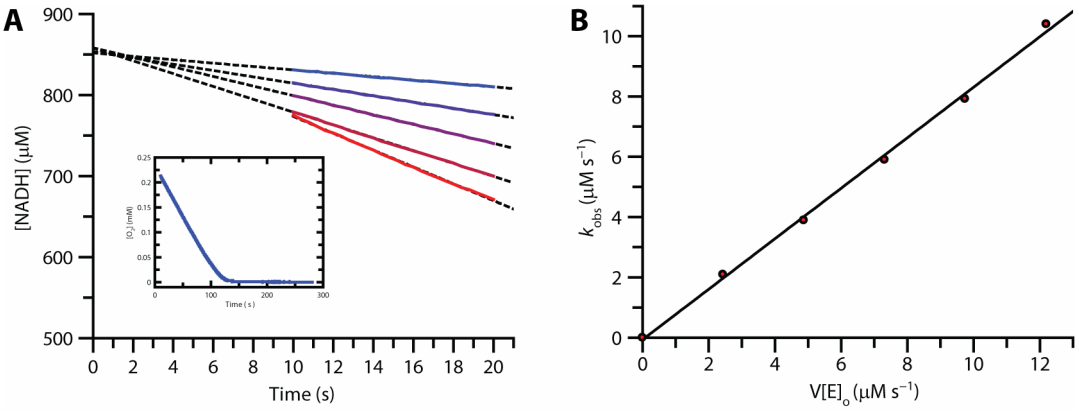

Figure 2.10. Estimation of K_m for molecular oxygen for the HpxO-catalyzed reaction of urate. HpxO (0.012 – 0.06 mM) was added to solutions of uric acid (0.5 mM) and NADH (1 mM) in 0.1 M potassium phosphate buffer, pH 8.0. (A) The absorbance at 385 nm was monitored until it had reached equilibrium on the time scale of the experiment (<600 s), corresponding to almost complete deoxygenation of the buffer by the urate oxidase reaction. Inset: Full time course (58 nM HpxO) showing saturation of the steady-state rate at $[O_2] \geq 0.05$ mM. A slow depletion of NADH on longer time scales reported on the rate of diffusion of oxygen into the buffer and spontaneous oxidation of the NADH. Interpolation of the linear time course data to the point of addition of the enzyme (t = 0 s) yielded the initial oxygen concentration from the difference in NADH concentrations (240 ± 6 μM, averaged over four enzyme concentrations) between the t = 0 and equilibrium concentrations. (B) A plot of the observed initial rate (from a linear fit to the A_{385} data at short times) as a function of $k_{cat}[E]_o$ has slope $[S]_o/(K_m + [S]_o)$, where $[E]_o$ is the HpxO concentration, k_{cat} is the turnover number (42 ± 2 s^{-1}), $[S]_o$ is the initial substrate concentration and K_m is the Michaelis constant. The slope q of the resulting linear plot allows estimation of $K_m = ([S]_o - q[S]_o)/q$.

2.3. Experimental.

2.3.1. Protein overexpression and purification

The plasmid coding the His_6-TEV-HpxO polypeptide was transformed into competent *Escherichia coli* BL21(DE3) using the heat-shock method. Briefly, 100 μL of competent cells were added to 2 μL of DNA in a sterile microcentrifuge tube. The mixture was incubated on ice for 30 minutes, then heat-shocked at 37 °C for two minutes. After incubation at room temperature for 10 minutes, 1 mL of sterile Luria-Bertani (LB) broth was added and the mixture was incubated at 37 °C for 75 minutes. After this incubation, the culture was centrifuged for five minutes at 8,000 × *g* and 1 mL of the supernatant was removed. The pellet was resuspended in the remaining 0.1 mL and this was plated out onto LB agar containing 40 mg/L kanamycin sulfate. The plate was incubated at 37 °C overnight. For overexpression of the protein, an overnight 37 °C starter culture in 10 mL LB broth (from a single colony of the transformants) was inoculated into 1 L of LB and grown at 37 °C until the optical density at 600 nm was 0.6. Protein overexpression was then induced by addition of isopropyl β-thiogalactopyranoside (1 mM). Induction was allowed to proceed at 37 °C for 6 h. The cells were then harvested by centrifugation and stored at −80 °C.

Purification was effected by Ni^{2+}-nitrilotriacetic acid (Ni-NTA) chromatography. The cell pellet from overexpression was resuspended in approximately 30 mL of lysis buffer (0.05 M NaH_2PO_4, 0.3 M NaCl and 10 mM imidazole, pH 8.0). Approximately 5 mg of FAD were added to the suspension at this time, along with approximately 10 mg of lysozyme. The cells were lysed by sonication (five cycles of 30 s duration during which 1.5 s sonicator pulses at medium power were followed by 1.5 s pauses) whilst the temperature was maintained at <10 °C. The resulting suspension was centrifuged (17,000 rpm, 25 minutes) and the supernatant was filtered through a sterile syringe filter (pore size 0.22 μm). The filtrate was then loaded onto the pre-charged

Ni-NTA resin (His•Bind, Novagen; bed volume 4.0 mL). The chromatography was carried out at room temperature but all buffers were kept at 4 °C on ice. The loaded resin was washed with 10 column volumes of lysis buffer and then with 15 column volumes of a buffer composed of 0.05 M NaH_2PO_4, 0.3 M NaCl and 20 mM imidazole, pH 8.0. The yellow protein was then eluted using a buffer composed of 0.05 M NaH_2PO_4, 0.3 M NaCl and 250 mM imidazole, pH 8.0. Yellow fractions were pooled (total volume ~6 mL) and buffer exchanged into 0.1 M potassium phosphate, pH 8.0 (10-DG desalting column, BioRad, Hercules, CA).

For long term storage (more than 3 days), 0.1 mL aliquots composed of 0.05 mL protein solution and 0.05 mL 80% glycerol were frozen in dry ice and stored at −80 °C.

2.3.2. Determination of ε_{450} for FAD in 6 M urea buffered with 0.1 M potassium phosphate, pH 8.0.

All buffered urea solutions were freshly prepared. Solid urea was dissolved to a final concentration of 6 M in 0.1 M potassium phosphate, pH 8.0. Serial dilutions from a 0.1 M FAD stock in the buffered urea solution were used for determination of the FAD absorbance spectra. Under these conditions the long-wavelength absorbance maximum was found at 450 nm. A Beer-Lambert plot of the absorbance-concentration data gave a value for ε_{450} of 9.7 mM^{-1} cm^{-1}. As a control for the effects of protein on the absorbance, BSA was added in a separate experiment to some of the samples, to a final concentration of 50 μg/mL. The presence of the BSA did not affect the absorbance at 450 nm. At all concentrations of FAD the A_{280}/A_{450} ratio was 1.84.

2.3.3. Computation of recombinant HpxO ε_{280} from the His$_6$-TEV-HpxO primary sequence.

The amino acid sequence of the recombinant, *N*-terminally tagged HpxO is given below:

MGSDKIHHHHHHSSGENLYFQGHMKAIVIGAGIGGLSAAVALKQSGIDCDVYEAVKEIKPVGA
AISVWPNGVKCMAHLGMGDIMETFGGPLRRMAYRDFRSGENMTQFSLAPLIERTGSRPCPVSR
AELQREMLDYWGRDSVQFGKRVTRCEEDADGVTVWFTDGSSASGDLLIAADGSHSALRPWV
LGFTPQRRYAGYVNWNGLVEIDEALAPGDQWTTFVGEGKRVSLMPVSAGRFYFFFDVPLPAG
LAEDRDTLRADLSRYFAGWAPPVQKLIAALDPQTTNRIEIHDIEPFSRLVRGRVALLGDAGHST
TPDIGQGGCAAMEDAVVLGAVFRQTRDIAAALREYEAQRCDRVRDLVLKARKRCDITHGKD
MQLTEAWYQELREETGERIINGMCDTILSGPLG

Analysis of this sequence by the method of Pace *et al.* (*20*) gives an estimate of ε_{280} = 57.4 mM^{-1} cm^{-1} for the HpxO polypeptide. This was computed using the formula

$$\varepsilon_{280}\ (M^{-1}\ cm^{-1}) = 5500n_{Trp} + 1490n_{Tyr} + 125n_{Cystine}$$

where n_i is the total number of the i^{th} residue in the protein sequence. The potential contribution from cystine residues was omitted in the analysis.

2.3.4. Steady-state kinetics with urate.

All stock solutions were prepared in 0.1 M potassium phosphate, pH 8.0 ("buffer"). Concentrations are final after mixing of all sample components. The concentration of NAD(P)H stocks was standardized using a molar extinction coefficient at 340 nm of 6.22 mM^{-1} cm^{-1}. For measurement of the steady-state rate, HpxO (40 nM, 0.04 mL of

a 400 nM stock) was pre-incubated with uric acid (0 – 70 μL of a 2 mM stock) and buffer was added to a final volume of 0.34 mL. The reaction was then initiated by addition of NADH (1.5 mM, 0.06 mL of a 10 mM stock), followed by rapid manual mixing. The absorbance was then measured at 285 nm as a function of time after mixing. The rates of the linear decreases in NADH concentration (ε_{385} = 0.745 mM^{-1} cm^{-1}) at each of the urate concentrations were obtained by linear regression. These were then plotted as a function of the urate concentration and the resulting rate-concentration dependence was fit to the Michaelis-Menten equation in order to determine the k_{cat} (42 ± 2 s^{-1}) and K_m (42 ± 8 μM) values. The errors are errors to the hyperbolic fit.

2.3.5. Steady-state kinetics with NAD(P)H.

All stock solutions were prepared in 0.1 M potassium phosphate, pH 8.0 ("buffer"). Concentrations are final after mixing of all sample components. In the case of NADPH, enzyme (0.25 μM, 0.01 mL of a 0.0126 mM stock) was pre-mixed with urate (0.5 mM, 0.125 mL of a 2 mM stock). The appropriate volume of NADPH solution (0.02 – 1 mM, 0 –50 μL of a 10 mM stock) was added to initiate the reaction after addition of buffer to produce a final volume of 0.5 mL. The rates of NADPH oxidation were measured by monitoring the absorbance at 340 nm (0 – 0.2 mM NAD(P)H) or at 385 nm (>0.2 mM NAD(P)H), using ε_{340} = 6.22 mM^{-1} cm^{-1} and ε_{385} = 0.745 mM^{-1} cm^{-1}. The measured rate at 0.2 mM substrate did not change when monitored at these two different wavelengths. A linear fit to the low-concentration NADPH data (≤ 200 μM) gives an estimate of k_{cat}/K_m of 9.7 ± 0.3 mM^{-1} s^{-1}. Reaction conditions in the case of NADH were as described above for NADPH, with the exception that the enzyme concentration was 25 nM. The hyperbolic fit estimates k_{cat}/K_m = 125 ± 30 mM^{-1} s^{-1}.

2.3.6. Anaerobic reduction of HpxO with NADPH.

A solution was prepared in 0.1 M potassium phosphate buffer, pH 8.0, which contained HpxO (6 μM), glucose (initial concentration 10 mM), glucose oxidase (10 units) and catalase (12.5 units). This solution was placed in a quartz spectrophotometer cuvette which was sealed with parafilm. The solution was allowed to equilibrate for 15 minutes, in order to remove the majority of dissolved oxygen. After this period the 400 – 550 nm spectrum of the solution was recorded. Next, a syringe was used to introduce a solution of NADPH (final concentration 0.50 mM) through the parafilm layer into the sealed cuvette. The resulting mixture was allowed to equilibrate for 10 minutes, in order to allow consumption of the small amounts of oxygen introduced by addition of the NADPH and by the mixing of the sample after NADPH addition. During this equilibration period, the absorbance peak centered at 450 nm decreased steadily in intensity, and this decrease was accompanied by a decrease in the absorbance at 340 nm derived from the NADPH (data not shown). These decreases were interpreted as reporting on the consumption of NADPH and the residual oxygen in the sample by completion of one or more rounds of catalysis. Once the absorbance had equilibrated, the 400 – 550 nm spectrum was re-recorded.

2.3.7. HPLC analysis of HpxO reaction products.

All reactions were assayed by reverse-phase HPLC on an Agilent 1100 HPLC system equipped with a quaternary pump and a 1.0 mL sample loop. The system also had a diode array UV-Vis detector (190 – 640 nm) and a fluorescence detector. The stationary phase was a Supelcosil LC-18-T column (15 cm × 4.6 mm, 3 μm particles), maintained at room temperature (21 ± 1 °C). The LC eluent consisted of a gradient of methanol in 10 mM potassium phosphate buffer, pH 6.6. In the analytical method the percentages P and M of phosphate buffer and methanol (balance water) at time t

varied according to the following scheme: {*t*,*P*,*M*}: {0,100,0}, {4,90,0}, {9,60,15}, {14,10,65}, {16,100,0}, {21,100,0}.

REFERENCES

1 Vogels, G. D., van der Drift, C. (1976) Degradation of purines and pyrimidines by microorganisms, *Bacteriol. Rev. 40*, 403–468.

2. Brondino, C.; Romão, M. J.; Moura, I.; Moura, J. J. G. (2006) Molybdenum and tungsten enzymes: the xanthine oxidase family, *Curr. Opin. Chem. Biol. 10* 109–114.

3. Oda, M., Satta, Y., Takenaka, O., Takenaka, N. (2002) Loss of urate oxidase activity in hominoids and its evolutionary implications, *Mol. Biol. Evol. 19*, 640–653.

4. Kahn, K., Serfozo, P., Tipton, P. A. (1997) Identification of the true product of the urate oxidase reaction, *J. Am. Chem. Soc. 119*, 5435–5442.

5. Imhoff, R., Power, N. P., Borrok, M. J., Tipton, P. A. (2003) General base catalysis in the urate oxidase reaction: evidence for a novel Thr-Lys catalytic diad, *Biochemistry 42*, 4094–4100.

6. Kahn, K.; Tipton, P. A. (1997) Kinetic mechanism and cofactor content of soybean root nodule urate oxidase, *Biochemistry 36*, 4731–4738.

7. Busi, E., Terzuoli, L., Basosi, R., Porcelli, B., Marinello, E. (2004) EPR spin trapping of a radical intermediate in the urate oxidase reaction, *Nucleosides, Nucleotides Nucleic Acids 23*, 1131–1134.

8. Ramazzina, I., Folli, C., Secchi, A., Berni, R., Percudani, R. (2006) Completing the uric acid degradation pathway through phylogenetic comparison of whole genomes, *Nat. Chem. Biol. 2*, 144–148.

9. Kim, K., Park, J., Rhee, S. (2007) Structural and functional basis for (*S*)-allantoin formation in the ureide pathway, *J. Biol. Chem. 282*, 23457–23464.

10. Cendron, L., Berni, R., Folli, C., Ramazzina, I., Percudani, R., Zanotti, G. (2007) The structure of 2-oxo-4-hydroxy-4-carboxy-5-ureidoimidazoline decarboxylase provides insight into the mechanism of uric acid degradation, *J. Biol. Chem. 282*, 18182–18189.

11. van der Drift, L.; Vogels, G. D.; van der Drift, C. (1975) Allantoin racemase, a new enzyme from pseudomonas species, *Biochim. Biophys. Acta*, *391*, 240–248.

12. Mulrooney, S. B., Hausinger, R. P. (2003) Metal ion dependence of recombinant *Escherichia coli* allantoinase, *J. Bacteriol. 185*(1), 126–134.

13. Pope, S. D., Chen, L.–L., Stewart, V. (2009) Purine utilization by *Klebsiella oxytoca* M5aI: genes for ring-oxidzing and -opening enzymes, *J. Bacteriol. 191*, 1006–1017.

14 de la Riva, L., Badia, J., Aguilar, J., Bender, R. A., Baldoma, L. (2008) The *hpx* genetic system for hypoxanthine assimilation as a nitrogen source in *Klebsiella pneumoniae*: gene organization and transcriptional regulation, *J. Bacteriol. 190*(24), 7892–7903.

15. Podschun, R., Ullmann, U. (1998) *Klebsiella* spp. as nosocomial pathogens: epidemiology, taxonomy, typing methods, and pathogenicity factors. *Clin. Microbiol. Rev. 11*(4), 589–603.

16. Keynan, Y., Rubinstein, E. (2007) The changing face of *Klebsiella pneumoniae* infections in the community, *Int. J. Antimicrob. Agents 30*(5), 385–389.

17. Harayama, S., Kok, M., Neidle, E. L. (1992) Functional and evolutionary relationships among diverse oxygenases, *Annu. Rev. Microbiol. 46*, 565–601.

18. Ortiz-Maldonado, M., Entsch, B., Ballou, D. P. (2004) Oxygen reactions in *p*-hydroxybenzoate hydroxylase utilize the H-bond network during catalysis, *Biochemistry 43*, 15246–15257.

19. Entsch, B., vanBerkel, W. J. H. (1995) Structure and mechanism of para-hydroxybenzoate hydroxylase, *FASEB J. 9*, 476–483.

20. Pace, C. N., Vajdos, F., Fee, L., Grimsley, G., Gray, T. (1995) How to measure and predict the molar absorption coefficient of a protein, *Protein Sci. 4*, 2411–2423.

21. Bradford, M. M. (1976) A rapid and sensitive method for the quantitation of microgram quantities of protein utilizing the principle of protein-dye binding, *Anal. Biochem. 72*, 248–254.

CHAPTER 3

Insights into the catalytic mechanism of HpxO from X-ray crystallographic studies and steady-state kinetic analysis of active site mutants.

3.1. Introduction

Our initial studies (*1*) on HpxO confirmed its assignment as a flavin adenine dinucleotide (FAD)-dependent urate oxidase (Figure 3.1). The primary sequence of HpxO, even in the absence of the biochemical data, allowed the reasonable proposal of its cofactor requirement. This was due to sequence similarity between HpxO and a variety of enzymes which catalyze similar oxygenation reactions, the prototype of which is 4-hydroxybenzoate hydroxylase (PHBH) (*2*). Such enzymes are known to possess conserved domains (and corresponding amino acid sequences) for binding of FAD and the nicotinamide co-substrate.

However, this homology information and the initial biochemical characterization did not provide detailed information on the chemical and kinetic mechanisms of formation of 5-hydroxyisourate **3.2** at the HpxO active site, nor did they identify the residues important for catalysis of oxygen transfer to the HpxO-bound uric acid **3.1**. These residues vary between members of the FAD-dependent monooxygenase family, owing to the chemical diversity of the enzymes' substrates, which necessitates differing arrangement of amino acid side chains at the active site to facilitate binding, substrate activation, and oxygenation (*3*,*4*).

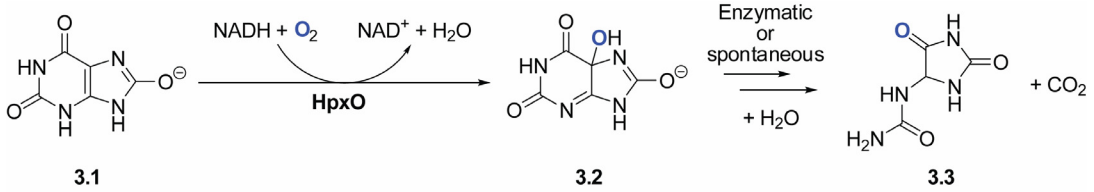

Figure 3.1. HpxO-catalyzed reaction of urate **3.1** and subsequent decomposition of HpxO-produced 5-hydroxyisourate **3.2** to allantoin **3.3**.

A further feature of members of this enzyme family is their ordered kinetic pathway, wherein binding of the substrate to be oxygenated triggers a conformational change in the protein that results in the movement of the FAD isoalloxazine ring to an "out" position where it is accessible for reduction by NAD(P)H (*5*). This "coupling" between substrate binding and flavin reduction has presumably evolved to prevent uncontrolled depletion of cellular NAD(P)H and the concomitant formation of hydrogen peroxide resulting from its abortive elimination from the flavin hydroperoxide intermediate in the absence of a bound oxygenation substrate. The coupling has been shown to be mediated through a complex network of amino acid residues and water molecules extending from the active site which is sensitive to the presence of substrate and can trigger the requisite conformational changes (*6*). Catalytically-relevant active site residues can thus be notionally grouped into two sets, consisting of amino acids important for the specificity and catalysis of the oxygen transfer reaction, and those important for maintaining the fidelity of the coupling between substrate binding and flavin reduction. Analysis of the structures of the HpxO protein in the absence and presence of uric acid could thus facilitate assignment of active site residues as members of one (or potentially both) of these sets. Kinetic studies on appropriately-chosen mutants of such residues can then confirm the assignment based on the structural data, providing an integrated picture on the HpxO catalytic mechanism. Here we report the results of these studies.

3.2. X-ray crystal structure of wild-type HpxO.

The X-ray crystal structure of the wild-type HpxO protein was solved by Katherine Hicks, Cornell University. This structure confirmed that HpxO co-purifies with FAD, and also that the FAD:HpxO stoichiometry is 1:1, as determined from the biochemical studies. The FAD was bound by the enzyme in a manner similar to related proteins

such as 4-hydroxybenzoate hydroxylase. The overall structural features of the protein are consistent with other members of the FAD-dependent monooxygenase family, which possess an *N*-terminal domain important for FAD and NAD(P)H binding, a central domain composed of a series of antiparallel β-sheets involved in substrate binding, often referred to as the "monooxygenase domain", and a *C*-terminal domain thought to be involved in dimerization of the protein in solution. The *C*-terminal domain exhibits variability in length and amino acid composition between members of the FAD-dependent monooxygenases.

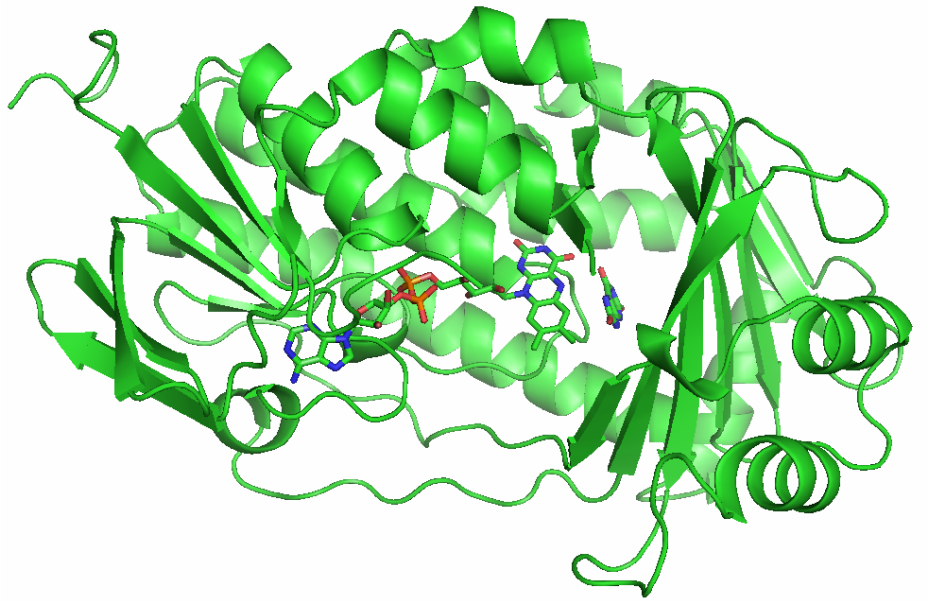

Figure 3.2. X-ray crystal structure of the HpxO-FAD-urate ternary complex.

3.3. X-ray crystal structure of the HpxO-FAD-urate ternary complex.

The X-ray crystal structure of the HpxO-FAD-urate ternary complex was also solved (Figure 3.2). This structure revealed uric acid bound at the HpxO active site (Figure 3.3) in close proximity to the isoalloxazine portion of the FAD. The urate interacts with a number of active site residues, principally involving hydrogen bonding interactions with the purine endocyclic nitrogen atoms and the exocyclic oxygen

atoms. A number of ordered water molecules were also observed in the active site. Several of these participate in a H-bond network which involves the urate molecule and the side chains of a number of polar active site residues. Individual interactions in this network are discussed in the context of the relevant active site residues, below. In 4-hydroxybenzoate hydroxylase, a hydrogen bond network extending from the active site to the protein surface has been shown to play a role in the conformational changes produced by substrate binding which allow movement of the FAD to its "out" position and its subsequent reduction by NAD(P)H.

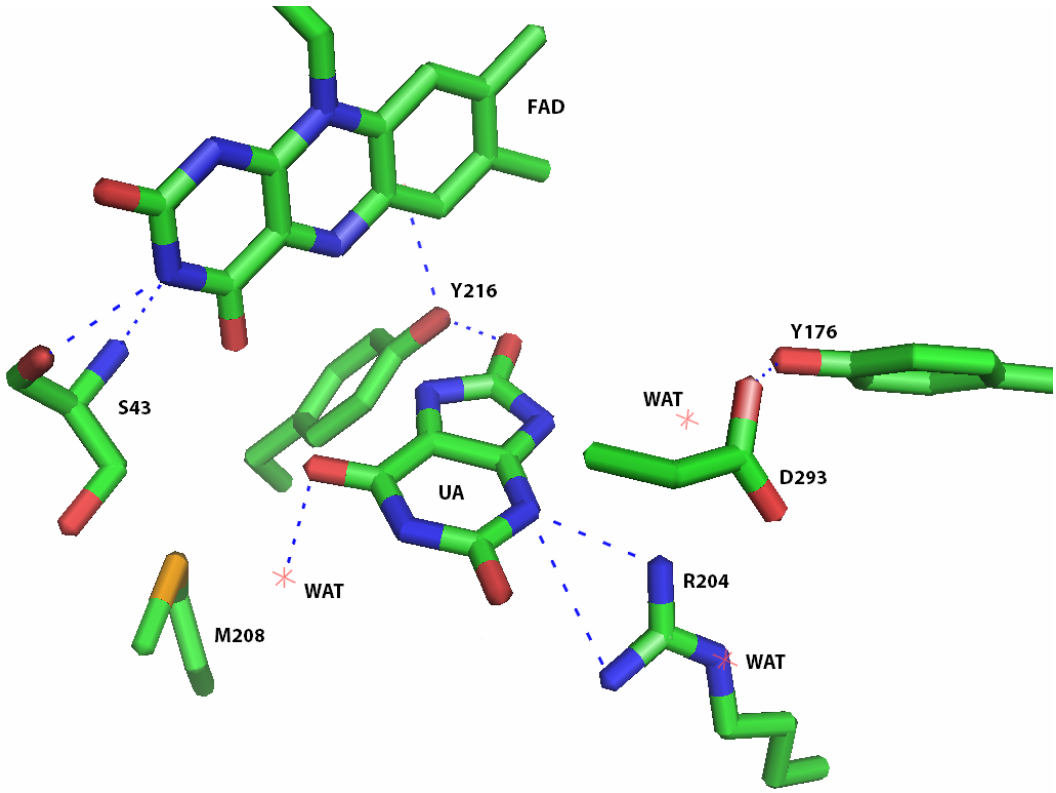

Figure 3.3. HpxO active site indicating positions of the FAD isoalloxazine ring, urate, and the residues mutated in the present study.

3.4. Choice of active site mutants for kinetic characterization.

Based on our inspection of the enzyme active site in the HpxO-FAD-urate complex, we selected seven residues which were likely to be important for catalysis, owing to either their direct interaction with, or proximity to, the uric acid molecule or the isoalloxazine portion of the FAD. The rationale for the choice of individual residues is discussed with the results, below. The kinetic data are summarized in Table 3.1.

3.5. HpxO R204K/Q mutants: activity and uncoupling.

The R204 residue is within hydrogen bonding distance (2.67 Å) of the uric acid N1 atom (Figure 3.4). It can thus serve as a general base to facilitate proton transfer from N1 of the urate molecule, which is likely to occur in concert with oxygenation of the urate C5 atom. Its positively charged side chain is also well-positioned to stabilize the negative charge which formally accumulates on the N1-C2-O2′ region of the urate during the oxygen transfer step. The residue may thus play a role in stabilization of the urate N1-C2-O2′ enol(ate) tautomer, both by hydrogen bonding and electrostatic interactions. We prepared the R204K and R204Q mutants of HpxO to investigate whether these interactions are important for catalysis.

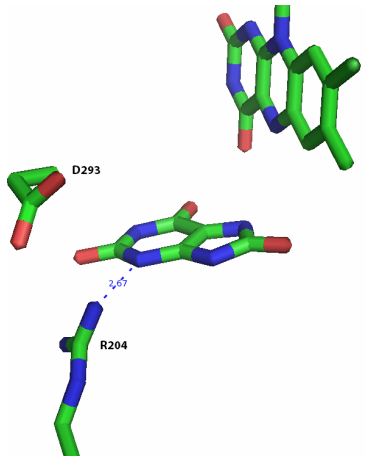

Figure 3.4. Location of HpxO R204 and D293 residues in the enzyme active site.

Table 3.1. Kinetic parameters for HpxO active site mutants. [a] V_{max}/E_o at 1 mM NADH; [b] V_{max}/E_o at 1.5 mM NADH; [c] $V_{max}/(E_o \times K_M)$ at 1 mM NADH; [d] $V_{max}/(E_o \times K_M)$ at 1 mM NADH; ND – not determined.

Protein	k_{cat} (s^{-1})	$K_{M,urate}$ (μM)	$K_{M,NADH}$ (μM)	$\sim k_{cat}/K_{M,urate}$ ($\mu M^{-1} s^{-1}$)	$\sim k_{cat}/K_{M,NADH}$ ($\mu M^{-1} s^{-1}$)
WT	42 ± 2	42 ± 8	~500	1.0 ± 0.2	0.125 ± 0.030
R204K	~0.05[a]	50 ± 20	ND	0.001[c]	ND
R204Q	0.26 ± 0.006	ND	640 ± 39	ND	$\sim 10^{-4}$
D293N	0.46 ± 0.02[b]	103 ± 19	293 ± 62	0.004[d]	0.001[d]
Y216F	8.4 ± 0.5	90 ± 20	100 ± 35	0.093	0.084
M208I	0.65 ± 0.05[a]	35 ± 7	>1,000	0.019[c]	$<6.5 \times 10^{-4}$ [c]
Y176F	~0.1[a]	ND	>1,000	ND	$<10^{-4}$ [c]
S43A	0.066 ± 0.002[a]	33 ± 5	920 ± 200	0.002[c]	$\sim 10^{-4}$

Both the R204K and R204Q mutants co-purified with sub-stoichiometric occupancy of FAD, The R204Q mutant could be reconstituted with the cofactor by a short incubation. The excess cofactor could then be removed by gel filtration. When the FAD-reconstituted proteins were treated with uric acid and NADH, the order of activity with respect to formation of allantoin **3.3** (Figure 3.5) was wt > R204K > R204Q (Table 3.1). This was consistent with the proposal that a cationic group in this region of the active site is important for catalysis.

However, these mutants showed a reversed trend with respect to their rates of NADH consumption. While wild-type HpxO tightly couples NADH and substrate oxidation, the R204K, and especially the R204Q mutants, showed elevated levels of uncoupling in this regard. Steady-state kinetic studies on HpxO R204Q indicated that the presence of uric acid in fact had little or no effect on the kinetics of oxidation of NADH (Figure 3.6). The K_M value for NADH was 0.64 ± 0.04 mM, close to the value for the wild-type enzyme in the presence of saturating concentrations of urate. The k_{cat} value was 0.26 s^{-1}, two orders of magnitude slower than the k_{cat} for urate consumption with wtHpxO. If the "uncoupling ratio" is defined as the ratio of the quantity of NADH oxidized to the quantity of allantoin formed in the enzymes' steady-state turnover, then this ratio is approximately one order of magnitude greater for HpxO R204K than for wild-type HpxO, and a further order of magnitude greater in the case of HpxO R204Q. This suggests that the R204 residue plays an important role in both the oxygen transfer step of the HpxO catalytic cycle and also in mediating the conformational change which translates substrate binding to flavin motion and reduction.

The R204 side chain potentially interacts with D293, in a salt bridge-type interaction. However, the electron density for these residues in the HpxO-FAD-urate ternary complex shows that the residues are not properly aligned to form the salt bridge. One

of the carboxyl oxygen atoms of D293 is located 3.51 Å away from the guanidinium group of R204, suggesting that these two residues could also be involved in a hydrogen bonding interaction.

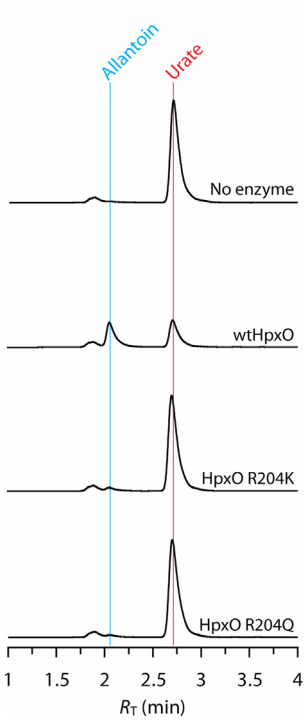

Figure 3.5. Reverse-phase HPLC analysis of HpxO R204Q/K conversion of urate to allantoin compared with wild-type enzyme. The enzymes (~1 μM) were incubated with urate (1 mM), NADH (5 mM) and FAD (0.1 mM) for 3 h at 25 °C. The protein was then removed by centrifugal ultrafiltration before analysis. Chromatograms were detected using the UV absorbance at 210 nm.

Thus the R204 residue may be notionally "bifunctional" in the case of the HpxO catalytic cycle, i.e., involved in gating the FAD "in" to "out" transition, and in a kinetic deprotonation of the urate required for oxygenation. An equivalent, charged residue is not observed in the structure of the 4-hydroxybenzoate hydroxylase active

site, where a complementary charged group with which it would interact is not present in the 4-hydroxybenzoate substrate.

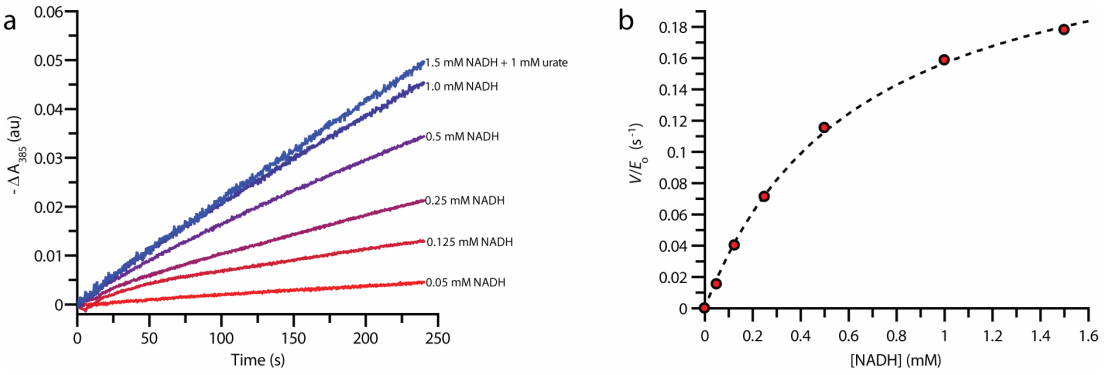

Figure 3.6. Steady-state oxidation of NADH catalyzed by HpxO R204Q. The enzyme (1.5 μM) was treated with NADH (0 – 1.5 mM) in 0.1 M potassium phosphate buffer, pH 8.0 at 25 ± 1 °C. The change in absorbance at 385 nm was recorded as a function of time after mixing. a) Time course data for the NADH oxidation. The linear phase was fit by linear regression to give the steady-state rate of NADH consumption at the varying concentrations of NADH. The presence of urate did not significantly affect the steady-state rate of urate consumption (top trace). b) Michaelis-Menten plot. The K_M for NADH was 0.64 ± 0.04 mM, k_{cat} was 0.26 ± 0.006 s^{-1}, with $k_{cat}/K_M \sim 10^{-5}$ μM^{-1} s^{-1},

Crystallographic studies are underway to determine the position of the FAD isoalloxazine ring in the HpxO R204Q-FAD-urate ternary complex, which the kinetic studies suggest may be largely in the "out" position.

3.6. HpxO D293N.

D293 potentially interacts with the R204 residue as discussed above (Figure 3.4), along with the side chain of Y176 (see section 3.9).

In the context of the results for the R204K/Q mutants, it could be proposed that D293 may be involved in modulation of the pK_a of the side chain of R204, in an interaction which would optimize proton transfer from the urate N1 atom accompanying oxygenation at C5. Additionally, D293 could be involved, along with R204, in the network of residues responsible for global conformational changes resulting in FAD reduction triggered by substrate binding.

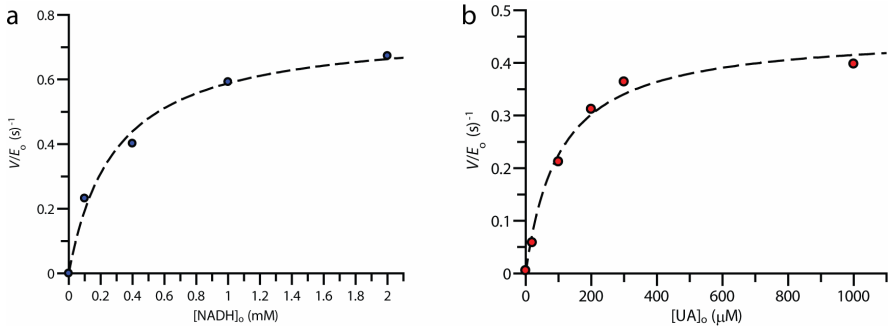

Figure 3.7. Michaelis-Menten steady-state kinetics of urate oxidation catalyzed by HpxO D293N. a) Dependence of steady-state rate on NADH concentration in the presence of 1 mM urate. The enzyme (0.6 μM) was treated with NADH (0 – 1.5 mM) in 0.1 M potassium phosphate buffer, pH 8.0 at 25 ± 1 °C. The change in absorbance at 385 nm was recorded as a function of time after mixing. The K_M for NADH was 293 ± 62 μM. b) Dependence of steady-state rate on urate concentration in the presence of 1.5 mM NADH under conditions otherwise identical to (a). The K_M for urate was 103 ± 19 μM. The k_{cat} value was 0.46 ± 0.02 s^{-1}

The D293N mutant showed impaired catalytic activity (Figure 3.7). The K_M for NADH was 293 ± 62 μM, approximately a two-fold decrease compared with the wild-

type enzyme. The K_M for urate was 103 ± 19 μM, an approximately two-fold increase over wtHpxO. The k_{cat}/K_M value for urate was ~0.007 μM^{-1} s^{-1}, ~10^3-fold less than for wtHpxO. Additionally, the FAD occupancy in the "as-isolated" protein was low, and this mutant could not be stably reconstituted with FAD as in the case of HpxO R204Q. However, the steady-state rate was insensitive to the presence of exogenous FAD in the 0 – 0.03 mM range (Figure 3.8).

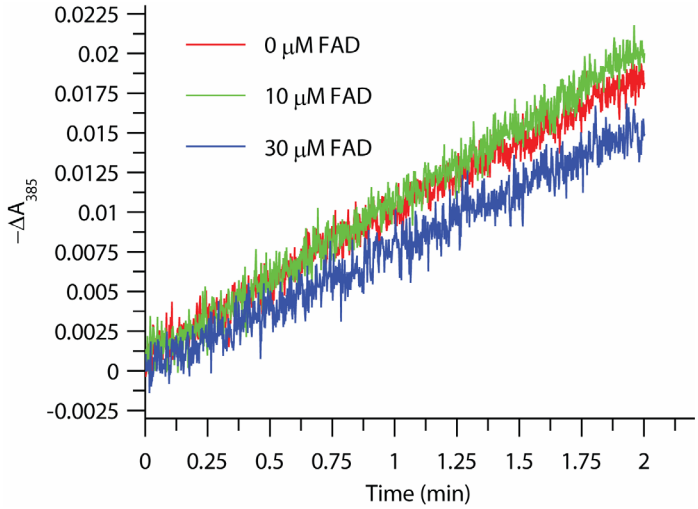

Figure 3.8. Changes in 385 nm absorbance due to oxidation of NADH by HpxO D293N in the presence of varying concentrations of FAD.

3.7. HpxO Y216F

The Y216 residue is appropriately positioned to hydrogen bond to the O8′ of the urate anion at the HpxO active site (2.76 Å), and also to an ordered water molecule which is the first in a chain of such molecules that extends outward from the active site to the protein surface (Figure 3.9).

The residue is located on one of the antiparallel β-sheets which form the "monooxygenase domain" of the protein. The amino acid residues in this domain are thought to be somewhat variable, in response to the necessity to bind different

substrates for oxygenation at the active site. The Y216 interaction with urate replaces the interaction of an arginine residue with the carboxylate group of 4-hydroxybenzoate in the PHBH structure.

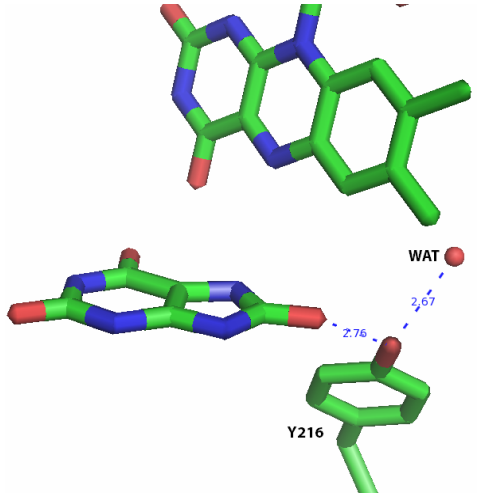

Figure 3.9. Position of Y216 residue at the HpxO active site.

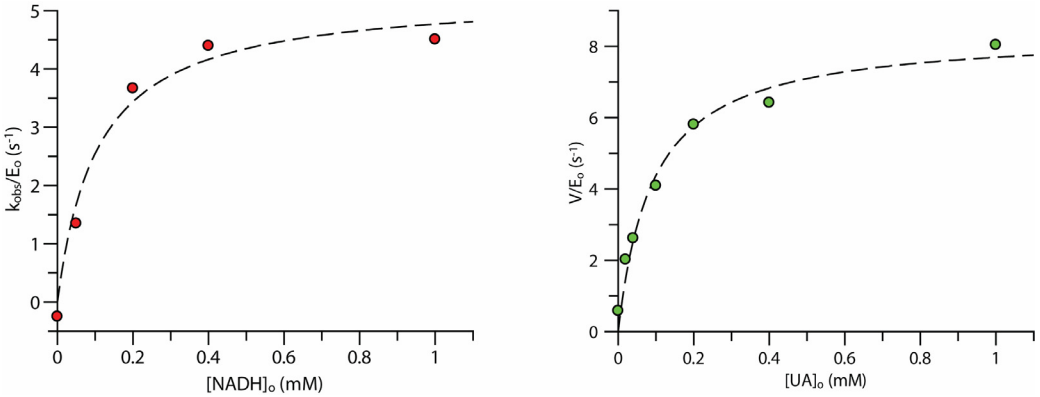

Figure 3.10. Steady-state kinetics of urate oxidation catalyzed by HpxO Y216F. Assays were carried out in 0.1 M potassium phosphate buffer, pH 8.0, in the presence of 0.01 mM FAD. The enzyme concentration was 140 nM. a) Dependence of steady-state rate on NADH concentration in the presence of 0.5 mM urate. The K_M for NADH was 0.100 ± 0.035 mM; b) Dependence of the steady-state rate on urate concentration in the presence of 0.5 mM NADH. The k_{cat} value for urate was 8.4 ± 0.5 s^{-1}. The K_M for urate was 90 ± 20 μM. These values give an estimate of k_{cat}/K_M of 0.093 μM^{-1} s^{-1}.

The HpxO Y216F mutant catalyzed the oxidation of urate and exhibited Michaelis-Menten kinetics (Figure 3.10). The k_{cat} was reduced by ~5-fold compared with the wild type enzyme. Interestingly, the K_M for NADH was 0.1 mM, about five times tighter than for wtHpxO. This suggests that this residue may be important for mediating the conformational changes involved in the flavin "in" to "out" transition during catalysis. The K_M value for urate was 0.09 mM, about two-fold higher than for wtHpxO. This is consistent with the prediction from the crystallographic study that Y216 is important for urate binding. The value of k_{cat}/K_M for urate was thus reduced by a factor of ~10 relative to wtHpxO, whereas that for NADH was essentially unchanged. The turnover rate for the Y216 mutant was enhanced by the addition of exogenous FAD (0.01 mM, Figure 3.11).

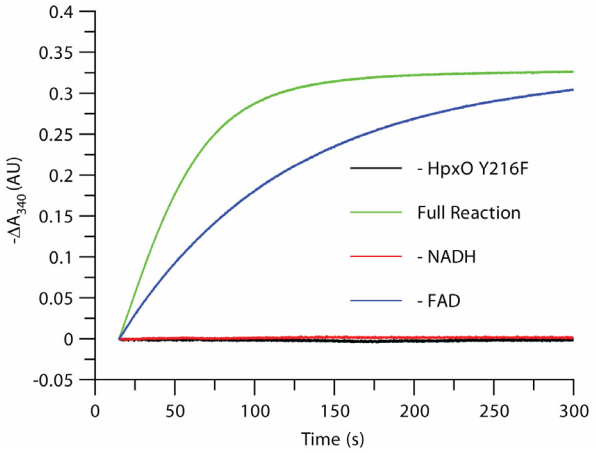

Figure 3.11. Time course of urate oxidation reactions catalyzed by HpxO Y216F. In the full reaction (green trace), the enzyme (250 nM) was incubated with urate (0.5 mM), NADH (0.1 mM) and FAD (0.01 mM) in 0.1 M potassium phosphate buffer, pH 8.0. The change in absorbance at 340 nm (decrease, plotted as $-\Delta A_{340}$) was plotted as a function of time after addition of the enzyme. The remaining traces correspond to controls where enzyme (black trace), NADH (red) or FAD (blue) were omitted. The full value of k_{cat} is not realized in the absence of exogenous FAD.

3.8. HpxO M208I.

This residue is more remote from the flavin and urate molecules than the other amino acids mutated in the present study (Figure 3.12). It is also located on the β-sheet region of the "monooxygenase domain", suggesting that it may have a role in substrate recognition or in mediating the conformational changes induced by substrate binding. The mutant showed impaired catalytic activity compared with wtHpxO. The most striking feature was change in the dependence of the steady-state rate on the NADH concentration (Figure 3.13). This dependence was linear up to 1 mM and could not be saturated even at 2 mM NADH, suggesting that the K_M value for NADH is > 1 mM. The enzyme still exhibited saturation kinetics with urate, with a V_{max}/E_o value of 0.65 ± 0.03 s^{-1} at 1 mM NADH, a reduction of two orders of magnitude over wtHpxO. However, the K_M value for urate was essentially unchanged, at 35 ± 7 μM.

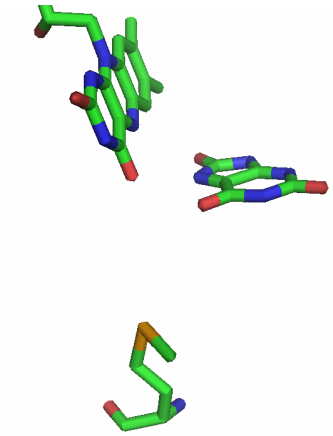

Figure 3.12. Position of the HpxO M208I residue.

These results implicate the M208I residue as being important for the conformational changes which result in flavin reduction during the catalytic cycle, and are consistent with the observations made for related FAD-dependent monooxygenases that residues remote from the active site participate in a network of amino acid side chains which facilitates global conformational changes of relevance to catalysis.

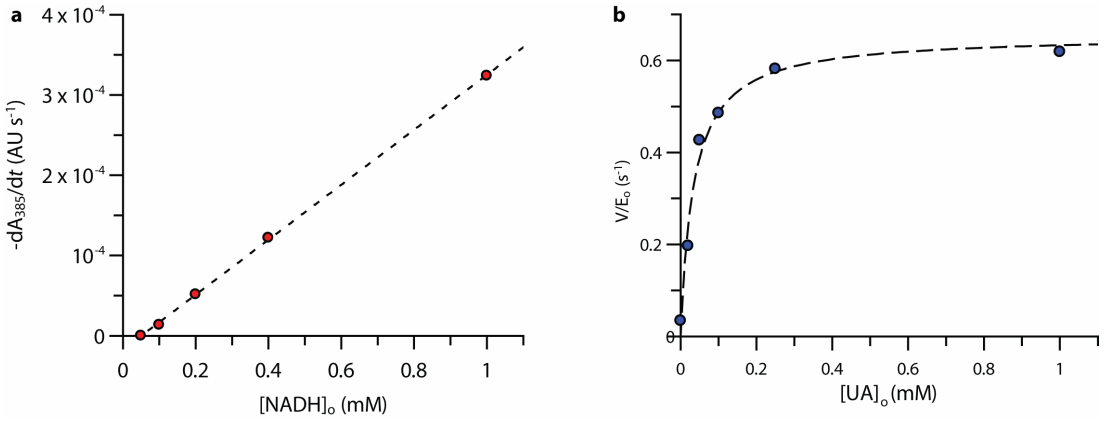

Figure 3.13. Steady-state kinetics of urate oxidation catalyzed by HpxO M208I. Assays were carried out in 0.1 M potassium phosphate buffer, pH 8.0, in the presence of 0.01 mM FAD. The enzyme concentration was 900 nM. a) Dependence of steady-state rate on NADH concentration in the presence of 1.0 mM urate. The K_M for NADH was > 1.0 mM; b) Dependence of the steady-state rate on urate concentration in the presence of 1.0 mM NADH. The V_{max}/E_o value for urate was 0.65 ± 0.03 s^{-1}. The K_M for urate was 35 ± 7 μM.

3.9. HpxO Y176F.

This residue forms hydrogen bonds with the side chain carboxylate group of D293 and may thus be part of an extended hydrogen bonding network involving that residue and R204 (Figure 3.14). The Y176 residue is also within hydrogen bonding distance of an ordered water molecule which in turn is hydrogen bonded to the N8 atom of the uric acid. This residue may thus be important both for substrate binding and for proton transfer steps in the oxygenation reaction.

Kinetic studies on HpxO Y176F were hampered by its extremely low activity. The protein appears to exhibit a very low affinity for FAD. The enzyme co-purifies with almost no detectable FAD.

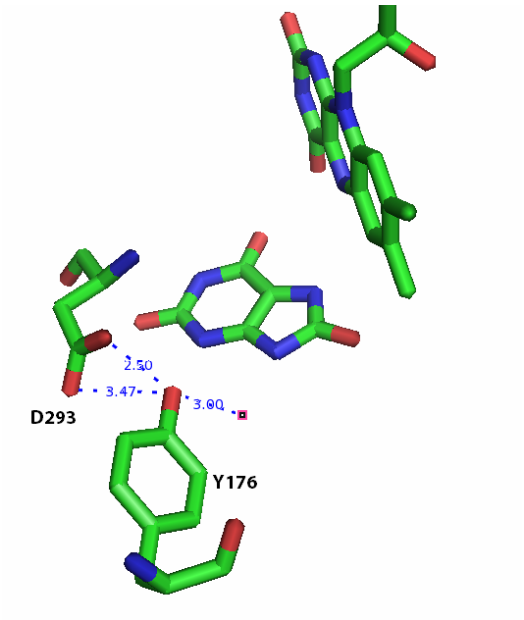

Figure 3.14. Position of the HpxO Y176 residue and its potential hydrogen bonding interactions with D293 and an ordered water molecule (pink dot).

Addition of a 50-fold molar excess of exogenous flavin (0.01 mM) resulted in only a small increase (≤ 25%) in enzymatic turnover, suggesting that this mutant, like many of the others, is impaired in flavin binding. The V/E_o value at 1 mM NADH and urate, and 0.01 mM FAD, was ~0.1 s^{-1}.

3.10. HpxO S43A

This residue is located close to the pyrimidyl portion of the FAD isoalloxazine ring and can form two hydrogen bonding interactions with the cofactor (Figure 3.15). S43 may thus be important for flavin binding and for determining the "out" or "in" position of the flavin during the HpxO catalytic cycle.

Consistent with this assignment of an important role for S43, the S43A mutant of HpxO was considerably less active than any of the other mutants studied here, with the exception of of R204K and Y176F. This was characterized by an increase in the K_M

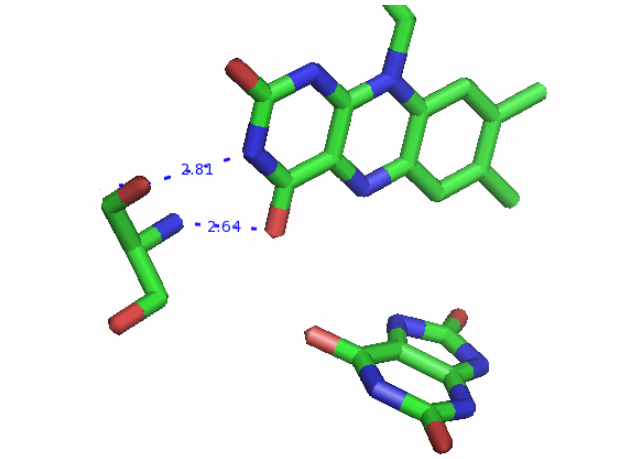

Figure 3.15. Position of HpxO S43 residue.

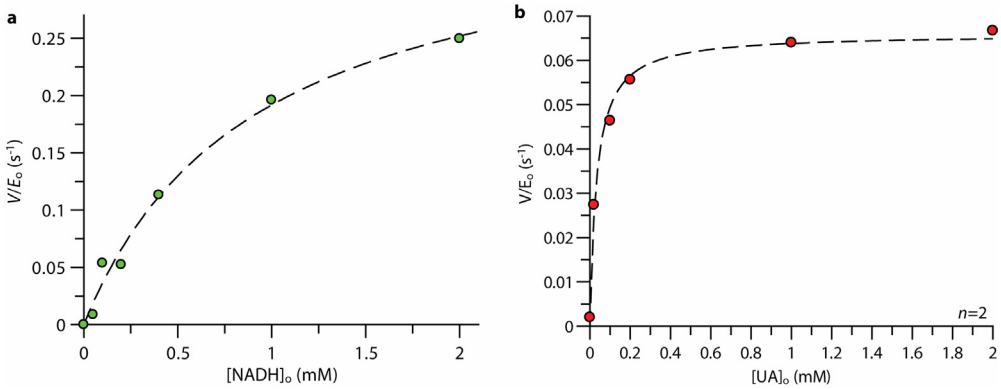

Figure 3.16. Steady-state kinetics of urate oxidation catalyzed by HpxO S43A. Assays were carried out in 0.1 M potassium phosphate buffer, pH 8.0, in the presence of 0.01 mM FAD. The enzyme concentration was 700 nM. a) Dependence of steady-state rate on NADH concentration in the presence of 1.0 mM urate. The K_M for NADH was estimated at 0.92 ± 0.2 mM; b) Dependence of the steady-state rate on urate concentration in the presence of 1.0 mM NADH. The V_{max}/E_o value was 0.066 ± 0.002 s^{-1}. The K_M for urate was 33 ± 5 μM.

for NADH (to ~0.9 mM) and an order of magnitude decrease in the turnover number. The K_M for urate was similar to that of wtHpxO (Figure 3.16).

3.11. Conclusion.

The steady-state kinetic parameters for seven active site mutants of HpxO were determined. All of the mutants showed impaired catalytic activity. The R204 residue is critically important for catalysis of the oxygenation reaction, most likely due both to stabilization of the transition state for oxygenation, by hydrogen bonding and electrostatic interactions with the N1-C2-O2′ region of the HpxO-bound uric acid. Additionaly, the R204Q mutant could catalyze the steady-state oxidation of NADH in a manner that was essentially independent of the presence of urate. This uncoupled reaction appears to implicate the R204 residue as being important for gating the conformational changes in the enzyme that follow substrate binding and allow flavin motion and reduction by NAD(P)H. The HpxO M208I mutant showed a dramatically altered K_M for NADH, which highlights the importance of residues remote from the active site, and by implication the importance of protein dynamics, for catalysis in HpxO and related flavin monooxygenases.

3.12. Experimental.

3.12.1. Protein production.

Overexpression vectors for each of the HpxO mutants were prepared by single-point mutagenesis of the vector encoding wtHpxO by Cynthia Kinsland (Protein Production Facility, Cornell University). The resulting plasmids were used for heterologous overexpression of the various mutants in *E. coli* using standard procedures. The proteins were stored at −80 °C in 0.1 M potassium phosphate buffer, pH 8.0, until use.

3.12.2. Steady-state kinetic assays.

Assays were carried out at 25 ± 1 °C in 0.1 M potassium phosphate, pH 8.0. NADH (10 mM), uric acid (2 mM), and FAD (1 mM) stock solutions were prepared freshly in this buffer on the day of the assay. Absorbance measurements were recorded on a Cary 300 Bio UV-Vis spectrophotometer (Varian). For analysis of NADH oxidation, an extinction coefficient of 0.745 mM^{-1} cm^{-1} at 385 nm was used. Protein concentrations were determined by the Bradford method (*7*). We previously showed that the concentrations of wild-type HpxO could be determined reliably by this method. For purposes of calculation of V/E_o, the active protein concentration was assumed to be equal to the total protein concentration in the presence of 0.01 mM FAD.

In assays where NADH concentration was varied, the uric acid concentration was typically fixed at 1 mM. Where the uric acid concentration was varied, the NADH concentration was fixed at 1 or 1.5 mM. In some cases as noted in the text, these NADH concentrations were less than saturating, but were the highest concentration of NADH which gave a Beer-Lambert response under the assay conditions. Calibration experiments indicated that this introduced an error of no more than 25% into the kinetic constants determined under these circumstances (data not shown).

In a typical experiment, enzyme (100–900 nM final concentration), uric acid (0–1 mM) and FAD (0.01 mM) were pre-incubated in 0.1 M potassium phosphate buffer, then added to an appropriate volume of NADH (0 – 2 mM) to initiate the reaction.

To minimize mixing effects, all other components of the HpxO reaction were typically added to the appropriate volume of NADH stock solution in order to initiate the reaction. The reaction mixtures were then manually mixed prior to observing the absorbance change at 385 nm as described above. The initial mixing step resulted in a delay of 12 ± 3 s between initiation of the reaction and the acquisition of the first

absorbance data point. The time domain for the absorbance data was chosen to produce the best linear fit to the initial change in 385 nm absorbance. In the cases of some of the mutants there was an initial rapid decrease in absorbance ($t_{1/2}$ ~ 20 s) which showed pronounced curvature and was followed by a longer linear phase. This initial data was poorly described by a "burst" type model and was attributed to mixing effects and omitted from the linear fit.

The absorbance data were analyzed by fitting the linear portions of the initial absorbance decay by linear least-squares regression to determine the rates of change of absorbance at 385 nm as a function of initial substrate concentration. These rates were converted to rates of change of NADH concentration and plotted as a function of $[NADH]_o$. The resulting data were fit by nonlinear regression to the Michaelis-Menten equation using the Grafit 5.0 software package (Erithacus Software, Surrey, UK). Kinetic traces presented in the Figures are typically representative traces from a single experiment. The kinetic constants were determined on the basis of at least two independent experiments. The standard errors reported in the text are the standard errors to the linear or nonlinear fits.

3.12.3. HPLC analysis of the products of the HpxO R204K/Q mutants.

All reactions were assayed by reverse-phase HPLC on an Agilent 1100 HPLC system equipped with a quaternary pump and a 1.0 mL sample loop. The system also had a diode array UV-Vis detector (190 – 640 nm) and a fluorescence detector. The stationary phase was a Supelcosil LC-18-T column (15 cm × 4.6 mm, 3 μm particles), maintained at room temperature (21 ± 1 °C). At the end of the incubation period for the enzymatic reaction, the protein was removed by centrifugal ultrafiltration of the reaction mixture (10 kDa MWCO membrane). Aliquots of 0.02 – 0.05 mL of the filtrate were then removed and analyzed for urate and allantoin. The LC eluent

consisted of a gradient of methanol in 10 mM potassium phosphate buffer, pH 6.6. In the analytical method the percentages P and M of phosphate buffer and methanol (balance water) at time t varied according to the following scheme: $\{t,P,M\}$: {0,100,0},{4,90,0},{9,60,15},{14,10,65},{16,100,0},{21,100,0}.

REFERENCES

1. O'Leary, S. E., Hicks, K. A., Ealick, S. E., Begley, T. P. (2009) Biochemical characterization of the HpxO enzyme from *Klebsiella pneumoniae*, a novel FAD-dependent urate oxidase, *Biochemistry 48*, 3033–3035.
2. Entsch, B., van Berkel, W. J. H. (1995) Structure and mechanism of *p*-hydroxybenzoate hydroxylase, *FASEB J. 9*, 476–483.
3. Entsch, B., Cole, L. J., Ballou, D. P. (2005) Protein dynamics and electrostatics in the function of *p*-hydroxybenzoate hydroxylase, *Arch. Biochem. Biophys. 433*, 297–311.
4. Ballou, D. P., Entsch, B. Cole, L. J. (2005) Dynamics involved in catalysis by single-component and two-component flavin-dependent aromatic hydroxylases, *Biochem. Biophys. Res. Comm. 338*, 590–598.
5. Gatti, D. L., Palfey, B. A., Lah, M. S., Entsch, B., Massey, V., Ballou, D. P., Ludwig, M. L. (1994) The mobile flavin of 4-OH benzoate hydroxylase, *Science 266*, 110–114.
6. Ortiz-Maldonado, M., Entsch, B., Ballou, D. P. (2004) Oxygen reactions in *p*-hydroxybenzoate hydroxylase utilize the H-bond network during catalysis, *Biochemistry 43*, 15246–15257.
7. Bradford, M. M. (1976) A rapid and sensitive method for the quantitation of microgram quantities of protein utilizing the principle of protein-dye binding, *Anal. Biochem. 72*, 248–254.

CHAPTER 4

Identification and initial characterization of a biosynthetic pathway for bacimethrin in *Clostridium botulinum A ATCC 19397*.

4.1. Introduction

Bacimethrin (**4.1**, Figure 4.1) was first isolated from strains of *Bacillus megaterium* in the early 1960s (*1*). The compound was observed to exhibit antibiotic activity against a variety of yeast species and several bacteria. The bacimethrin antibiotic activity was found to be attenuated in the presence of thiamin pyrophosphate **4.9** (vitamin B_1) and pyridoxine (vitamin B_6). The first chemical synthesis of the compound was reported in 1962 (*2*). The efficacy of the compound as an antibiotic in a mouse model was then assessed, and was found to be slight to moderate against a variety of clinically-relevant pathophysiological states (*3*). The results of these studies suggested that bacimethrin may have limited utility as an antibiotic.

Two decades later, the production of bacimethrin was also observed in *Streptomyces albus* (*4*). A further synthesis was described and data was presented which suggested that bacimethrin might inhibit the phosphorylation of its close structural analogue HMP-OH **4.2**, a key pyrimidine intermediate in thiamin biosynthesis. A third chemical synthesis of bacimethrin was reported subsequently (*5*).

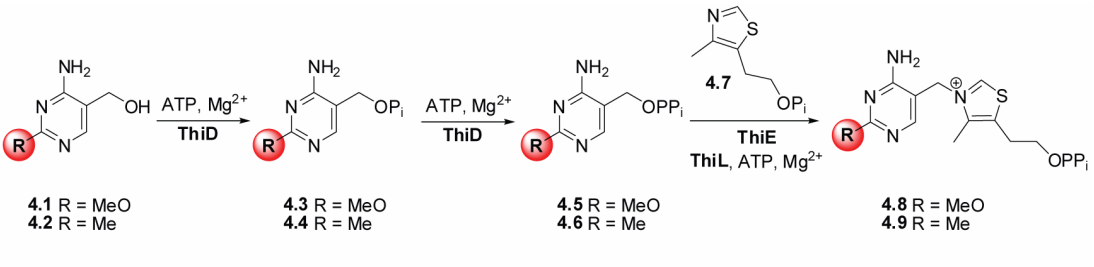

Figure 4.1. Bacimethrin **4.1** and HMP-OH **4.2**, and their enzymatic conversion to methoxythiamin pyrophosphate **4.8** and thiamin pyrophosphate **4.9**.

Later studies assessed in greater detail the molecular basis for the effects of bacimethrin on bacterial growth. Zilles *et al*. reported that the bacteriostatic effects of bacimethrin had their origin in modulation of thiamin biosynthesis (*6*). In particular, *Salmonella enterica* serovar *Typhimurium* mutants that exhibited increased expression of the *thi* operon, which codes for the thiamin biosynthetic genes, or mutants with defects in *thiD*, the gene product of which (phosphomethylpyrimidine kinase) phosphorylates HMP-OH **4.2** and HMP-P **4.4**, showed increased resistance to bacimethrin. This led to the proposal that bacimethrin could either inhibit thiamin biosynthesis in competition with HMP-OH, by binding to thiamin biosynthetic enzymes which process HMP-OH or its downstream products. An alternative hypothesis postulated that bacimethrin could enter into thiamin biosynthesis, resulting in production of methoxythiamin pyrophosphate (MeOThDP) **4.8**, which was proposed in this model to be the true bacteriostatic agent. Subsequent studies showed that bacimethrin is enzymatically converted to methoxythiamin pyrophosphate six-fold faster *in vitro* than HMP-OH is converted to thiamin pyrophosphate **4.9** (*7*). Bacimethrin pyrophosphate is a substrate (*8*) for thiamin phosphate synthase (ThiE, Figure 4.1). Later pre-steady-state kinetic studies on ThiE showed that the key ThiE intermediate, a pyrimidine-derived carbocation, forms 16 times faster from bacimethrin pyrophosphate than from HMP-PP at the ThiE active site (*9*). Cell-based studies also concluded that the observed effects of bacimethrin on bacterial growth were due to inhibition by MeOThDP of metabolic pathways dependent on the thiamin-dependent enzymes α-ketoglutarate dehydrogenase, transketolase, and deoxy-D-xylulose-5-phosphate synthase (*7*).

Bacimethrin was later used in a genetic screen to identify thiamin metabolic genes (*10*). The screen identified genes which conferred resistance to bacimethrin, including five genes of previously unknown function. Of these five, two gene products (YmfB

and Cof) catalyzed the hydrolysis of HMP-PP to HMP-P. YmfB was also shown to catalyze conversion of thiamin pyrophosphate to thiamin phosphate.

One curious conclusion from the cell-based studies (*7*) on bacimethrin/MeOThDP toxicity was the following. While the effects of bacimethrin treatment on sensitive bacteria were interpreted as arising from blockade of metabolic pathways dependent on thiamin pyrophosphate-utilizing enzymes, the effects of bacimethrin could be reversed by providing the bacteria with *any one* of the nutrient sets for which organisms bearing mutations in the genes coding for the thiamin-dependent enzymes in question were auxotrophic. The *combination* of *all* the sets of nutrients was not required to antagonize the effects of bacimethrin. It was unclear how this effect was produced.

The present work had two principal aims. The first was to characterize a putative biosynthetic operon for bacimethrin in *Clostridium botulinum*. The second was to further understand the molecular basis for the bacteriostatic effects of bacimethrin.

4.2. Identification of a gene cluster responsible for bacimethrin production in Clostridium botulinum A ATCC 19379.

Inspection of the sequenced genome of *C. botulinum* reveals a gene cluster potentially involved in bacimethrin biosynthesis. We had previously hypothesized that bacimethrin could be produced from cytosine in two steps (Figure 4.2). This could

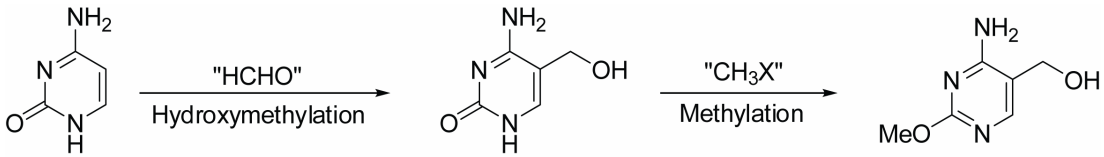

4.10 **4.11** **4.1.**

Figure 4.2. Proposed biosynthesis of bacimethrin **4.1** from cytosine **4.10**.

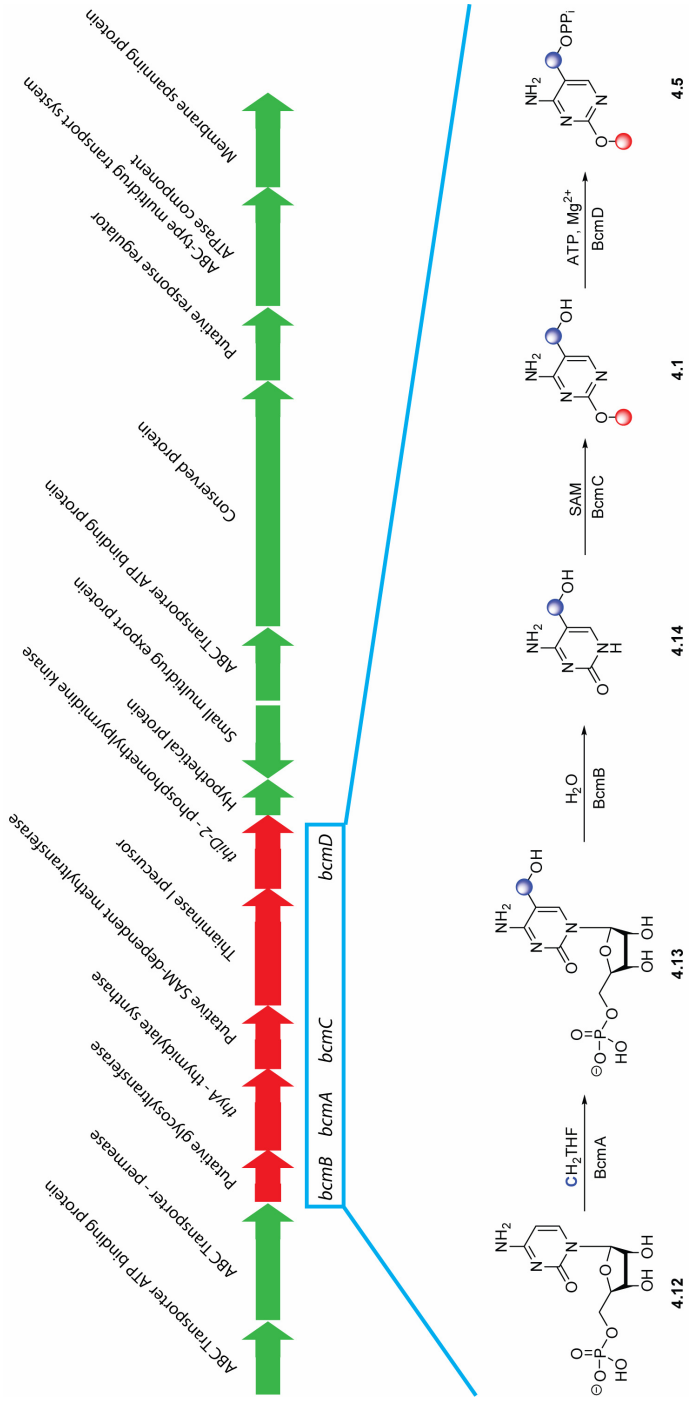

Figure 4.3. Genetic organization and homology-based annotated enzymatic activities for the bacimethrin biosynthetic cluster in *Clostridium botulinum* A ATCC 19397. CH_2-THF is 5,10-methylenetetrahydrofolate **4.16**; SAM is *S*-adenosyl-L-methionine **4.17**; ABC is "ATP-binding cassette".

occur by hydroxymethylation of the 5-position of cytosine using a formaldehyde equivalent, followed by methylation at the O-2′ position of the pyrimidine. The order of these steps could also be reversed in the biosynthetic pathway. We found that the *C. botulinum A ATCC 19397* genome contains a gene cluster (Figure 4.3) with genes annotated as thymidylate synthase, a putative glycosyltransferase, a SAM-dependent methyltransferase, and a phosphomethylpyrimidine kinase (*thiD-2*). Additionally, the cluster contained genes proposed to code for an ABC transporter and a putative thiaminase I.

Thymidylate synthase is closely related to cytidylate hydroxymethylase; both enzymes catalyze a methylenetetrahydrofolate-dependent hydroxymethylation at the 5-position of pyrimidine nucleotides (dUMP or CMP **4.12** respectively) (*11*,*12*). The *C. botulinum* enzyme in the putative bacimethrin biosynthetic cluster also showed high sequence similarity with the MilA enzyme from *Streptoverticillium rimofaciens* ZJU5119, which catalyzes the same reaction in the biosynthesis of the peptidyl nucleoside antibiotic mildiomycin (*13*). The MilA enzyme was shown to exhibit specificity for CMP as its nucleotide substrate. We thus proposed that bacimethrin could be synthesized from CMP **4.12** in *C. botulinum*, rather than directly from cytosine. We assigned the name *bcmA* to the *C. botulinum* gene.

A second putative enzyme-encoding gene in the cluster, which we designated *bcmB*, was annotated as a hypothetical protein possessing a conserved domain homologous to the nucleoside 2-deoxyribosyltransferase enzyme family (*14*). Moreover, this enzyme also showed considerable sequence homology with the second enzyme of the mildiomycin biosynthetic pathway, MilB. The MilB enzyme catalyzes the conversion of 5-hydroxymethylcytidine monophosphate **4.13** to 5-hydroxymethylcytosine **4.14**. We thus proposed this step to also be the second step in bacimethrin biosynthesis.

The third enzyme in the cluster was annotated as putative methyltransferase and contained a conserved domain proposed to bind the methyl donor *S*-adenosylmethionine (*15*). We thus proposed that this enzyme, which we designated as BcmC, could catalyze transfer of a methyl group from *S*-adenosylmethionine (SAM) to the O-2 position of 5-hydroxymethylcytosine, producing bacimethrin **4.1**.

The fourth enzyme in the putative biosynthetic cluster, which we designated BcmD, was annotated as a kinase with homology to ThiD, the kinase responsible for phosphorylation of HMP-OH **4.2** and HMP-P **4.4** in the late biosynthetic steps of thiamin phosphate biosynthesis. Consequently we proposed that *C. botulinum* could produce bacimethrin pyrophosphate, which could be endogenously coupled to thiazole phosphate **4.7** by the ThiE enzyme (thiamin phosphate synthase), producing methoxythiamin pyrophosphate. The genome of *C. botulinum* A ATCC 19397 contains a gene (CLB_0490) which is proposed to encode the ThiE protein.

The bacimethrin biosynthetic cluster also appears to contain the components of an ABC transporter. The presence of such transporters in the biosynthetic gene clusters of antibiotics is well-precedented, and is thought to be involved in export of the biosynthesized toxin (*16*). In the present context, the role of such an ABC transporter could be to export bacimethrin, or its phosphorylated derivatives, or methoxythiamin itself, constituting a detoxification mechanism for the thiamin analogue in the producing organism.

The presence of the thiaminase I in the cluster could also aid in this detoxification process. Thiaminase I catalyzes the substitution of the thiazolium portion of thiamin (and its phosphorylated analogues) with a variety of nucleophiles (*17*), but in contrast to thiaminase II (*18*), the nucleophilic substrate cannot be water. Thus thiaminase I does not catalyze formation of HMP-OH from thiamin. In the case of thiaminase II, water is the only nucleophilic substrate. Thiaminase II has been implicated in salvage

of HMP-OH from thiamin derivatives in which the thiazolium portion of the cofactor has been degraded (*19*,*20*). The function of thiaminase I has remained unclear to date.

4.3. Functional characterization of the bcm cluster.

The *bcmA*, *bcmB*, *bcmC* and *bcmD* genes were separately cloned into vectors encoding an *N*-terminal 6×His tag and heterologously overexpressed in *E. coli* using standard procedures, by Lisa Cooper (Texas A&M University). The resulting proteins were purified by Ni^{2+}-affinity chromatography using standard conditions. We then examined whether the enzymes exhibited the proposed catalytic activities *in vitro*.

4.3.1. BcmA and BcmB.

4.3.1.1. Activity.

Treatment of cytidine monophosphate **4.12** with BcmA and either commercially-available 5,10-methylenetetrahydrofolate **4.16**, or the compound produced *in situ* (Figure 4.4) from the reaction of formaldehyde with an excess of tetrahydrofolic acid **4.15** (*21*), resulted in conversion of the CMP to a less polar product (Figure 4.5d).

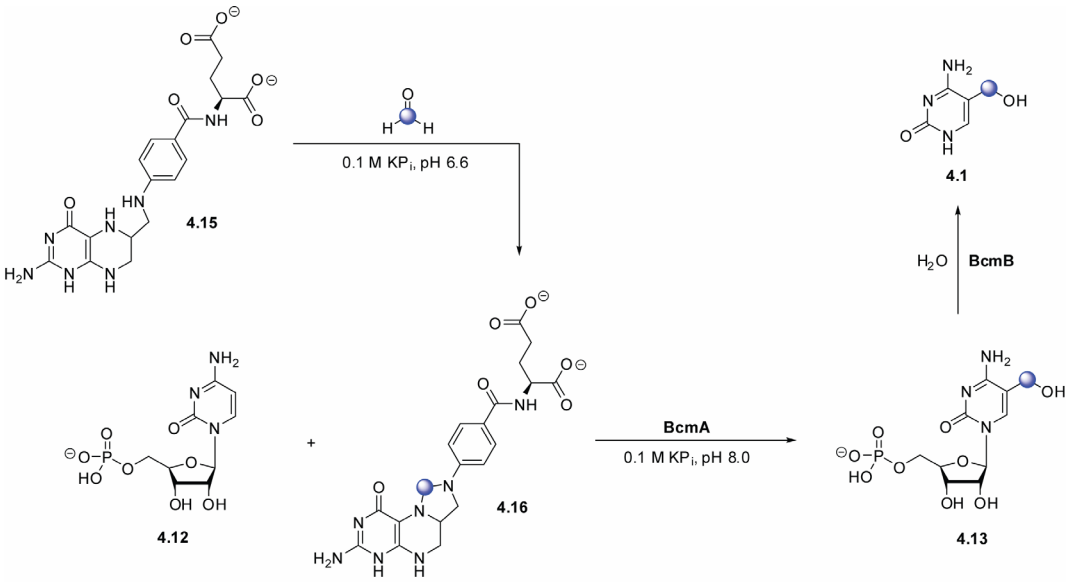

Figure 4.4. Reactions catalyzed by BcmA and BcmB.

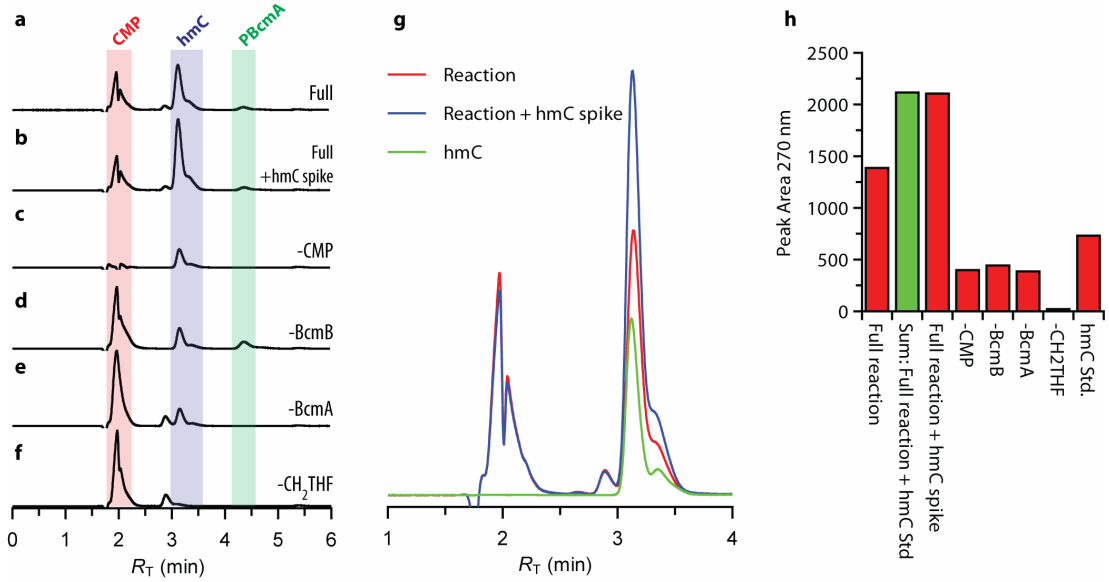

Figure 4.5. Analysis of activity of BcmA and BcmB. CMP **4.12** (R_T 2.0 minutes) was treated with BcmA or a combination of BcmA and BcmB in the presence of 5,10-methylenetetrahydrofolate **4.16**. The reactions were analyzed by reverse-phase HPLC after a 3 h incubation. Chromatograms were detected at 270 nm. a) HPLC chromatogram of the BcmAB reaction mixture; b) Full reaction spiked with authentic 5-hmC; c) control reaction omitting CMP, and showing the presence of a CH_2THF-derived compound which co-elutes with 5-hmC at 3.1 minutes; d) control reaction omitting BcmB, showing accumulation of the BcmA product ("PBcmA", 4.35 minutes) and lack of accumulation of 5-hmC; e) control reaction omitting BcmA, showing lack of accumulation of the BcmA product and 5-hmC; f) control reaction omitting 5,10-methylenetetrahydrofolate; g) overlay of expanded chromatograms in the 5-hmC region: red - full reaction, blue - full reaction spiked with 5-hmC, green – 5-hmC standard at the same concentration used to spike sample (g); h) relative integration values for the 5-hmC region (3.0–3.5 minutes) in chromatograms (a)-(f), in red, and the sum of the value for the full reaction (a) and the value contributed only by the added standard 5-hmC, in green.

The UV absorbance spectrum of this product suggested it was a cytosine derivative. The product was also sensitive to treatment with alkaline phosphatase, indicating that it was phosphorylated. This product was not formed in the absence of BcmA, CMP, or methylenetetrahydrofolate, and was proposed to be 5-hydroxymethyl-CMP **4.13**. Treatment of this product with BcmB resulted in its consumption and formation of 5-hydroxymethylcytosine **4.14**. This latter assignment was confirmed by reverse-phase HPLC, where the BcmB product co-eluted with an authentic standard of 5-hydroxymethylcytosine (Figure 4.5a, 4.5b). Where BcmA and BcmB were incubated with CMP and the methylenetetrahydrofolate preparation, the BcmA product did not accumulate to the extent observed when only BcmA was present, suggesting that BcmB can efficiently catalyze the reaction of the BcmA product. No product was observed when BcmA, or both BcmA and BcmB were incubated with dCMP. This data is consistent with the proposed activities for BcmA and BcmB, particularly when considered along with the sequence homology of BcmA and BcmB to the MilA and MilB enzymes which are known to catalyze the sequential formation of **4.13** and **4.14**, respectively.

4.3.1.2. Steady-state kinetic parameters for BcmA.

The steady-state hydroxymethylation of CMP catalyzed by BcmA was monitored by following the decrease in absorbance at 290 nm, which results from the conversion of 5,10-methylenetetrahydrofolate to tetrahydrofolate. This method has been used previously in kinetic studies on the formation of 5,10-methylenetetrahydrofolate (*21*). The enzyme exhibited saturation kinetics with both CMP and 5,10-methylenetetrahydrofolate. The K_m for CMP was estimated at 12 μM (Figure 4.6), while that for 5,10-methylenetetrahydrofolate was ≤ 2 μM. A more sensitive assay will be required to accurately determine the K_m value for the

methylenetetrahydrofolate. The k_{cat} value was estimated at ~0.02 s^{-1}, using a value of 3.0 mM^{-1} cm^{-1} for $\Delta\varepsilon_{290}$ between methylenetetrahydrofolate and tetrahydrofolate (*22*). Under the assay conditions there was no evidence that the hydroxymethylation reaction produced a significant change in absorbance at 290 nm for the cytidine chromophore.

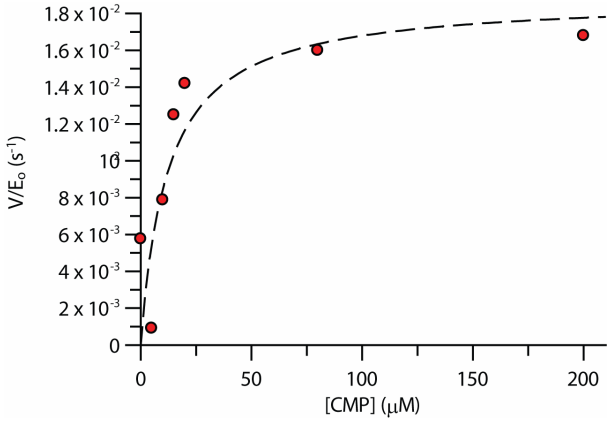

Figure 4.6. Representative Michaelis-Menten plot for the BcmA-catalyzed reaction of CMP with 5,10-methylenetetrahydrofolate. The values of $K_{m,CMP}$ and k_{cat} were estimated at 12 μM and 0.02 s^{-1}, respectively. The K_m value for methylenetetrahydrofolate was ≤ 2 μM. The rates were determined by following the change in absorbance at 290 nm, which reports on conversion of methylenetetrahydrofolate to tetrahydrofolate.

4.3.2. BcmC

To investigate whether BcmC could catalyze the formation of bacimethrin **4.1** from 5-hydroxymethylcytosine **4.14**, we incubated substrate and enzyme in the presence of *S*-adenosyl-L-methionine iodide **4.17**. This resulted in formation of bacimethrin and *S*-adenosylhomocysteine **4.18** (Figures 4.7, 4.8). Initial assignment of the products was made on the basis of co-elution with authentic standards. Bacimethrin was not detected in controls where enzyme, CMP, or SAM were omitted. Formation of

bacimethrin was also confirmed by positive-mode ESI-TOF mass spectrometry (Figure 4.9). An ion was detected in the mass spectrum of the reaction mixture at 156.078 *m*/*z*, which was not present in a control where enzyme was absent. The mass-to-charge ratio of this ion agrees with the calculated value for the bacimethrin $[M+H]^+$ ion within 2.6 ppm. Fragmentation of this ion by collisionally-induced dissociation resulted in the accumulation of daughter ions at 138 *m*/*z* (loss of water) and 81 *m*/*z*, consistent with the bacimethrin structure and the fragmentation pattern known for HMP-OH (*23*).

4.3.3. BcmD

This enzyme is annotated as *thiD-2* in the *C. botulinum* genome, and thus is predicted to catalyze formation of, sequentially, bacimethrin phosphate **4.3** and bacimethrin pyrophosphate **4.5**. Incubation of bacimethrin with BcmD, ATP and $MgCl_2$ resulted in consumption of ATP and bacimethrin (Figure 4.10). Controls where ATP or the enzyme were omitted showed no reaction of the bacimethrin. A more polar product was observed in the reverse-phase HPLC chromatogram of the reaction mixture which was consistent with formation of bacimethrin phosphate. Efforts to confirm the identity of this product are ongoing.

4.3.4. 2'-Methoxythiamin is not a substrate for the C. botulinum thiaminase I.

2′-Methoxythiamin **4.19** was treated with the thiaminase I found in the bcm cluster (CbtThia-I) in the presence of β-mercaptoethanol, which acts as a nucleophilic substrate (Figure 4.11). Under conditions where this enzyme efficiently cleaved thiamin **4.20**, no reaction of methoxythiamin was observed. This result is intriguing in that it suggests the thiaminase may have a function other than detoxification of the methoxythiamin derived from bacimethrin. Further investigation of this is underway.

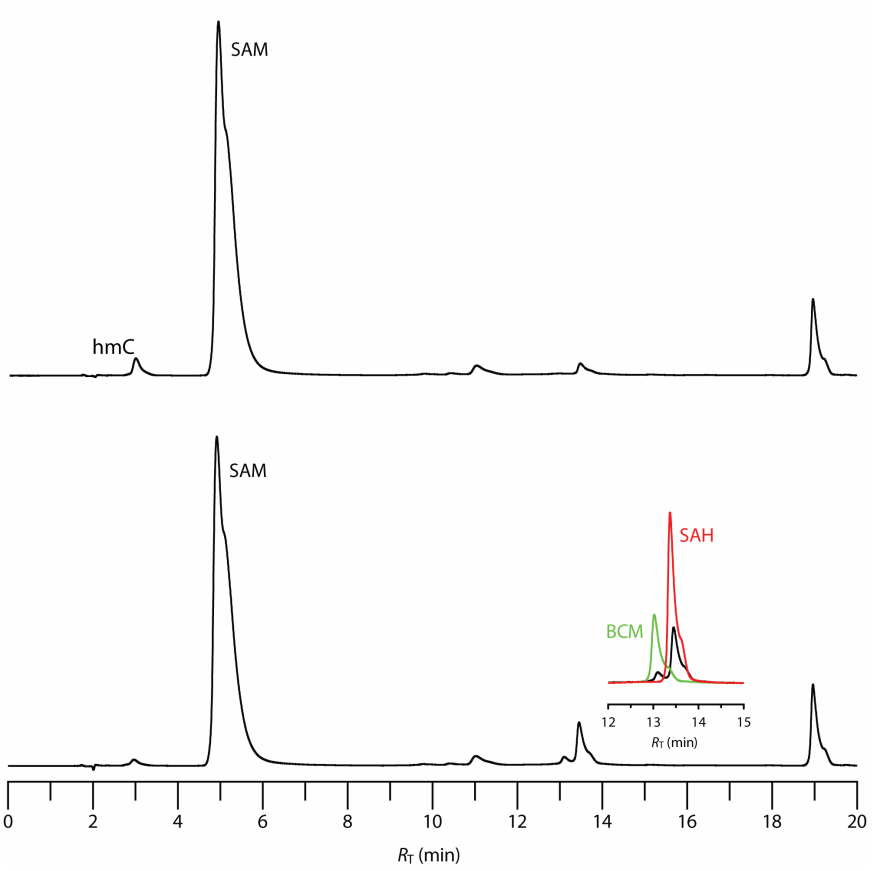

Figure 4.7. Activity of BcmC. 5-Hydroxymethylcytosine (hmC **4.14**, 0.2 mM) was treated with S-adenosylmethionine iodide (SAM **4.17**, 2 mM) in the presence of BcmC (5 μM) for 2.5 h in 50 mM HEPES, pH 7.5 at 25 ± 1 °C. Top – control lacking enzyme; Bottom – full reaction. Inset: expanded section of the chromatogram in which the bacimethrin (BCM) and S-adenosylhomocysteine (SAH) products eluted, overlaid with chromatograms (in color) produced from analysis of authentic standards of these compounds.

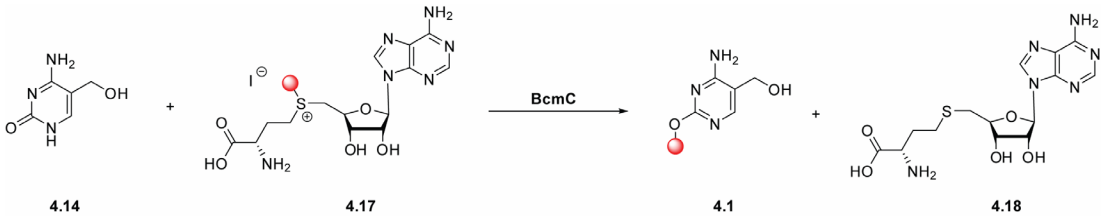

Figure 4.8. Reaction catalyzed by BcmC.

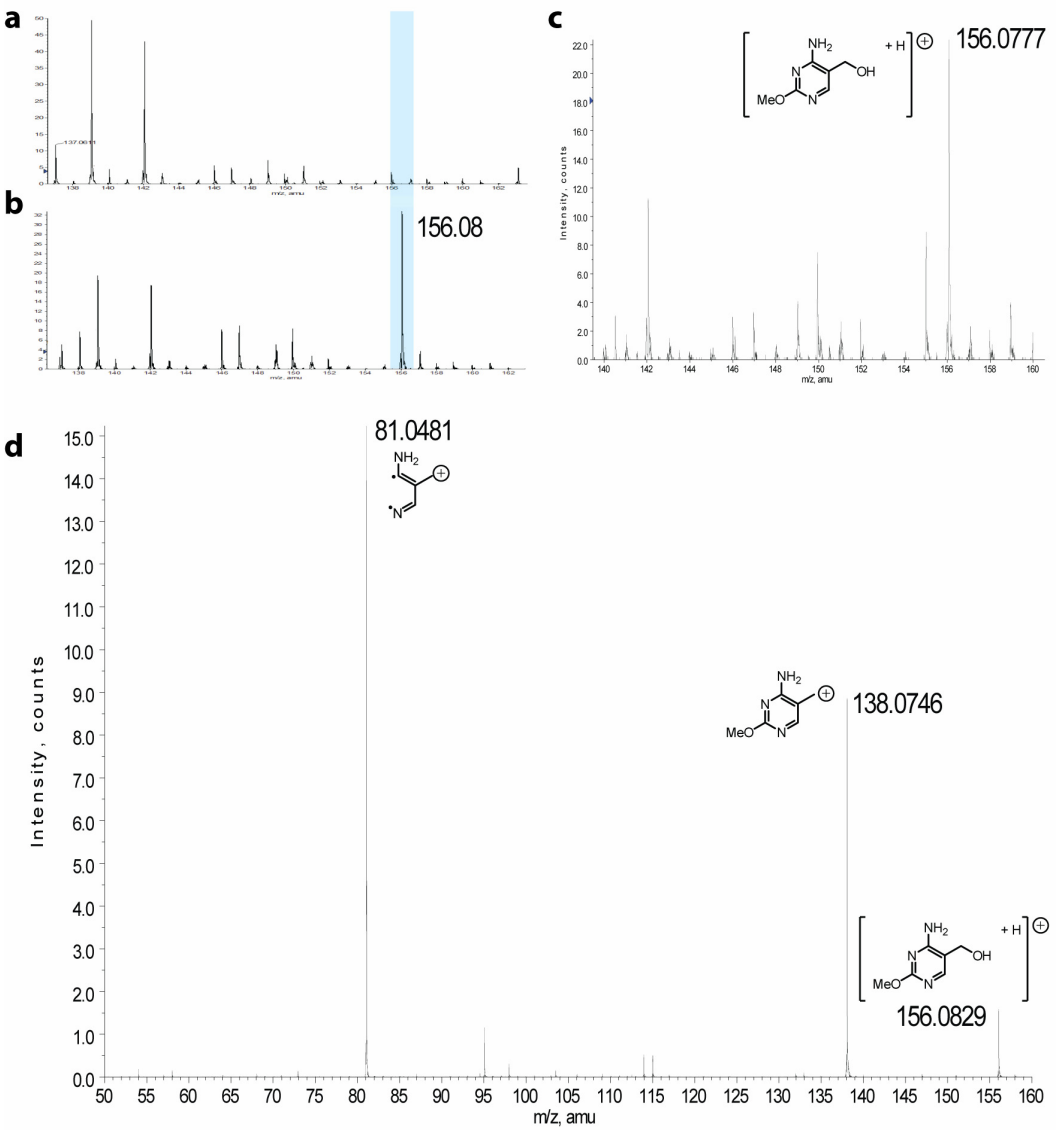

Figure 4.9. ESI-TOF MS analysis of bacimethrin produced by BcmC. The enzyme (2.75 μM) was incubated with 5-hydroxymethylcytosine (0.25 mM) and *S*-adenosyl-L-methionine iodide (0.3 mM) in 25 mM ammonium acetate, pH 6.2, for 3.5 h. The reaction mixture was then analyzed by ESI-TOF +MS after removal of the enzyme by centrifugal ultrafiltration. a) ESI-TOF +MS of a control reaction lacking BcmC; b) MS of reaction mixture showing ion at 156.1 *m/z*; c) Exact mass determination of bacimethrin-derived ion (theoretical $[M+H]^+$ 156.0773, accuracy 2.6 ppm); d) ESI-MS/MS spectrum of BcmC product showing fragmentation expected for bacimethrin.

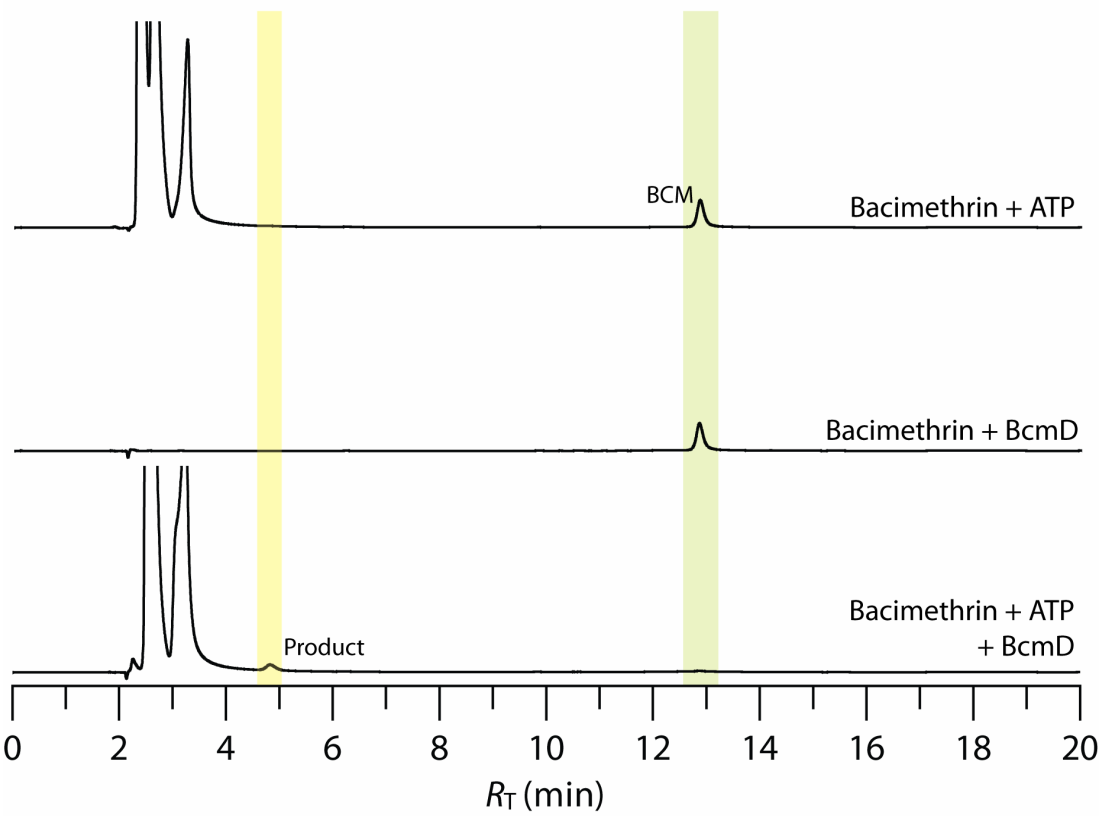

Figure 4.10. *In vitro* activity of BcmD. Bacimethrin (BCM, 0.48 mM) was incubated with ATP (10 mM) and $MgCl_2$ (5 mM) in the presence of BcmD (0.125 mM), in 50 mM HEPES, pH 7.5 for 2.5 h at 25 ± 1 °C. The reaction mixture was then diluted with water to 0.3 mL and the protein was removed by centrifugal ultrafiltration (3 kDa MWCO membrane). 0.05 mL aliquots of the filtrate were analyzed by reverse-phase HPLC. Top – control omitting BcmD; Middle – control omitting ATP; Bottom – full reaction mixture indicating ATP- and BcmD-dependent consumption of bacimethrin.

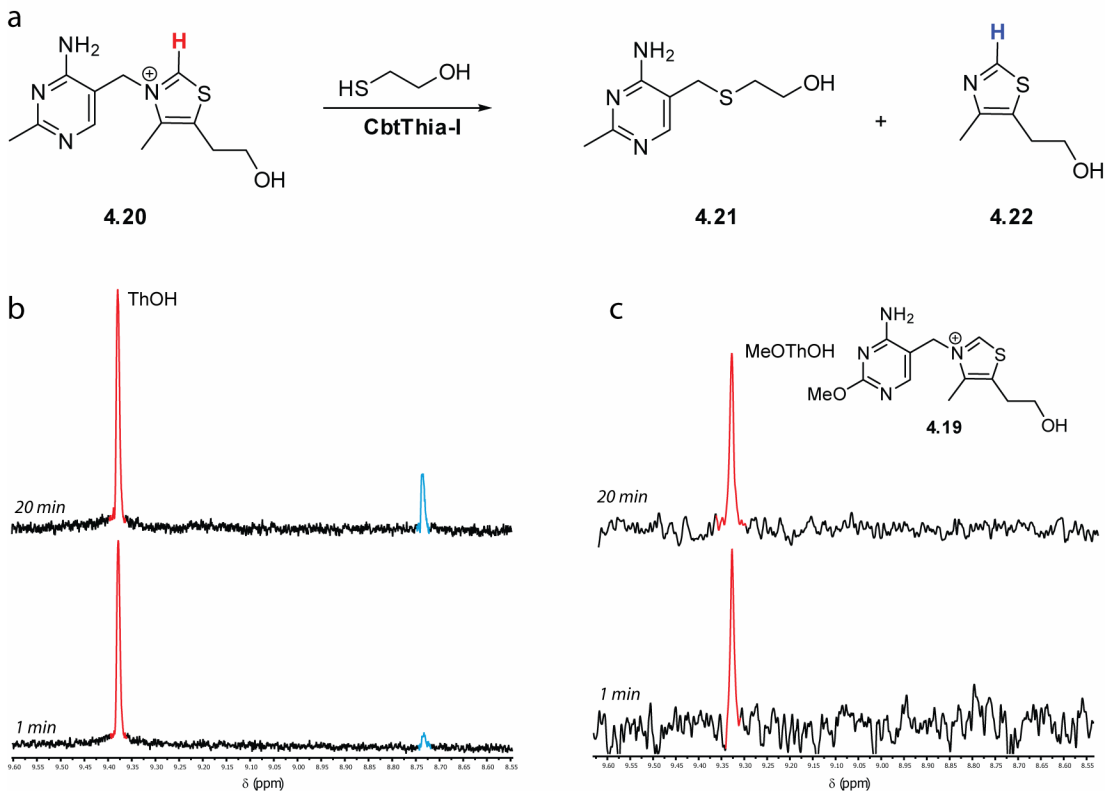

Figure 4.11. Activity of thiaminase I from *C. botulinum A ATCC19397* (CbtThia-I). a) Reaction catalyzed by thiaminase I, which converts thiamin **4.20** or its phosphorylated derivatives to thiazole **4.22** (or phosphorylated derivatives) and a pyrimidyl product derivatized with the nucleophilic substrate, which cannot be water; b) Reaction of thiamin with CbtThia-I in the presence of β-mercaptoethanol, monitored by ^{1}H NMR spectroscopy. The resonance marked in red is due to the thiazolium C2-proton (δ_H 9.38 ppm), which is converted to the resonance marked in blue (8.73 ppm) by the enzymatic activity. The small amount of thiazole present at the commencement of the NMR experiment is due to the interval (~45 s) between addition of the β-mercaptoethanol and acquisition of the first spectrum. Controls lacking enzyme also lack this resonance (not shown); c) Incubation of methoxythiamin **4.19** under conditions identical to those for the reaction of thiamin shows no accumulation of thiazole.

4.4. Discussion.

The results described here constitute the identification of the biosynthetic pathway for bacimethrin in *C. botulinum A ATCC 19397*. The molecule can be produced from CMP in three enzymatic steps using well-precedented chemical transformations. Additionally, the presence of the thiaminase I protein in the biosynthetic cluster, which can degrade thiamin but not methoxythiamin, leads to several intriguing questions relating to the mechanism of toxicity of bacimethrin. The first of these questions is whether thiaminase I can potentiate the bacteriostatic activity of bacimethrin *in vivo*. The thiaminase I protein was previously shown to be an extracellular enzyme in the cases of a variety of organisms, including *Bacillus thiaminolyticus*. The *C. botulinum* thiaminase I gene also encodes the *N*-terminal signal peptide which targets the protein for export (*24*). If *C. botulinum* exports both bacimethrin and thiaminase I, are these employed synergistically to both deplete thiamin available to competing microorganisms, and simultaneously provide the competitors a structural analogue of the cofactor which inhibits their metabolism?

A second, related question is whether *C. botulinum* and other organisms can in fact utilize methoxythiamin pyrophosphate as a cofactor, instead of thiamin pyrophosphate. To our knowledge, no detailed biochemical studies on isolated thiamin-dependent metabolic enzymes from *Clostridium* have been carried out. This latter issue is probably due to the practical difficulties associated with studying the highly pathogenic *C. botulinum*. Ideally, another bacimethrin- and thiaminase I-producing organism which is non-pathogenic would be an invaluable model with which to address the questions posed above. BLAST analysis starting from the thiaminase I protein reveals that the bacimethrin biosynthetic cluster containing the thiaminase I-coding gene is present in a number of the *Clostridia* and also is likely to be present in several strains of *Burkholderia pseudomallei*, as well as in *Burkholderia*

thailandensis E624. Identification of organisms which produce both bacimethrin and the thiaminase protein, but are relatively non-pathogenic, will be important for further *in vivo* characterization of the biological mechanisms underlying bacimethrin toxicity.

Further analysis of the genome sequence of *C. botulinum A ATCC19397* reveals an idiosyncratic genotype with respect to thiamin biosynthesis. This was previously identified based on comparative genomic analysis (*25*). The organism lacks most of the genes for biosynthesis of the thiamin thiazole, including the thiazole synthase (*thiG*, *26*) and the genes (*thiS*, *thiF*) responsible for delivery of sulfur to the thiazole during the thiazole synthase reaction (*27*). The organism also does not appear to possess a gene encoding a protein with homology to THI4p, the single eukaryotic thiazole biosynthetic enzyme (*28*). However, the *C. botulinum* genome contains the *thiM* gene, proposed to encode thiazole kinase. This gene is required to produce a thiazole substrate which can efficiently undergo the thiamin phosphate synthase (ThiE) reaction. The organism is thus either incapable of producing the thiazole moiety of thiamin by itself, or does so by an as-yet uncharacterized pathway. This genotype appears to be conserved among members of the *Clostridia* which possess the thiaminase I gene and the bacimethrin biosynthetic pathway.

C. botulinum also possesses the *thiC* gene, which is responsible for HMP biosynthesis in a variety of organisms (*29*). However, the *C. botulinum* ThiC appears to contain a mutation in the important conserved region responsible for ligation of the [4Fe-4S] cluster required for the enzyme's activity. This involves deletion of a conserved proline residue which converts the archetypal HMP-P synthase (ThiC) CX_2CX_4C motif to a CX_2CX_3C sequence. This differs also from the conserved CX_3CX_2C motif observed in other members of the radical SAM superfamily (*30*). It is consequently unclear at the present time whether *Cbt*ThiC is an active HMP-P synthase.

The organism's genotype thus suggests that *C. botulinum A ATCC 19397* could produce thiamin pyrophosphate if it were supplied exogenous thiazole and if the ThiC protein were active. The available data also suggest that the organism could produce methoxythiamin from bacimethrin under the same conditions. One of the most fascinating questions remaining to be answered is whether the thiaminase I enzyme, which obligatorily produces thiazole from thiamin, is exported by *C. botulinum* (and other organisms with similar genotypes) to simultaneously destroy thiamin available to competing microorganisms and to produce thiazole which can be scavenged by the thiaminase-producing bacterium for biosynthesis of endogenous (methoxy)thiamin for

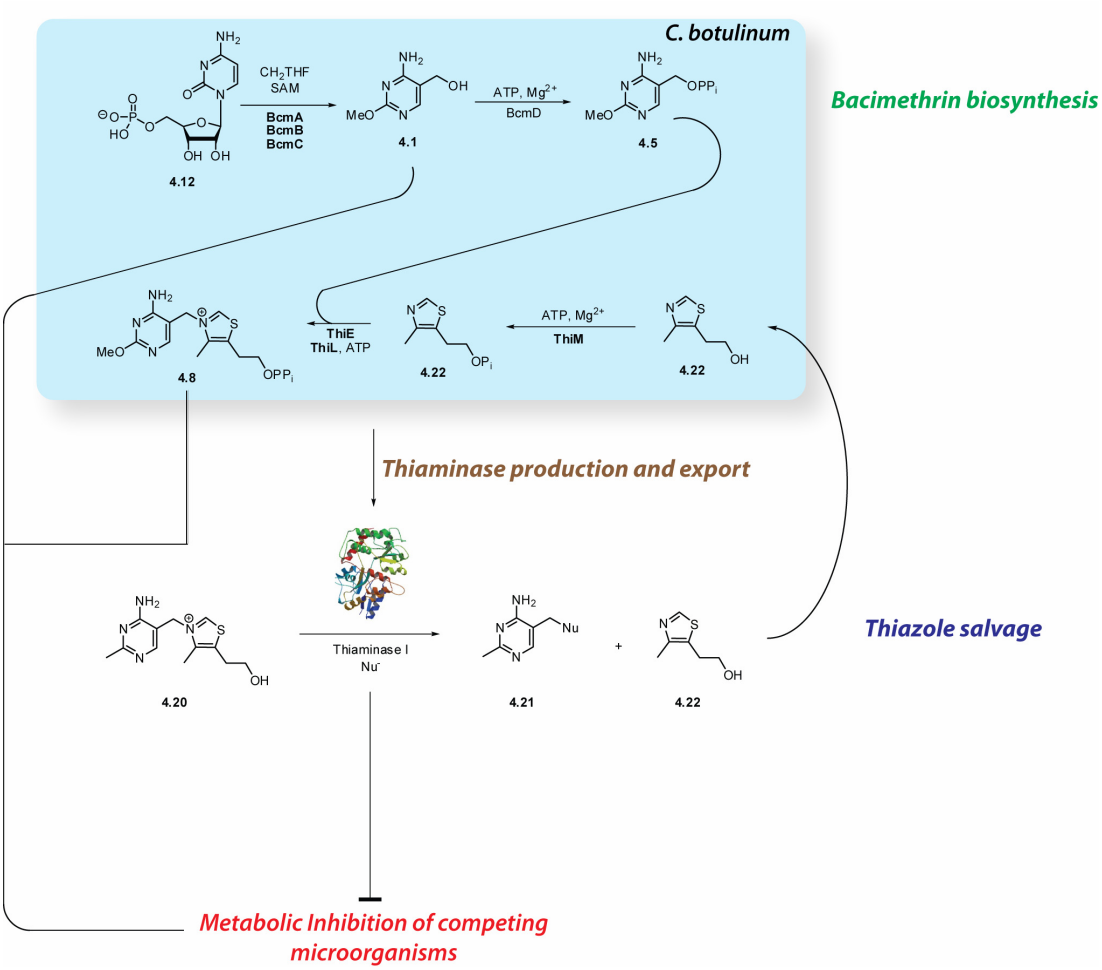

Figure 4.12. Proposed roles for thiaminase I, bacimethrin and methoxythiamin.

use in its metabolism (Figure 4.12). If this is the case, the function for thiaminase I from *C. botulinum* as a combined thiazole scavenger and potentiator of the toxicity of bacimethrin could be assigned. Investigation of these questions is underway presently.

4.5. Experimental

Protein concentrations were determined by the Bradford method (*31*).

4.5.1. Analytical HPLC method

All reactions were assayed by reverse-phase HPLC on an Agilent 1200 HPLC system equipped with a quaternary pump, and thermostatted autosampler (14 °C) with a 0.1 mL sample loop. The system also had a diode array UV-Vis detector (80 Hz full spectral sampling, 190 – 640 nm) and a fluorescence detector. The stationary phase was a Supelcosil LC-18-T column (15 cm × 4.6 mm, 3 μm particles), maintained at 26 °C. The LC eluent consisted of a gradient of methanol in 10 mM potassium phosphate buffer, pH 6.6. In the analytical method the percentages *P* and *M* of phosphate buffer and methanol (balance water) at time *t* varied according to the following scheme: {*t*,*P*,*M*}:{0,100,0},{5,90,0},{11,60,15},{23.5,10,65},{25,100,0},{30,100,0}.

4.5.2. **In vitro** *activity of BcmA and BcmB*

CMP (0.125 mM) and (6*R*,*S*)-5,10-methylenetetrahydrofolate (0.125 mM) were incubated with BcmA (7 μM) in 0.1 M potassium phosphate buffer, pH 8.0, containing 0.15 M potassium chloride and β-mercaptoethanol (10 mM). Reactions were incubated in darkness for 3 h at 25 ± 1 °C. Control reactions identical to the above but lacking, variously, CMP, methylenetetrahydrofolate, and BcmA were also prepared. The protein was then removed by centrifugal ultrafiltration through a 3 kDa MWCO membrane (Microcon, Millipore) and 50 μL aliquots of the filtrate were

analyzed by reverse-phase HPLC. Chromatograms were detected using the absorbance at 254 nm. UV-Vis spectra of substrate and product peaks were also collected.

For analysis of the BcmB activity, a sample identical to the above was prepared but which included BcmB (8 μM).

In a separate experiment, 5,10-methylenetetrahydrofolate was also prepared *in situ* by addition of formaldehyde. (final concentration 1 mM) to a 0.5 mL solution of tetrahydrofolic acid (~5 mM, Sigma) in 0.1 M potassium phosphate buffer, pH 6.6. Aliquots (0.04 mL of this solution were then quenched into the BcmA reaction mixture (0.2 mL final volume). In this case the reactions were incubated overnight in darkness.

4.5.3. In vitro *activity of BcmC.*

S-Adenosyl-L-methionine (SAM, 2 mM) and 5-hydroxymethylcytosine (0.2 mM) were incubated with BcmC (0.01 mM) in 50 mM HEPES, pH 7.5 for 1.5 h at 25 ± 1 °C. The reaction mixtures (0.05 mL) were then diluted to 0.3 mL with water and the protein was removed by centrifugal ultrafiltration (3 kDa MWCO membrane). 0.05 mL aliquots of the filtrate were then analyzed by reverse-phase HPLC using a modification of the method described above, with {*t*,*M*,*P*}: {0,0,100}, {5,0,90}, {8,10,75}, {14,15,60}, {20,35,50}, {25,65,10}, {28,0,100}, {33,0,100}. Chromatograms were detected using the absorbance at 254 nm. UV-Vis spectra of substrate and product peaks were also collected.

4.5.4. In vitro *activity of BcmD.*

Bacimethrin (0.48 mM) was incubated with ATP (10 mM) and $MgCl_2$ (5 mM) in the presence of BcmD (0.125 μM), in 50 mM HEPES, pH 7.5 for 2.5 h at 25 ± 1 °C. The reaction mixture was then diluted with water to 0.3 mL and the protein was removed

by centrifugal ultrafiltration (3 kDa MWCO membrane). 0.05 mL aliquots of the filtrate were analyzed by reverse-phase HPLC.

4.5.5. Reaction of thiamin and methoxythiamin catalyzed by C. botulinum thiaminase I.

^{1}H NMR spectra were acquired on a Varian INOVA 500 MHz instrument equipped with an autoswitchable probe and a *Z*-axis pulsed field gradient. Methoxythiamin **4.19** (MeOThOH) was synthesized by Ahmed Al-Harrasi, Cornell University. The thiaminase I enzyme was heterologously overexpressed and purified using standard procedures by Lisa Cooper, Texas A&M University. Thiamin (**4.20**, ThOH) was from Sigma. For assessment of the enzyme activity, the substrate (MeOThOH or ThOH 10 mM) was treated with thiaminase I (300 nM) in a solution prepared from 0.2 mL of 0.1 M potassium phosphate buffer, pH 8.0, 0.4 mL deuterium oxide, and 0.06 mL 1 M KCl. The ^{1}H NMR spectrum of this solution was acquired and used for optimization of the instrument *Z*-shims. The HDO resonance was suppressed using a shaped excitation pulse generated by the Varian "Wet1d" pulse sequence. To initiate the reaction, β-mercaptoethanol was added (2.1 μL, 50 mM) to the NMR tube and the solution was mixed manually and replaced in the magnet (dead time ~45 s). The ^{1}H NMR spectrum of the resulting solution was then monitored over time. The data for the reaction of thiamin were processed by application of a 0.35 Hz exponential multiplication, and the data for the reaction of methoxythiamin were processed by application of a 2.2 Hz exponential multiplication prior to Fourier transformation.

4.5.6. Identification of the BcmC product as bacimethrin by ESI mass spectrometry.

5-Hydroxymethylcytosine (0.25 mM) and *S*-adenosyl-L-methionine iodide (0.3 mM) were incubated with BcmC (2.75 μM) in 25 mM ammonium acetate, pH 6.2, for 3.5 h.

The enzyme was then removed by centrifugal ultrafiltration (10 kDa MWCO membrane, Pall Life Sciences, Ann Arbor, Michigan), and formic acid was added to the filtrate (final concentration 0.1 % (v/v)). The samples were thne analyzed by ESI-TOF +MS on an Applied Biosystems Q-STAR instrument in the Laboratory for Biological Mass Spectrometry, Texas A&M University.

4.5.7. Steady-state kinetics of the BcmA-catalyzed hydroxymethylation of CMP.

5,10-Methylenetetrahydrofolate was from Schircks Laboratories, Jona, Switzerland. In a typical assay, BcmA (760 nM) was incubated with 5,10-methylenetetrahydrofolate (0.05 mM) and CMP (0 – 0.2 mM) in 50 mM HEPES, pH 7.5 containing 0.15 M potassium chloride. The addition of potassium chloride was required to prevent precipitation of the enzyme. β-Mercaptoethanol was also included at 10 mM. The reaction was initiated by addition of the methylenetetrahydrofolate. In control experiments where the enzyme or CMP was omitted, the methylenetetrahydrofolate absorbance at 290 nm did not measurably decrease on the time scale of the experiment (typically 100 s).

The value of V/E_o was estimated from the relation

$$\frac{V}{E_o} = \frac{1}{\Sigma\Delta\varepsilon_{PS}}\frac{dA_{290}}{dt} \qquad (4.1)$$

where $\Sigma\Delta\varepsilon_{PS}$ is the difference between the sums of the 290-nm extinction coefficients of the products and reactants. There was no evidence for changes in the absorbance spectrum other than those attributable to interconversion of the pterin compounds.

REFERENCES

1. Tanaka, F., Takeuchi, S., Tanaka, N., Yonehara, H., Umezawa, H., Sumiki, Y. (1961) Bacimethrin, a new antibiotic produced by *Bacillus megaterium*, *J. Antibiotics A*, *14*, 161–162.
2. Koppel, H. C., Springer, R. H., Robins, R. K., Cheng, C. C. (1962) Synthesis of bacimethrin, *J. Org. Chem. 27*, 1492.
3. Nishimura, T., Tanaka, N. (1963) Biological studies on bacimethrin, a pyrimidine antibiotic, and monazomycin, *J. Antibiotics A 16*, 179–181.
4. Drautz, H., Messerer, W., Zähner, H., Breiding-Mack, S., Zeeck, A. (1987) Metabolic products of microorganisms. 239. Bacimethrin isolated from *Streptomyces albus*. Identification, derivatives, synthesis and biological properties, *J. Antibiotics 40*, 1431–1439.
5. Ple, N., Turck, A., Fiquet, E., Queguiner, G. (1991), Metabolism of diazines. III. New synthesis of analogs of trimethoprim and of bacimethrin, *J. Heterocyc. Chem. 28*, 283–287.
6. Zilles, J. L., Croal, L. R., Downs, D. M. (2000) Action of the thiamine antagonist bacimethrin on thiamine biosynthesis, *J. Bacteriol. 182*, 5606–5610.
7. Reddick, J. J., Saha, S., Lee, J., Melnick, J. S., Perkins, J., Begley, T. P. (2001) The mechanism of action of bacimethrin, a naturally occurring thiamin antimetabolite, *Bioorg. Med. Chem. Lett. 11*, 2245–2248.
8. Reddick, J. J., Nicewonger, R., Begley, T. P. (2001) Mechanistic studies on thiamin phosphate synthase: evidence for a dissociative mechanism, *Biochemistry 40*, 10095–10102.

9. Hanes, J. W., Ealick, S. E., Begley, T. P. (2007) Thiamin phosphate synthase: the rate of pyrimidine carbocation formation, *J. Am. Chem. Soc. 129*, 4860–4861.

10. Lawhorn, B. G., Gerdes, S. Y, Begley, T. P. (2004) A genetic screen for the identification of thiamin metabolic genes, *J. Biol. Chem. 279*, 43555–43559.

11. Newby, Z., Lee, T. L., Morse, R. J., Liu, Y., Liu, L., Venkatraman, P., Santi, D. V., Finer-Moore, J. S., Stroud, R. M. (2006) The role of protein dynamics in thymidylate synthase catalysis: variants of conserved 2′-deoxyuridine 5′-monophosphate (dUMP)-binding Tyr-261, *Biochemistry 45*, 7415–7428.

12. Butler, M. M., Graves, K. L., Hardy, L. W. (1994) Evidence from ^{18}O exchange studies for an exocyclic methylene intermediate in the reaction catalyzed by T4 deoxycytidylate hydroxymethylase, *Biochemistry 33*, 10521–10526.

13. Li, L., Xu, Z., Xu, X., Wu, J., Zhang, Y., He, X., Zabriskie, M. T., Deng, Z. (2008) The mildiomycin biosynthesis: initial steps for sequential generation of 5-hydroxymethylcytidine 5′-monophosphate and 5-hydroxymethylcycosine in *Streptoverticillium rimofaciens* ZJU5119, *ChemBioChem 9*, 1286–1294.

14. Short, S. A., Armstrong, S. R., Ealick, S. E., Porter, D. J. T. (1996) Active site amino acids that participate in the catalytic mechanism of nucleoside 2′-deoxyribosyltransferase, *J. Biol. Chem. 271*, 4978–4987.

15. Martin, J. L., McMillan, F. M. (2002) SAM (dependent) I AM: the *S*-adenosylmethionine-dependent methyltransferase fold, *Curr. Opin. Struct. Biol. 12*, 783–793.

16. Davidson, A. L., Chen, J. (2004) ATP-binding cassette transporters in bacteria, *Annu. Rev. Biochem. 73*, 241–268.

17. Wittliff, J. L., Airth, R. L. (1970) Thiaminase I (thiamine:base 2-methyl-4-aminopyrimidine-5-methenyltransferase, E.C. 2.5.1.2), *Methods Enzymol. 18* 229 – 234.

18. Wittliff, J. L., Airth, R. L. (1970) Thiaminase II (thiamine hydrolase, E.C. 3.5.99.2), *Methods Enzymol. 18*, 234–238.

19. Toms, A. V., Haas, A. L., Park, J.–H., Begley, T. P., Ealick, S. E. (2005) Structural characterization of the regulatory proteins TenA and TenI from *Bacillus subtilis* and identification of TenA as a thiaminase II, *Biochemistry 44*, 2319–2329.

20. Haas-Jenkins, A., Schyns, G., Potot, S., Sun, G., Begley, T. P. (2007) A new thiamin salvage pathway, *Nat. Chem. Biol. 3*, 492–497.

21. Kallen, R. G., Jencks, W. P. (1966) The mechanism of the condensation of formaldehyde with tetrahydrofolic acid, *J. Biol. Chem. 241*, 5851–5863.

22. Osborn, M. J., Talbert, P. T., Huennekens, F. M. (1960) The structure of "active formaldehyde" (N^5,N^{10}-methylene tetrahydrofolic acid), *J. Am. Chem. Soc. 82*, 4921–4927.

23. Tazuya, K., Yamada, K., Kumaoka, H. (1960) Incorporation of histidine into the pyrimidine moiety of thiamin in *Saccharomyces cerevisiae*, *Biochim. Biophys. Acta 990*, 73–79.

24. Costello, C. A., Kelleher, N. L., Abe, M., McLafferty, F. W., Begley, T. P. (1996) Mechanistic studies on thiaminase I, *J. Biol. Chem. 271*, 3445–3452.

25. Rodionov, D. A., Vitreschak, A. G., Mironov, A. A., Gelfand, M. S. (2002) Comparative genomics of thiamin biosynthesis in prokaryotes. New genes and regulatory mechanisms, *J. Biol. Chem. 277*, 48949–48959.

26. Hazra, A., Chatterjee, A., Begley, T. P. (2009) Biosynthesis of the thiamin thiazole in *Bacillus subtilis*: identification of the product of the thiazole synthase-catalyzed reaction, *J. Am. Chem. Soc. 13*, 3225–3229.

27. Lehmann, C., Begley, T. P., Ealick, S. E. (2006) Structure of the *Escherichia coli* ThiS-ThiF complex, a key component of the sulfur transfer system in thiamin biosynthesis, *Biochemistry 45*, 11–19.

28. Chatterjee, A., Schroeder, F. C., Jurgenson, C. T., Ealick, S. E., Begley, T. P. (2008) Biosynthesis of the thiamin-thiazole in eukaryotes: identification of a thiazole tautomer intermediate, *J. Am. Chem. Soc. 130*, 11394–11398.

29. Chatterjee, A., Li, Y., Zhang, Y., Grove, T. L., Lee, M., Krebs, C., Booker, S. J., Begley, T. P., Ealick, S. E. (2008) Reconstitution of ThiC in thiamin pyrimidine biosynthesis expands the radical SAM superfamily, *Nat. Chem. Biol. 4*, 758–765.

30. Frey, P. A., Hegeman, A. D., Ruzicka, F. J. (2008) The radical SAM superfamily, *Crit. Rev. Biochem. Mol. Biol. 43*, 63–68.

31. Bradford, M. M. (1976) A rapid and sensitive method for the quantitation of microgram quantities of protein utilizing the principle of protein-dye binding, *Anal. Biochem. 72*, 248–254.

CHAPTER 5

Summary and outlook.

5.1. CysM.

5.1.1. Summary.

Our kinetic studies on CysM led to the conclusion that the amino acid substrate for this enzyme is not *O*-acetyl-L-serine, as had been previously thought. Instead, the enzyme selectively uses *O*-phospho-L-serine as the amino acid precursor for L-cysteine. This had not been observed previously in bacteria, and had been observed only once in total, in the hyperthermophilic archaeon *Aeropyrum pernix*.

This study also was the first to offer a detailed kinetic characterization of the transfer of sulfur from a small sulfur carrier protein to an enzyme-bound biosynthetic intermediate. The kinetic results complemented a crystallographic study which showed that the CysM active site containing the α-aminoacrylate intermediate is occluded from solvent in the absence of CysO, and that very specific interactions between CysM and CysO are required to open the small channel through which the sulfur atom is delivered on the flexible CysO-COSH *C*-terminus (*1*,*2*). Importantly, the kinetics show that CysO does not bind tightly to CysM, and that the sulfur delivery is a kinetically-controlled event, presumably involving rapid sampling of the CysO/CysM interface for a configuration of the two proteins that triggers conformational changes allowing access to the α-aminoacrylate intermediate at the CysM active site. This protein-mediated selectivity is exquisite, with second order rate constants for the CysO-COSH/CysM-aminoacrylate reaction more than two orders of magnitude greater than for the reaction of the CysM-bound intermediate with the small anion, bisulfide.

Around the same time as our study was published, a second study carried out by Ågren *et al.* arrived at similar conclusions about the substrate specificity for CysM. They also identified the residue responsible for selectivity for *O*-phosphoserine as Arg220. Mutating this residue greatly reduces the selectivity for the amino acid substrate (*3*).

5.1.2. Outlook.

5.1.2.1. Biomedical relevance of CysM.

The unexpected substrate specificity of CysM for *O*-phosphoserine may be of biomedical relevance. The extent of flux through the CysM-dependent cysteine biosynthetic pathway in *M. tuberculosis* as it infects humans is still unclear. While gene expression studies have shown that expression of CysM is upregulated under conditions of oxidative stress, an alternate school of thought suggests that regulation is not necessarily an indicator of essentiality of the gene product for survival of *M. tuberculosis*, at least during the latent stages of infection when the organisms are living in macrophages (*4*). Genes required for survival in macrophages were shown to frequently be constitutively expressed. Nevertheless, if a potent inhibitor of CysM were to be found, it could potentially be a useful therapeutic agent. High-throughput screening strategies with this aim could be developed.

5.1.2.2. Biophysical aspects.

The CysM/CysO-COSH system involves an interesting protein-protein interaction, where the selective recognition of CysO-COSH by CysM containing the α-aminoacrylate intermediate results in a kinetically controlled atom transfer reaction that appears to be limited by association of the proteins. Mapping out the structural features of the proteins that facilitate this recognition interaction would add to our

understanding of transient protein-protein interactions in general, and also in the particular case of the small sulfur carrier proteins. The crystallographic study carried out by Ågren *et al.* Showed that the *C*-terminal portion of CysM is at least partly responsible for determining specificity for the nucleophilic substrate (*1*), however further studies are needed to fully describe the determinants of the CysO-CysM interaction which result in opening of the active site to the *C*-terminus of CysO-COSH. Comparative similar studies on the equivalent ThiSG complex in thiamin biosynthesis may aid understanding of the recognition elements and other features which facilitate the function of this sulfur transfer system. Kinetic studies on suitably chosen mutants of the proteins, and also time-resolved NMR studies, could shed further light on the key interactions which mediate the recognition event.

5.2. HpxO.

5.2.1. Summary.

We confirmed the proposals, arising from two genetic studies, that the urate oxidase enzyme in *Klebsiella pneumoniae* depends on a flavin adenine dinucleotide cofactor for its activity. All previously-studied urate oxidase enzymes are cofactor-independent. We showed that HpxO selectively utilizes NADH over NADPH (*V*/*K* ratio of ~10) and that the enzyme utilizes molecular oxygen at least an order of magnitude more efficiently than the cofactor-independent urate oxidase. This latter effect is a possible reason for the evolution of this activity in *K. pneumoniae*, which is apparently found frequently in relatively oxygen-depleted habitats, such as humans.

We also characterized the steady-state kinetics of seven active site mutants of the HpxO enzyme. The choice of these mutations was determined on the basis of the X-ray crystal structure of the protein. Most of these enzymes are highly impaired in their ability to oxidize uric acid. In particular, the R204Q mutant can catalyze the oxidation

of NADH in a manner that is essentially independent of urate, suggesting that this residue may be an important component of the machinery that couples substrate binding to flavin motion to the "out" position, allowing for its reduction and the subsequent oxygenation reactions in the catalytic cycle. A hydrogen bonding network between a number of active site residues which may be important for substrate binding or proton transfer reactions during catalysis was identified from the crystallographic data.

5.2.2. Outlook.

5.2.2.1 Biological significance.

The sequenced genomes of a variety of organisms which appear to contain the HpxO enzyme also contain a gene coding for the cofactor-independent urate oxidase. In some cases the two urate oxidase genes are contiguous on the chromosome of the organism in question, in others they both appear to be present in the purine catabolic cluster, and in others they are found quite removed from each other on the chromosome. It is this unclear whether such organisms employ one or both enzymes for urate oxidation at a given time, or whether they are differentially regulated or expressed. Genomic and proteomic profiling experiments aimed at investigating the regulation and expression of these genes would add to our understanding of purine catabolism and nitrogen assimilation in these bacteria.

Since humans cannot assimilate nitrogen from uric acid, which is excreted, an inhibitor of one or both of the bacterial urate oxidase enzymes may be of clinical relevance. A modified version of the cofactor-independent urate oxidase is currently employed as a therapeutic agent for cases of gout (build-up of crystalline urate in human joints) which is unresponsive to conventional therapies such as xanthine oxidase inhibitors. However, this therapeutic strategy suffers from the production of

one equivalent of hydrogen peroxide per equivalent of urate oxidized. HpxO administered in a similar context would not produce this hydrogen peroxide side product.

5.2.2.2. Mechanistic studies.

The steady-state kinetic studies on the HpxO active site mutants identified a number of residues which are important for catalysis. While enzymes closely related to HpxO, such as 4-hydroxybenzoate hydroxylase, have been intensely studied, in particular the role of R204 of HpxO in coupling of urate binding to flavin reduction by NADH merits more detailed examination. A series of pre-steady-state kinetic experiments and biophysical measurements aimed at determining how this residue contributes to the HpxO catalytic cycle will provide additional insights into the function of FAD-dependent monooxygenases.

5.3. Bacimethrin.

5.3.1. Summary.

We identified and characterized a biosynthetic pathway for the bacteriostatic natural product in *Clostridium botulinum A ATCC 19397*. This pathway proceeds in three steps from cytidine monophosphate, involving sequential hydroxymethylation of the 5-position of the nucleotide, followed by glycosyl bond cleavage, and methylation of the O2′-position of the resulting 5-hydroxymethylcytosine. We also demonstrated that the ThiD-2 gene product in the biosynthetic cluster can catalyze the reaction of bacimethrin in an ATP-dependent manner, presumably producing bacimethrin phosphate and pyrophosphate. The thiaminase I gene product, also expressed from the biosynthetic cluster, efficiently cleaves thiamin but not the methoxythiamin which

would be derived from bacimethrin, suggesting that the purpose of this thiaminase is not detoxification of endogenously-produced methoxythiamin.

5.3.2. Outlook.

5.3.2.1. The bacimethrin-derived product of C. botulinum **BcmD.**

While this enzyme unambiguously catalyzes the reaction of bacimethrin in the presence of ATP, the product or products have not yet been isolated and fully characterized. This will be accomplished by a combination of LC-MS and NMR analyses.

5.3.2.2. Substrate specificity of **BcmD.**

The *bcmD* gene is one of two copies of the *thiD* gene in the *C. botulinum* chromosome. The second copy is clustered with the genes encoding thiamin phosphate synthase (*thiE*) and hydroxyethylthiazole kinase (*thiM-1*). Two copies of ThiD are found in a range of bacterial taxa including several strains of *Clostridium botulinum*. ThiD-1 is generally found clustered with genes involved in thiamin metabolism, while ThiD-2 is found in a variety of genetic contexts. The primary sequences of the *C. botulinum A ATCC 19397* ThiD-1 and ThiD-2 proteins show 52% amino acid identity and 73% similarity. As part of an assessment of the relative utilization of methoxythiamin and thiamin in *C. botulinum*, the selectivity of the BcmD enzyme for bacimethrin over HMP-OH will be measured.

5.3.2.3. Activity of C. botulinum **ThiC.**

Sequence alignment of this protein with other ThiC enzymes showed a mutation in the highly-conserved sequence motif involved in ligation of the enzyme's catalytically essential [4Fe–4S] cluster. It thus remains to determine whether this protein is in fact

active. Synthesis of the *C. botulinum thiC* gene using *E. coli*-optimized codons and its subsequent overexpression, purification and characterization are currently underway.

5.3.2.4. The role of methoxythiamin.

Given that methoxythiamin is likely to be produced *in vivo* by *Clostridium botulinum*, what is its role in the organism? Previous studies have shown that methoxythiamin is bacteriostatic in *Escherichia coli* and other bacteria, but can methoxythiamin itself be used in place of thiamin in *C. botulinum*, making it the first naturally-occurring functional structural analogue of thiamin to be discovered? If this is the case, is methoxythiamin *selectively* used over thiamin by *C. botulinum* and other bacimethrin-producing organisms? Owing to the technical difficulties of working with *C. botulinum*, a model organism with a similar bacimethrin biosynthetic cluster, but which is not highly pathogenic, would be an invaluable tool in addressing these questions. Efforts are presently underway to determine whether *Bacillus thiaminolyticus*, which produces thiaminase I, also contains the bacimethrin biosynthetic cluster. Additionally, analysis of the cofactor dependence of thiamin-dependent enzymes from *C. botulinum* can partially address some of these questions in *in vitro* experiments. This can be achieved in the most practical and expedient fashion by synthesis of the relevant genes and their subsequent heterologous expression, followed by *in vitro* characterization of the proteins. Such studies are presently underway.

5.3.2.5. The role of thiaminase I.

The function of thiaminase I has remained unclear since discovery and initial characterization of the enzyme in the mid-20th century. Our present studies have shown that thiaminase I, which has been proposed by others to be an extracellular

enzyme, is likely produced in concert with bacimethrin in *C. botulinum*. It remains to be determined whether thiaminase is thus a virulence factor which potentiates the toxicity of bacimethrin for this organism. Comparative genomic analysis does not indicate that bacimethrin is produced by all organisms which possess a gene encoding thiaminase I. However, *C. botulinum* appears to lack the ability to biosynthesize the thiazole moiety of thiamin. Thiaminase I obligatorily produces this thiazole from thiamin. Could the role of thiaminase I in *C. botulinum* be dual – to potentiate the toxicity of bacimethrin, and to scavenge thiazole for use by *C. botulinum* itself? These questions can best be addressed by suitable studies on a model organism, as described above, and efforts towards addressing these questions are underway.

REFERENCES

1. Ågren, D., Schenll, R., Schneider, G. (2009) The *C*-terminal of CysM from *Mycobacterium tuberculosis* protects the aminoacrylate intermediate and is involved in sulfur donor selectivity, *FEBS Lett. 583*, 330–336.
2. Jurgenson, C. T., Burns, K. E., Begley, T. P., Ealick, S. E. (2008) Crystal structure of a sulfur carrier protein complex found in the cysteine biosynthetic pathway of *Mycobacterium tuberculosis*, *Biochemistry 47*, 10354–10364.
3. Ågren, D., Schnell, R., Öhlmann, W., Singh, M., Schneider, G. (2009) Cysteine synthase (CysM) of *Mycobacterium tuberculosis* is an *O*-phosphoserine sulfhydrylase: evidence for an alternative cysteine biosynthesis pathway in mycobacteria, *J. Biol. Chem. 283*, 31567–31574.
4. Rengarajan, J., Bloom, B. R., Rubin, E. J. (2005) Genome-wide requirements for *Mycobacterium tuberculosis* adaptation and survival in macrophages, *Proc. Natl. Acad. Sci. USA 102*, 8327–8332.